DISCRETE MODELING OF SHAPE MEMORY ALLOYS

S MOHANRAJ

NATIONAL UNIVERSITY OF SINGAPORE
2009

DISCRETE MODELING OF SHAPE MEMORY ALLOYS

S MOHANRAJ

(M.Sc. Materials Science and Engineering, NUS, 2003)

A THESIS SUBMITTED FOR THE DEGREE OF

DOCTOR OF PHILOSOPHY

DEPARTMENT OF MECHANICAL ENGINEERING

NATIONAL UNIVERSITY OF SINGAPORE

2009

Acknowledgements

I would like to express my deepest gratitude to Dr. Srikanth Vedantam, for providing me the tremendous opportunity of doing the research under his guidance. He took me to the world of mathematical modeling and taught me the fundamentals and applications in the real world. I always felt I was learning something new during each and every visit at his office. He motivates without pressurizing and subtly corrects without being at all discouraging. I am confident that the extremely perceptive and appropriate knowledge taught by him will lead me to greater heights in my intellectual career.

I would like to extend my sincere thanks to Dr. Vincent Tan. Many thanks to the Institute of Microelectronics for providing me the opportunity to work in Singapore and the conducive research environment which motivated me to seek higher graduate studies. I would like to thank my friends Judy, Terrence, Ravi, Siva and Raju who were supportive and made my moments pleasurable during coursework. I would like to thank my roommates Ganesh, Siva, Akella, Rajeev for their kindness and for providing a wonderful and friendly environment.

A very special word of thanks goes to my parents Soundarapandian and Poonkodi and my sister Viji, for their support and encouragement over the years. My wife Swarna deserves special acknowledgment for sacrificing her time and providing constant help and encouragement throughout my studies. Our sweet baby girls Niju and Rewa, are precious and real bundles of joy.

Contents

Summary

First order structural phase transitions arise from diffusionless rearrangement of the solid crystalline lattice and are known to cause exotic behaviour in materials. These are mainly a result of the characteristic complex microstructure which accompanies such transitions. An open problem in constitutive modeling of materials is in developing approaches which tie material information at different length scales in a consistent manner. In materials undergoing phase transitions such as shape memory alloys, this problem takes on added significance due to the evolution of microstructure of several different length scales during operation. It is thus imperative to develop constitutive models which incorporate information from several length scales and study the overall effect on the macroscopic properties.

Purely continuum models of materials have not been very successful in *multiscale modelling*: constitutive modelling incorporating the effect of several length scales. Commonly, multiscale models use a combination of discrete and continuum viewpoints. Discrete approaches incorporate the physics of small length scale features of the microstructure more directly whereas continuum approaches allow the problem to remain tractable.

Most multiscale models developed earlier have neglected thermal effects. During phase transitions, thermal effects are important and in this thesis we study discrete models for such problems. We first study the origin of structural phase transitions arising from vibrational entropy effects. Using statistical mechanics arguments we isolate a phase transforming mode whose properties determine those of the phase transitions. We then perform numerical simulations for a chain of atoms

with a potential energy possessing these properties and study the dependence of the phase transformation on the shape of the potential well. We also incorporate a gradient energy term and study its effect on hysteresis and the length scale of the resulting microstructure. While these simulations are performed to confirm the role of the properties of the potential energy, these properties do not provide a guide for a direct empirical fit of the interatomic potentials. In light of this, we develop two phenomenological approaches for a discrete description of thermal phase transitions.

Our first approach is a mean field description in which the effect of the surrounding atoms on a particular atom is provided through a temperature dependent substrate potential. It is important that the effect of the kinetic energy of the discrete particles is accounted for consistently and not twice: in the interatomic potential and in the kinetic energies of the particles. Using statistical mechanics calculations we confirm that this is not the case. We derive macroscopic properties such as the latent heat of transformation and the transformation temperatures for this model.

Next, we modify the previous model to neglect the substrate potential and instead consider purely temperature dependent nearest neighbour interactions. The reason for this to facilitate extension of this model to two- and three-dimensional cases which is not possible in the presence of a substrate potential. The configuration of the surrounding atoms (which depends on temperature) changes the energy of the interaction potential and the location of its minimum. We use a polynomial Falk-type free energy, which is a polynomial expansion of a single strain component, to describe the interaction potential. We restrict our studies in this work to a one-dimensional chain of identical atoms with an additional gradient energy term to penalize the presence of phase boundaries. We show numerically that these models realistically depict thermal solid-solid structural phase transitions.

List of Figures

Chapter 1

Introduction

1.1 Materials with microstructure

Atoms are the basic constituents of a material and they group themselves in repeating or periodic arrays over large atomic distances to form crystals or grains. There may be several grains in the material with different orientations of the crystalline lattice. Grain boundaries are the interfaces between grains of different crystal orientations. The presence of grains forms distinctive patterns, with lengths ranging from a few nanometres to a few micrometres and is an example of microstructure in metallic materials. Many interesting phenomena demonstrated by materials have been governed by their microstructure. Structural phase transitions are crystallographic structural changes in a material due to applied mechanical and/or thermal loads. These phase transitions result in rich microstructure and concomitant change in the mechanical response.

Structural phase transitions are of great interest due to their role in fostering technologically useful behavior in many materials such as metals, alloys and ceramics [1, 2]. The mechanical effects of structural phase transitions range from influencing commonplace properties such as hardness, strength or the elastic modulus [1] to causing more esoteric effects such as pseudoelasticity, shape memory [3] and ferroelectricity [4]. The structural phase transitions of most interest are the re-

versible, diffusionless, solid-solid transitions often referred to as 'weak' martensitic transformations [5].

Martensitic phase transitions occur between a high-temperature parent phase, in which the crystalline lattice is of relatively high-symmetry and a low-temperature lower-symmetry product phase. This phase change is usually first-order and is accompanied by the generation and absorption of latent heat during the forward (parent to product) and reverse (product to parent) transformations, respectively. Since the product phase is of low crystalline symmetry, it arises in many energetically equivalent variants and is anisotropic. This results in an important feature of these transformations, which is the formation of rich microstructure. The microstructure that is formed is quite complex and is easily changed with applied mechanical or thermal loads. Moreover the nature of the microstructure, such as the orientation of the domain walls or the volume fraction of the particular variant of the low-symmetry phase, has great influence on the mechanical response of the bulk material. For example, the orientation of the interfaces in a twinned structure affects dislocation and ledge motion on the twin boundary and thus the motion of the twin boundary [6]. Since this microstructure ranges from length scales of a few nanometers [7] to a few millimeters [8, 9], the nano and micromechanical aspects require careful consideration. Thus a proper account of the effect of this microstructure on the bulk response requires physical understanding of materials from atomic scale to macroscopic scale.

1.2 Shape Memory Alloy behaviour

Phase transitions occur in Shape memory alloys (SMA) through a diffusionless rearrangement of atoms in the form of a displacive *first-order phase transition*. At high temperatures SMA exist in a relatively higher symmetry austenite structure and at lower temperatures a low symmetry, multivariant martensite structure is preferred. The material thus undergoes *martensite phase transformations* with changes in

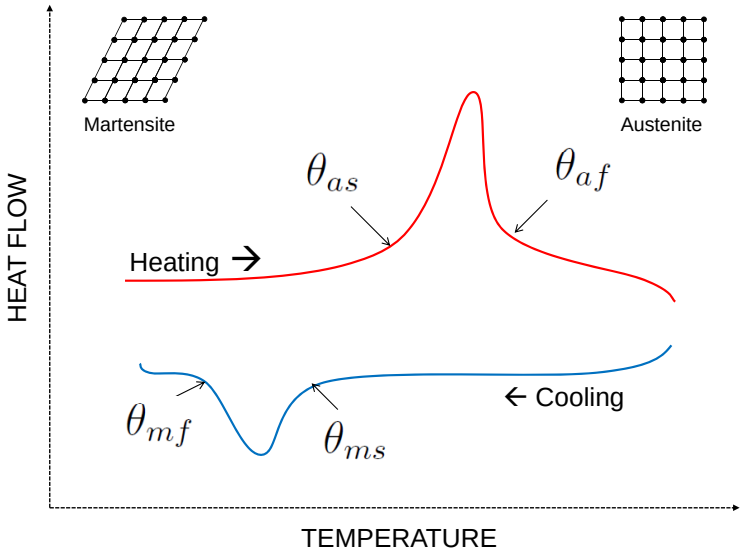

Figure 1.1: Typical Differential Scanning Calorimetry curve of a SMA alloy.

temperature. The martensite phase usually consists of orthorhombic, trigonal or monoclinic lattice structures. Differential Scanning Calorimetry (DSC) is a useful method for monitoring and characterizing the temperature-induced transformation. A typical DSC curve of a SMA alloy is schematically shown in Figure 1.1. The exchange of minima of the free energy of two phases at different temperatures is the driving factor for the phase transformation. The forward transformation (austenite-to-martensite) occurs when the free energy of martensite becomes less than the free energy of austenite at a temperature below a critical temperature θ_o at which the free energies of the two phases are equal. However, the transformation does not begin exactly at θ_o but, in the absence of stress, at a temperature θ_{ms} (martensite start), which is less than θ_o. The transformation continues to evolve as the temperature is lowered until a temperature θ_{mf} (martensite finish) is reached. When the SMA is heated from the martensitic phase in the absence of stress, the reverse transformation (martensite-to-austenite) begins at the temperature θ_{as} (austenite start), and at the temperature θ_{af} (austenite finish) the material is fully in the austenite phase. First-order phase transitions are char-

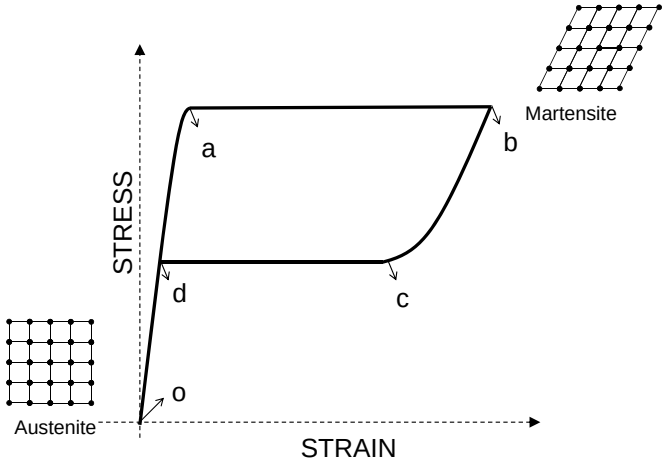

Figure 1.2: A schematic of a pseudoelastic behaviour.

acterized by the generation of latent heat. Latent heat is the quantity of heat that must be extracted/added to a system to transform from one phase to other, while keeping the temperature of the system constant. The area below the peak of the DSC curve in between transformation-start and finish temperatures gives *exothermic* and *endothermic* transition of the latent heat of forward and reverse transformation respectively.

Above the transformation temperature these alloys can be deformed by stressing and they recover their undeformed shape from large strains. Figure 1.2 shows a schematic of the stress-strain response of a SMA under an isothermal extension experiment. The material is initially in the austenite phase and stress causes only elastic distortions of the austenite lattice $\mathbf{o} - \mathbf{a}$. At a critical stress (point **a**), austenite becomes unstable and martensite starts to form. The stress plateau $\mathbf{a} - \mathbf{b}$ indicates the martensite transformation in the specimen without any additional stress. Unloading results in a elastic unloading of the martensite phase $\mathbf{b} - \mathbf{c}$ followed by reverse transformation to austenite from point **c** to point **d**. Further unloading simply follows the initial loading path. The strain is fully recovered

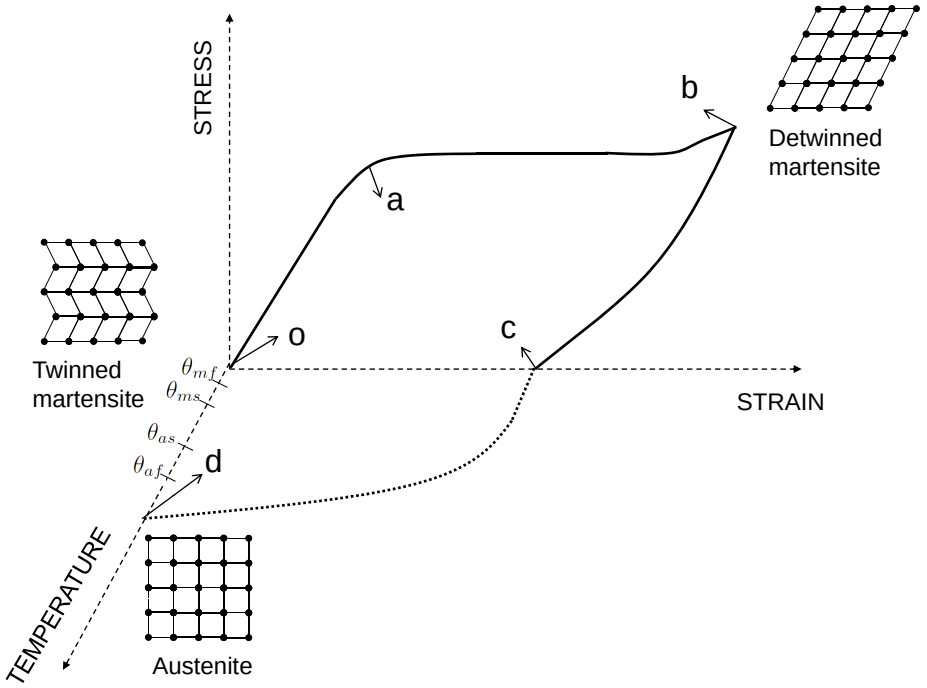

Figure 1.3: A schematic of a shape memory effect.

but not the applied mechanical work. This macroscopic phenomenon is called as *pseudoelasticity* and also referred to as a *stress-induced transformation*.

Below the transformation temperature a similar deformation of these alloys results in an apparently plastic strain as seen in Figure 1.3. However, this deformation can be recovered by increase in temperature. This phenomenon is termed the *shape memory effect*. In Figure 1.3 the material is initially in a twinned martensite phase (point **o**). Applied stress causes the detwinning along the path $\mathbf{o} - \mathbf{a} - \mathbf{b}$. Unloading results in elastic recovery of the detwinned material with some residual strain (point **c**). This residual strain is completely recovered by heating the material above austenite finish temperature θ_{af}. Along the path $\mathbf{c} - \mathbf{d}$, detwinned martensite transforms to austenite. Cooling the material at this stage results in the formation of twinned martensite without any change in the macroscopic length, this process is called as *self-accommodation*.

1.3 Multiscale modeling

Modeling of materials is an efficient way to understand, predict and control the properties of materials. The scientific investigation of materials with microstructure greatly depends on the mathematical models and simulations of materials at different length and time scales. Insofar as materials modeling are concerned, the smallest length scale considered is the atomic scale at which the quantum-mechanical (QM) state of electrons determine the property of the atoms and their interaction through the Schrodinger equation. Two computational schemes to solve the QM problem are the Quantum Monte Carlo (QMC) and Quantum Chemistry (QC) methods which can be used accurately to study a few tens of electrons. On the other hand, methods based on density functional theory (DFT) and local density approximation (LDA) can be employed for a few thousands of atoms. Tight binding approximation (TBA) can be extended to reach the simulations to a few nanometers and a few nanoseconds in time scale with concomitant loss in accuracy.

The *atomistic* problem is also studied at a length scale in which electronic interactions are ignored, but instead the effects of bonding govern the interaction between atoms. The interaction between atoms is represented by a potential function that depends on the atomic configuration. The interatomic potentials can be developed from a quantum-mechanical description of the material or empirical or semiempirical potentials obtained by fitting the lattice constants and elastic moduli. Dynamic evolution of the atomic system is governed by classical Newtonian mechanics and numerical methods are used to study the simultaneous motion and interaction of atoms. Molecular Dynamics (MD) and Monte Carlo (MC) simulations are widely used to provide insight in to atomic processes. MD simulations can go up to approximately 10^9 atoms and time scales up to microseconds can be reached. The *mesoscopic* scale in which dislocations, grain boundaries, and other microstructural elements dictate the property of a material is another important length scale at which materials are studied. The atomic degrees of freedom are

not explicitly treated and only larger scale entities are modeled. Approaches like Dislocation Dynamics (DD) and Statistical Mechanics (SM) are derived from phenomenological theories to study the kinetics of dislocations and consequently the macroscopic mechanical response. DD models can be used to study systems a few tens of microns in size. At the *macroscopic* scale, continuum fields such as density, velocity, temperature, displacement and stress fields play a major role, and constitutive laws are used to describe the behavior of the physical system. The governing equations are discretized and the finite element method (FE) is used to examine the mechanical behaviour of materials.

The macroscopic behaviour of a material is influenced by the phenomena at all the length scales outlined above. The models discussed above are efficient and specialized in their respective scales, but they are inefficient in describing effects at different length and time scales. Thus the current focus in the mechanics literature is in developing methods to couple and address these multiscale phenomena. The present multiscale approaches can be broadly categorized into two distinct kinds: *sequential* and *concurrent* approaches.

Sequential approaches try to describe phenomena at the different scales separately but with the aim of passing relevant information between scales. These are also referred to as serial, implicit or message-passing methods. For example, the Peierls-Nabarro model incorporates information obtained from *ab initio* calculations directly into continuum models. This approach can be applied to problems associated with dislocation core structure and cross slip process [10] which neither atomistic nor conventional continuum models can handle separately. Complex microstructure evolution during phase transformations can be studied using a phase-field model in which the microstructural constituents are described by a set of continuous order-parameter fields [11]. The temporal microstructural evolution is obtained from solving kinetic equations that govern the time-dependence of the spatially inhomogeneous order-parameter fields. The Kinetic Monte Carlo (KMC) model is another approach which provides the means for coarse-graining the atom-

istic degrees of freedom to a few mesoscopic degrees of freedom. For example, KMC models have been used to study epitaxial growth [12].

Concurrent approaches tend to simultaneously use two or more models applicable to different length scales with appropriate matching conditions. These are also referred to as parallel or explicit methods. For example, the Macroscopic Atomistic Ab initio Dynamics (MAAD), developed by Abraham et al. [13, 14] dynamically couples different length scales along their interface. The FE and MD regions are coupled by scaling down the FE mesh to atomic dimension at the interface of the two regions. MD atoms at the interface of quantum tight binding (TB) region, include neighbour atoms whose positions are determined by the dynamics of atoms in the TB region. This approach was used to study different problems like dislocation dynamics [15], crack propagation [16, 17] and energetic particle-solid collisions [18, 19]. The quasicontinuum method proposed by Tadmor et al. [20, 21] systematically coarsens the atomistic regions using kinematic constraints. These kinematic constraints are selected and designed so as to preserve the full atomistic resolution where required. This method has been applied to a variety of problems like dislocation structures [20, 21] and the interaction of dislocations with grain boundaries in Aluminium [22].

In this thesis we take the sequential multiscale model as our paradigm and develop discrete models for reversible, diffusionless, solid-solid structural phase transitions such as those seen in shape memory alloys. In section 1.4 we review different models developed to study phase transitions and highlight the need for incorporation of an atomistic description. In section 1.5 we discuss different approaches used to derive the interatomic potential for phase transition.

1.4 Models for martensitic phase transitions

The behaviour of materials with microstructure has been described by a non-linear elasticity theory [23] incorporating the crystallographic aspects of martensites [24].

Global energy minimization used in this theory to address the static regime. For example, it was shown by Bhattacharya [25], that certain microstructures are geometrically possible only if their lattice parameters satisfy highly restrictive conditions. Although these theories provide useful information about the type of microstructure formed, they do not completely determine the length scales due to the dynamic origin of these aspects. To study the dynamics models were proposed by Ball et al. [26], Friesecke et al. [27]. These relative energy minimizers predict the formation of infinitely fine patterns, in contrast to static models which use a global minimizer.

Continuum theories for shape memory alloys assume the dynamics to take place isothermally. The free energy density as a function of deformation gradient is the key to determining the stress. For martensite, the energy has to meet a symmetry condition imposed by the austenite phase. The free energy symmetry function with minimizers, appropriate elastic moduli and transition strains and phenomenological dependence on temperature are the main constitutive information needed for continuum theories. Non-isothermal dynamics in the continuum setting has been considered by several authors [28, 29, 30, 31, 32, 33, 34, 35]. The coexistence of phases and interface propagation under applied thermal or mechanical loads poses an additional challenge in their incorporation into constitutive equation. Kinetic relations for phase boundaries was first introduced by Truskinovsky [36] and Abeyaratne and Knowles [37] as additional constitutive information to determine the macroscopic response of the body.

Traditional continuum theories have been shown to be ill-equipped to study multiscale problems since they do not incorporate length scale effects. Phase field models [38, 39, 40, 41, 42] and strain-gradient theories [43, 44, 37, 45, 46, 30, 47, 48] are being considered in order to incorporate length scales. The papers by Triantafyllidis and Bardenhagen [45, 46] derive static gradient elasticity models from discrete models. Predictions of discrete and strain-gradient continuum models for martensitic materials are directly compared by Truskinovsky and Vainchtein

[49, 50]. However, it is still difficult to incorporate nanoscale effects into the constitutive equations of these augmented theories. Hence some of the recent efforts in multiscale modelling involve discrete atomistic descriptions of the microstructure coupled with mesoscopic or macroscopic approaches in the more homogeneous regions [51].

The complex nature of martensitic phase transitions casts some additional difficulties in determining appropriate kinetic relations. Some first models to obtain kinetic relations use discrete masses connected by nonlinear springs. Travelling wave solutions for these lattice models have been studied by Truskinovsky and Vainchtein [52] and show the radiation of lattice waves carrying energy away from the propagating front, resulting in macroscopic dissipation. Abeyaratne and Vedantam [6] use a Frenkel-Kontorova model [53, 54] to derive appropriate continuum kinetic relations for twin boundary motion. More recently dynamics of steps along a martensitic phase boundary have been studied by Zhen and Vainchtein [55, 56].

1.5 Interatomic potentials for phase transforming materials

One of the main difficulties in the atomistic calculations (apart from the computational time and memory expense) is in selecting appropriate interatomic potentials. While developing the interatomic potentials from a quantum mechanical description of the material is the most physically appealing approach, it proves to be computationally prohibitive. Instead, empirical and semi-empirical potentials are most commonly used. Empirical potentials usually fit the parameters to lattice constants and elastic moduli. However, for materials undergoing phase transitions, the lattice constants and elastic moduli properties of multiple crystalline lattices (multiple phases) need to be fitted in addition to other properties associated with the phase transition such as the transformation temperature and latent heats. Most of these

materials are binary or ternary alloys and reliable potentials for such multielement materials are generally not available. In spite of these difficulties, there have been some notable attempts to study phase transitions from an atomistic viewpoint using a single Lennard-Jones potential [57], multiple Lennard-Jones potentials between different types of atoms [58, 59, 60] or many-body potentials [61]. The main empirical fit to these potentials is the lattice spacing and the lattice structure of the parent and product phases. In theory, one of the elastic moduli in the parent or product phases may also be fitted empirically to these potentials. However, the other important parameters of phase transitions such as the transformation temperature and latent heat of transformation cannot be easily incorporated into these potentials. In fact, little is known about the particular features of the interatomic potential which determine these parameters. An alternative approach which has been recently proposed to obtain appropriate interatomic potentials for materials undergoing phase transitions is the use of temperature-dependent Lennard-Jones parameters [62, 63]. While no molecular dynamics simulations were performed in these studies, a detailed stability analysis revealed the existence of multiple stable phases. The energy density as a function of the deformation and temperature of a bi-atomic crystal was calculated using this method for use in continuum theories. In another approach, vibrational entropy effects were incorporated into a discrete model through domain wall stiffening [64]. While temperature-dependent potentials are phenomenological, they prove to be useful in developing an understanding of phase transitions from a discrete viewpoint.

1.6 Outline of thesis

In Chapter 2, we show the origin of structural phase transitions in vibrational entropy effects. Using statistical mechanics arguments we isolate a phase transforming mode which is the key to materials undergoing structural phase transitions. The properties of the potential energy in the phase transforming mode determine

the properties of the phase transformation. In particular the potential energy slice along the phase transforming mode is required to have a low-energy wells corresponding to the low-temperature phase and low-curvature region corresponding to the high-temperature phase. We then perform numerical simulations for a chain of atoms with a potential energy possessing these properties and study the dependence of the phase transformation on the shape of the potential well. We also incorporate a gradient energy term and study its effect on hysteresis and the length scale of the resulting microstructure. While these simulations are performed to confirm that these properties of the potential energy affect the phase transformation, it is still not easy to fit an interatomic potential to obtain these properties. In the subsequent chapters we focus on more phenomenological approaches.

While we studied the origin of vibrational entropy-driven structural phase transitions in Chapter 2, in Chapter 3 we focus on a mean field approach to structural phase transitions. The reasons for this are twofold: (1) the fundamental interatomic potential is not known — only the properties of the total potential energy along a particular mode and (2) the large differences in curvature of the potential energy slice causes computational difficulties. Instead, here we propose a mean field approach and assume that each atom experiences a substrate potential which depends on the effect of the surrounding atoms (and is, therefore, temperature-dependent). Such an approach is fraught with the possibility of counting the kinetic energy component of the system twice: once in the interatomic potential and explicitly in the kinetic energies of the particles. Using statistical mechanics calculations we confirm that this is not the case. We derive the macroscopic properties such as the latent heat of transformation and the transformation temperatures. We perform statistical mechanical calculations for a system of N uncoupled oscillators. We obtain analytical results for the Helmholtz free energy, entropy and the specific heat.

In Chapter 4 we modify the previous model to neglect the substrate potential and instead consider purely temperature-dependent nearest-neighbour inter-

actions. The reason for this to facilitate extension of this model to two- and three-dimensional cases which is not possible in the presence of a substrate potential. The configuration of the surrounding atoms (which depends on temperature) changes the energy of the interaction potential and the location of its minimum. We use a polynomial Falk-type free energy, which is a polynomial expansion of a single strain component, to describe the interaction potential. We restrict our studies in this work to a one-dimensional chain of identical atoms with an additional gradient energy term to penalize the presence of phase boundaries.

In Chapter 5 we summarize the results of our findings and propose future directions for extension of these results.

1.7 Key contributions of this thesis

In this thesis we have studied discrete models for materials undergoing structural phase transformations. We have shown for the first time that the origin of the vibrational entropy-driven phase transformations is in the properties of a parametric slice of the total potential energy of the system. We then developed a phenomenological discrete model for phase transitions and showed the connection to the macroscopic properties using statistical mechanics. In particular, the calculations show that it is possible to use a form of the continuum free energy for the interatomic potential energy. Finally, we presented a modified model which allows extension to two- and three- dimensional systems.

Chapter 2

Interatomic potentials for phase transforming materials

2.1 Introduction

One of the most successful applications of classical statistical physics in the solid state has been the prediction of the high-temperature specific heats of solids. Though the interaction between individual atoms in a solid is complicated, recognizing that the amplitude of vibration relative to interatomic distances is small allows the effect of the surrounding atoms on a given atom to be approximated by a harmonic potential field independent of neighboring atoms. In this uncoupled harmonic approximation, the kinetic and potential energies of each degree of freedom contribute $\frac{1}{2}k_B\theta$ (k_B is the Boltzmann constant and θ is the absolute temperature) to the internal energy and the resulting specific heat value matches closely the empirical observations of Dulong and Petit [65].

Some materials, notably those known as shape memory alloys (SMAs), undergo first-order diffusionless solid-solid structural phase transformations also called martensitic transformations. These transitions are marked by a spike in the heat capacity indicating the release or absorption of latent heat during the transformation. This feature is not described by the simple model outlined above since an atom in a

harmonic potential is incapable of undergoing a phase transition; anharmonic effects are essential. Moreover, the exchange in stability of the phases is due to an increase in entropy associated with the high-temperature phase. The high entropy of the high-temperature phase is related to softer phonons and large amplitude vibrations of the lattice in certain phase transforming modes [66]. There have been few simple models capable of delineating these effects, particularly the role of large amplitude vibrations and high entropy of the high-temperature phase in the phase transition.

In this chapter we present a simple model in the spirit of the above classical calculation of specific heats which is capable of describing vibrational entropy-driven phase transitions occurring above the Debye temperature of the solid.

Previous models of entropy-driven transitions employed a Hamiltonian consisting of a temperature independent three-well on-site potential (external field) and anharmonic intersite coupling terms [64]. The presence of the on-site potential allowed the model to overcome [64] the well-known absence of phase transitions in one-dimensional models with finite range interactions [67]. The anharmonicity of the *intersite coupling* strength effected a change in the stiffness of the low-temperature phonons which was responsible for driving the phase transition [64]. In contrast, our model is motivated by a crystallographic consideration of the phase transforming modes and a physical interpretation of the on-site potential. The entropy changes arise from the on-site potential which stabilizes the high-temperature phase. The intersite coupling represents the domain wall energy and is assumed to be harmonic.

In this chapter we examine the properties of interatomic potentials for phase transforming materials. A review of the relevant basic statistical mechanics concepts is included in Appendix A. We begin with a description of the classical calculation of the high-temperature specific heats of crystalline solids.

2.2 Calculation of specific heat of solids

Consider a crystalline solid at finite temperature. All atoms in a crystal vibrate about their equilibrium positions and interact with their neighbors through an interatomic potential. To calculate the potential energy of the solid we require knowledge of the interatomic potential and the trajectories of all the atoms which is quite difficult in practice. Instead, the approach taken in a *mean field* model is to assume that the effect of all the neighboring atoms provides a harmonic potential field for each atom and that the vibration of each atom is independent of the positions of its neighboring atoms. This assumption allows us to treat the solid as a system of *uncoupled harmonic oscillators*.

The energy of a harmonic oscillator of frequency ω is, in one-dimension,

$$E = \frac{1}{2M}p^2 + \frac{1}{2}M\omega^2 q^2, \tag{2.1}$$

where p is the momentum and q is the position of the oscillator of mass M. Using the classical formula for the average quantity in a canonical ensemble (given in Appendix A), the average energy of the oscillator in thermal equilibrium is

$$< E >= \frac{\int_{-\infty}^{+\infty}(\frac{1}{2M}p^2)e^{-p^2/2Mk_B\theta}dp}{\int_{-\infty}^{+\infty}e^{-p^2/2Mk_B\theta}dp} + \frac{\int_{-\infty}^{+\infty}\frac{M\omega^2}{2}q^2e^{-M\omega^2q^2/2k_B\theta}dq}{\int_{-\infty}^{+\infty}e^{-M\omega^2q^2/2k_B\theta}dq}. \tag{2.2}$$

Each term on the right is equal to $\frac{1}{2}k_B\theta$ and so

$$< E >= k_B\theta \tag{2.3}$$

for the simple harmonic oscillator in one-dimension.

The internal energy of N harmonic oscillators in three dimensions is then

$$U = 3N < E >= 3Nk_B\theta, \tag{2.4}$$

or, for a mole of substance

$$U_M = 3R\theta, \tag{2.5}$$

where $R = N_A k_B$ is the gas constant, and N_A is Avogadro's number, 6.023×10^{23}.

If we may consider that the atoms in a solid behave as harmonic oscillators about their equilibrium positions, we see that classical theory predicts the lattice contribution to the molar heat capacity at constant volume

$$C_V = \left(\frac{\partial U_M}{\partial \theta}\right)_V \tag{2.6}$$

of a solid should be, for a mole of atoms,

$$C_V = 3R. \tag{2.7}$$

This value, which is known as the Dulong and Petit value, is in good agreement with the observed total heat capacity of many solids at elevated temperatures.

2.3 Vibrational entropy in first-order phase transitions

Our focus in this thesis is on systems capable of undergoing martensitic transformations. The high-temperature phase (also known as the parent phase) is termed *austenite* and is not stable at low-temperatures. The low-temperature phase (also known as the product phase) is termed *martensite* and is not stable at high-temperatures.

From the macroscopic point of view the latent heat of system undergoing first-order phase transformation is given by

$$\lambda_T = \theta_T(S_M - S_A), \tag{2.8}$$

where θ_T is the transformation temperature and S_M and S_A are the molar entropies of the final and initial phase respectively. At the atomic scale, entropy is also viewed as the amount of disorder in a system: the more disordered a system, the greater its entropy. In the case of a crystalline solid with atoms localised on lattice sites, the disordering is associated with its excitations, i.e., its phonons. From the microscopic point of view, we show the vibrational phonon entropy difference between a martensite and austenite phase drives the phase transformation.

Consider a material capable of undergoing phase transitions. When the material is in the martensite state, we will describe it using a harmonic mean field model and thus the Hamiltonian is

$$H_M = \frac{p^2}{2M} + \frac{1}{2}K_M q^2 \tag{2.9}$$

where K_M is the spring constant of martensite phase. The partition function $\mathcal{Z}$ for a Hamiltonian in Eq. 2.9 is given by

$$\mathcal{Z}_M = \int_{-\infty}^{\infty} dp \int_{-\infty}^{\infty} \mathrm{d}q \exp(-H_M/k_B\theta) \tag{2.10}$$

The Helmholtz free energy of the martensite phase is given by

$$F_M = -k_B\theta \ln \mathcal{Z}_M = -\frac{k_B\theta}{2} \ln(\frac{4\pi^2 M(k_B\theta)^2}{K_M}) \tag{2.11}$$

At absolute zero temperature the austenite state has higher energy (and is therefore not the stable phase). Thus consider a harmonic Hamiltonian H_A for austenite having a higher-energy

$$H_A = \frac{p^2}{2M} + E_0 + \frac{1}{2}K_A q^2 \tag{2.12}$$

where $E_0 > 0$ and K_A is the spring constant of austenite phase. The free energy of the austenite phase is given by

$$F_A = E_0 - \frac{k_B\theta}{2} \ln(\frac{4\pi^2 M(k_B\theta)^2}{K_A}) \tag{2.13}$$

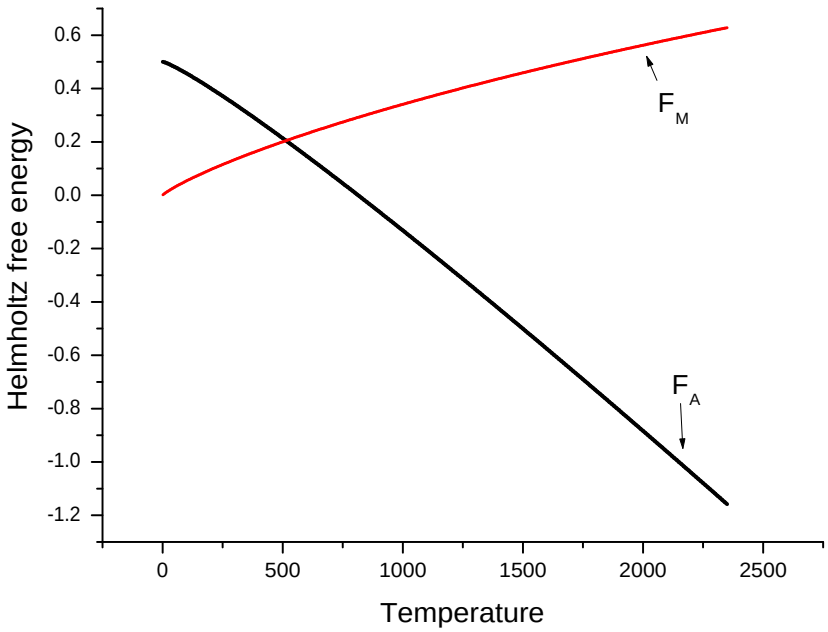

Figure 2.1: The Helmholtz free energy of martensite shown in red and austenite shown in black.

If at higher temperatures, $F_A < F_M$, exchange of phase stability is possible. It can easily be seen that this is possible only if $K_A/K_M < 1$. In Figure 2.1 we show the schematic plot of Helmholtz free energy with temperature in the case of $K_A/K_M < 1$. It is seen that at higher temperatures, the free energy of austenite is lower and thus a phase transformation is possible.

The dependence of the transition temperature θ_T on E_0 and K_A/K_M is found from equating free energies $F_A = F_M$. This yields $k_B\theta_T = -\frac{2E_0}{\ln K_A/K_M}$ (note that this result does not depend on M). As expected, the greater the difference in $\theta = 0$ energies, the greater the transition temperature. And on the other hand the smaller the K_A/K_M, the lower the transition temperature. Thus at high-temperatures there is sufficient vibrational entropy to stabilize the parent state. Further, if the vibrations are the same in the two states, state A will never be the equilibrium state, i.e. $\theta_T \to \infty$ as $K_A/K_M \to 1$. The parent phase would never be the stable equilibrium structure if its phonon entropy were not lower than that of

the martensitic phase.

It is clear from the two harmonic potentials that what leads to the lower free energy of austenite state is the softer spring constant i.e. the lower frequencies of its vibrations. Note that these spring constants are not directly related to elastic moduli of austenite and martensite phases. These spring constants are related to the curvature of the *interatomic potential*, whereas the elastic moduli are related to the curvature of the *free energy*. One simple way of seeing how this leads to an increased entropy as the temperature is increased is by noting that as the curvature of the potential is reduced, the particle can spread out more easily, i.e. it is more disordered than in a stiffer potential at a given temperature. The two harmonic potentials that have been used in the description are heuristic and the connection to a mean field approach is tenuous. The mean field model we propose in the next section makes the connection through crystallographic considerations.

2.4 Mean field model for phase transitions

2.4.1 Crystallography

Our model is motivated by a crystallographic consideration of the phase transformation and provides a physical interpretation of the on-site potential. For simplicity of exposition, consider a unit cell in two dimensions of a material capable of undergoing square to rectangle transitions as shown in Figure 2.2 (the argument can easily be extended to phase transitions between any two parent and product lattices in three dimensions). Taking the square lattice as the reference, the Bain stretch matrices describing the two variants of the low-temperature phase are given by

$$\mathbf{U}_1 = \begin{pmatrix} \alpha & 0 \\ 0 & \beta \end{pmatrix}, \quad \mathbf{U}_2 = \begin{pmatrix} \beta & 0 \\ 0 & \alpha \end{pmatrix}, \tag{2.14}$$

where α and β are the stretches of the sides of the unit cell. Now, consider a parametrization of the stretch matrices given by

$$\mathbf{U}(q) = \begin{pmatrix} s_1 q^2 + s_2 q + 1 & 0 \\ 0 & s_1 q^2 - s_2 q + 1 \end{pmatrix} \tag{2.15}$$

with $s_1 = (\alpha + \beta)/2 - 1$ and $s_2 = (\alpha - \beta)/2$. q represents a homogeneous deformation parameter for the unit cell; $q = 0$ represents the square phase and $q = \pm 1$ represent the two rectangular variants. Thus, if $\mathbf{x}_i$ represent the position vectors of atoms in the square lattice and $\mathbf{y}_i$ the current position of the atoms, we can express the current position of any atom in terms of its displacement as a part of a homogeneous deformation of the unit cell plus orthogonal shuffles. The homogeneous deformation of the unit cell contributes to the structural phase transformation and we will refer to this as the phase transforming mode (PTM). The orthogonal shuffles do not contribute to the phase transformations. We write

$$\mathbf{y}_i = \mathbf{R}\mathbf{U}(q)\mathbf{x}_i + \boldsymbol{\xi}_i, \tag{2.16}$$

for each atom i of the unit cell. $\mathbf{R}$ is a rigid rotation of the unit cell and $\boldsymbol{\xi}_i$ represent the displacements of atoms from the PTM positions.

Note that, in the simple lattice under consideration, we have one atom per unit cell and therefore two degrees of freedom. One degree of freedom is provided by the PTM and the other by the non-PTM.

2.4.2 Hamiltonian

The Hamiltonian for the system with sites labeled i is given by

$$\mathcal{H} = \sum_i \frac{p_i^2}{2m} + V(\mathbf{y}_i) \tag{2.17}$$

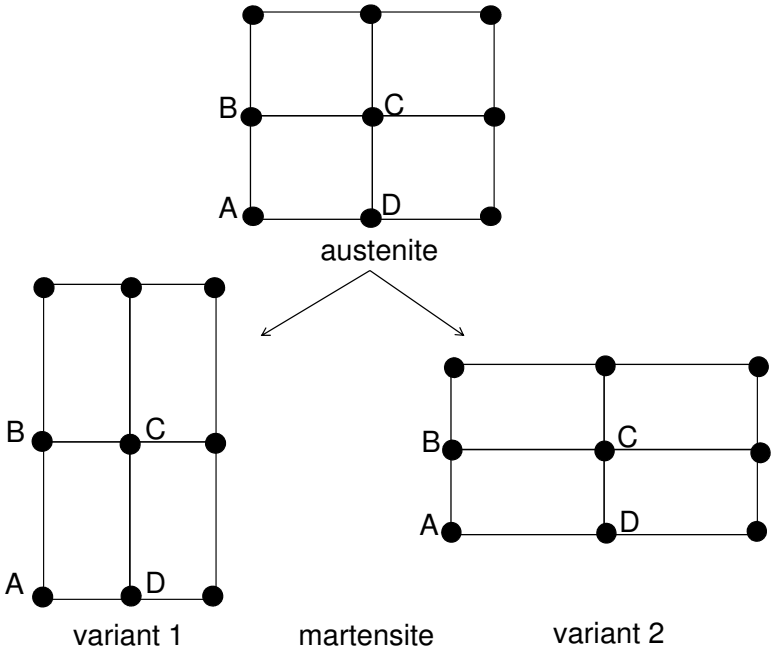

Figure 2.2: A schematic of a square high-temperature parent phase (austenite) and two variants of the low-symmetry product phase (martensite). The two variants arise from the fact that the bond AB in the parent phase stretches to two different lengths in the product phase.

where the potential energy $V(\mathbf{y}_i)$ depends on the positions of all the atoms. In the classical calculation, this potential is replaced by an effective harmonic field on each atom irrespective of the positions of the surrounding atoms.

In our model we view the current position of the each atom as a superposition of low-amplitude oscillations on the large amplitude PTMs of a unit cell to which the atom belongs. Thus we consider a simple additive decomposition of the potential energy

$$V(\mathbf{y}_i) = \sum_j \left(V_\xi(\boldsymbol{\xi}_i) + V_q(\mathbf{R}\mathbf{U}(q)\mathbf{x}_i) \right), \tag{2.18}$$

Where V_ξ is the potential energy contribution of the non-PTM which we choose to be harmonic. V_q is the potential energy of anharmonic phase transforming mode.

In order to understand the form of the potential $V_q(\mathbf{R}\mathbf{U}(q)\mathbf{x}_i)$ consider an equilibrium homogeneous deformation of the unit cell in the lattice. Note that,

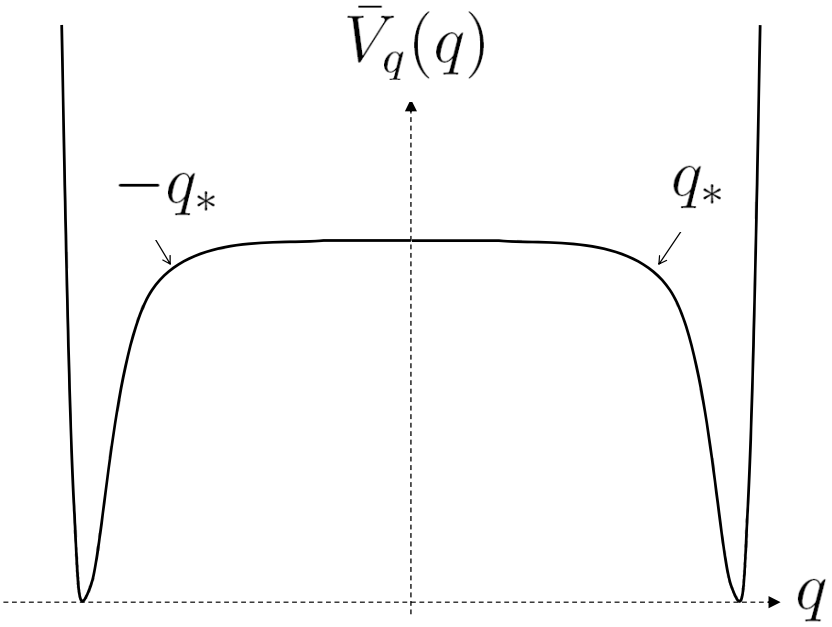

Figure 2.3: A schematic of the anharmonic potential energy.

since the potential energy of the unit cell is unaffected by rigid rotations we may write $V_q(\mathbf{RU}(q)\mathbf{x}_i) = \bar{V}_q(q)$. At absolute zero temperature the rectangular variants are stable whereas the square phase is unstable and has higher energy. Thus the potential will have minima at $q = \pm 1$ but not at $q = 0$ as shown in Figure 2.3. For simplicity, we choose a piecewise quadratic form for the anharmonic potential

$$\bar{V}_q(q) = \begin{cases} \frac{1}{2}k_m(q+1)^2, & q \leq -q_* \\ E_0 - \frac{1}{2}k_a q^2, & -q_* \leq q \leq q_* \\ \frac{1}{2}k_m(q-1)^2, & q \geq q_*. \end{cases} \tag{2.19}$$

where $E_0 > 0$ is the barrier height between the variants and $k_m > 0,\ k_a > 0$. q_* is chosen such that the potential energy is continuous.

At low-temperatures, the unit cell is in one of the martensite variants and the thermal vibrations will be localized to the corresponding minimum at $\langle q \rangle = \pm 1$. Where $\langle q \rangle$ represents the time average. At higher temperatures, the amplitude

of the vibrations increases and at the critical temperature the vibration spans both the wells. Due to the symmetry of the chosen potential, $\langle q \rangle = 0$ at high-temperatures. However, for this state to be characterized as the parent phase and *not a heterophase state*, the time spent in $q \in (-q^*, q^*)$ should be substantially larger than the time spent in $|q| > q^*$. The probability of finding the cell in the parent phase will then be larger than in either variant.

At high-temperatures, the vibration spans both wells, the ratio of time spent around $q = 0$ and the side wells is $t_p/t_m = \mathcal{O}(1/\sqrt{k_a/k_m})$. For $t_p/t_m \gg 1$, we require $k_a/k_m \ll 1$ and the magnitude of curvature at $q = 0$ should be small compared to the curvature at $q = \pm 1$. The softer potential at $q = 0$ implies that a larger volume of phase space is sampled by the system and the vibrational entropy is thus greater. Note, as stated earlier softer potential is not related to the elastic moduli of the material.

2.4.3 Calculation of thermodynamic properties

Using the potential energy for the uncoupled system in Eq. (2.19) and the Hamiltonian Eq. (2.17), we calculate the thermodynamic quantities. The canonical ensemble partition function in this case is given by $\mathcal{Z} = \mathcal{Z}_p \mathcal{Z}_\xi \mathcal{Z}_q$ where

$$\begin{aligned} \mathcal{Z}_q &= \int_{-\infty}^{+\infty} \exp\left(-\frac{\bar{V}_q(q)}{k_B\theta}\right) dq \\ &= \int_{-\infty}^{-q_*} \exp\left(-\frac{k_m(q+1)^2}{2k_B\theta}\right) dq + \int_{-q_*}^{q_*} \exp\left(-\frac{2E_0 - k_a q^2}{2k_B\theta}\right) dq \\ &\qquad + \int_{q_*}^{+\infty} \exp\left(-\frac{k_m(q-1)^2}{2k_B\theta}\right) dq \end{aligned} \tag{2.20}$$

Since the terms in the Hamiltonian corresponding to p and ξ are quadratic, Z_p and Z_ξ each contribute $\frac{1}{2}k_B$ to the specific heat and will not be explicitly considered henceforth. The partition function for the phase transforming mode can be

explicitly evaluated to be

$$\begin{aligned}\mathcal{Z}_q &= \sqrt{\frac{2\pi k_B\theta}{k_m}}\left[\frac{1}{\sqrt{k_a/k_m}}\exp\left(-\frac{E_0}{k_B\theta}\right)\mathrm{erfi}\left(\sqrt{\frac{k_a}{2k_B\theta}}q_*\right)\right] \\ &\quad +\sqrt{\frac{2\pi k_B\theta}{k_m}}\left[\mathrm{erfc}\left(\sqrt{\frac{k_m}{2k_B\theta}}(q_*-1)\right)\right] \qquad (2.21)\end{aligned}$$

in which erfi denotes the imaginary error function and erfc $= 1 -$ erf is the complementary error function. Thus the free energy is given by

$$F = -k_B\theta \ln \mathcal{Z}, \qquad (2.22)$$

and the entropy is given by

$$S = -\frac{\partial F}{\partial \theta}. \qquad (2.23)$$

The internal energy is thus

$$U = F + \theta S = -k_B\theta \ln \mathcal{Z} - \theta\frac{\partial F}{\partial \theta}, \qquad (2.24)$$

and the specific heat capacities

$$c_V = \frac{\partial U}{\partial \theta}. \qquad (2.25)$$

Since the partition function is explicitly known the above expression can be evaluated. The free energy as a function of temperature is shown in Fig. 2.4(a) for a set of chosen parameters, $E_0 = 0.01$, $k_a/k_m = 10^{-4}$ and $q = 0.99$. Figure 2.4(b) and Figure 2.5(a) show the entropy and internal energy respectively. The entropy does undergo a step change indicating that this represents an entropy-driven transition.

In Figure. 2.5(b) we show the specific heat as a function of temperature for two different values of α holding the other values fixed. For larger k_a/k_m the spike in the specific heat curve widens out. In a first-order transition, the spike in the specific heat curve approaches a delta function. Thus we see from the form of

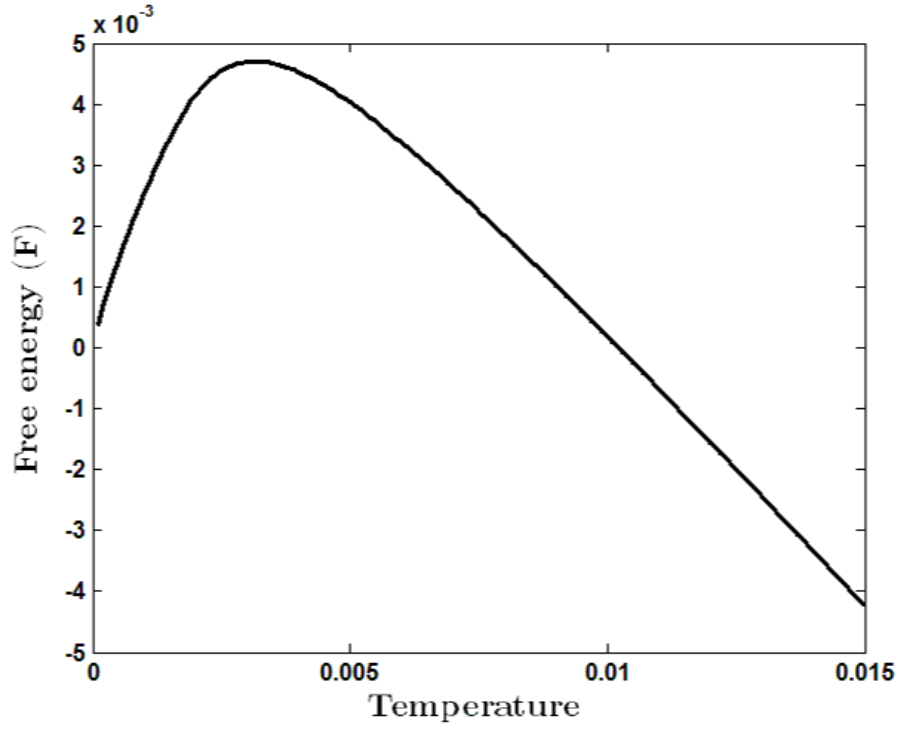

(a)

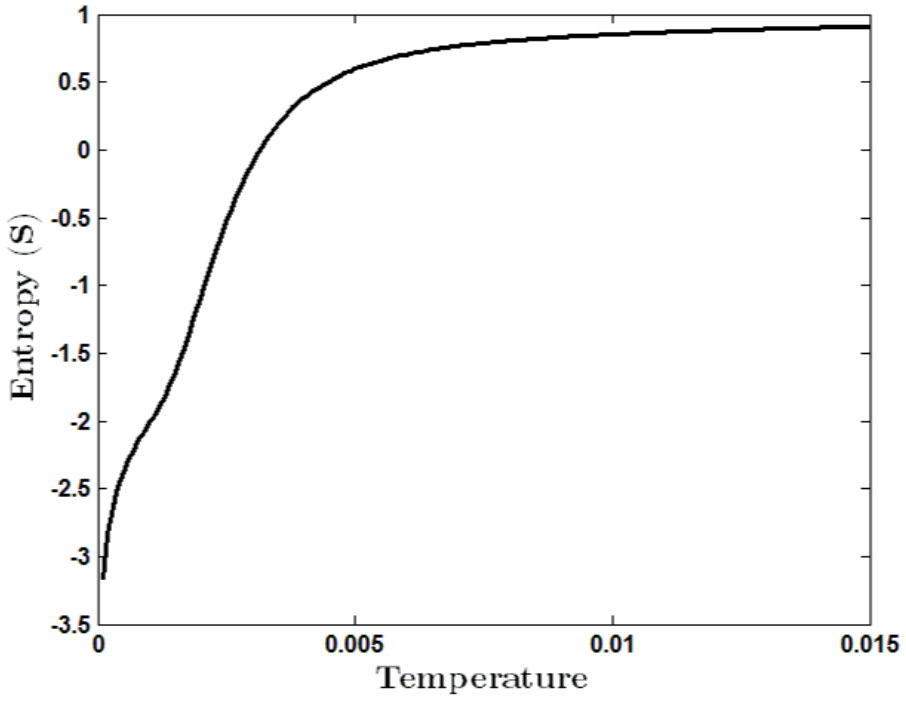

(b)

Figure 2.4: (a) Free energy as a function of temperature. (b) Entropy as a function of temperature

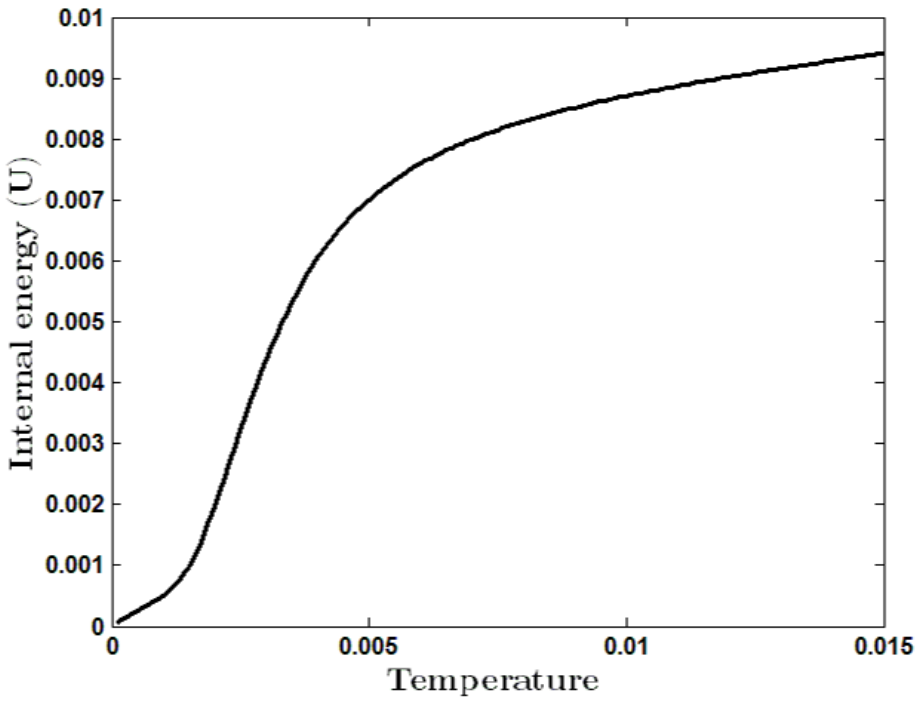

(a)

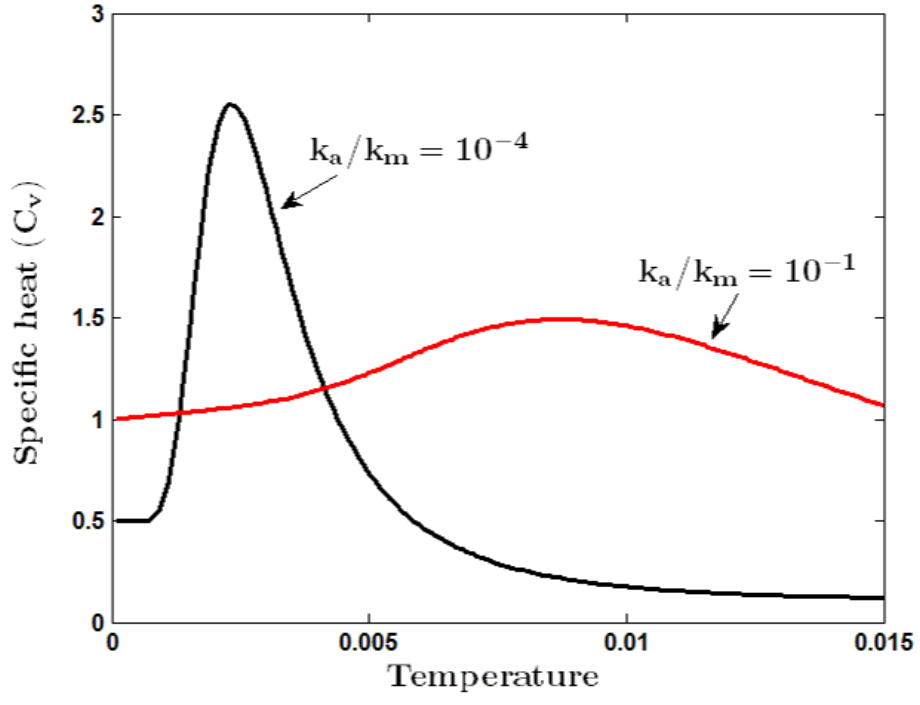

(b)

Figure 2.5: (a) Internal energy as a function of temperature. (b) Specific heat as a function of temperature for $k_a/k_m = 10^{-4}$ and $k_a/k_m = 10^{-1}$.

the potential that the curvatures of the austenite and martensite regions of the potential well govern the first-order phase transition.

2.5 Phase transformations in one-dimensional chain

We next consider a one-dimensional system of coupled oscillators in which the coupling potential has the properties described above. For ease of computations we choose a smoother potential instead of the potential in Eq. (2.19).

2.5.1 Interatomic potential

Since we restrict attention to a one-dimensional setting, we describe an analog of the above lattice configurations.

Consider a chain of N equidistant atoms separated by distance a as shown in Figure 2.6. This is the reference configuration and is taken to represent the austenite lattice. Thus a is the lattice constant of the austenite phase. We take the lattice constants of the two variants of martensite ($M^{\pm}$) to be $a \pm u_M$.

Let the reference equilibrium positions of the atoms (in the austenite phase) from a fixed origin be given by x_i; thus $x_i = ia$. Let the current position of the atom i be given by y_i. Then $y_i = ia + u_i$ where u_i is the displacement of the i atom from its reference position. The interatomic potential between adjacent pairs of atoms i and $i+1$ is chosen so that the minima are at $u_{i+1} - u_i = 0$ for the austenite phase and $u_{i+1} - u_i = \pm u_M$ for the two variants of the martensite phase. The energy of the ith bond is chosen as a function of the bond length $\ell_i = y_{i+1} - y_i$,

$$\begin{aligned} W(\ell_i) &= \frac{1}{2}\Big(A\exp(-k_a\ell_i^2) + B[1-\exp(-k_m(\ell_i+u_M))]^2 \\ &\quad + B[1-\exp(k_m(\ell_i-u_M))]^2 + C \Big) \end{aligned} \tag{2.26}$$

where k_m, k_a determine the curvatures of martensite and austenite wells. The depth and height of the austenite well is represented by A and B respectively. The

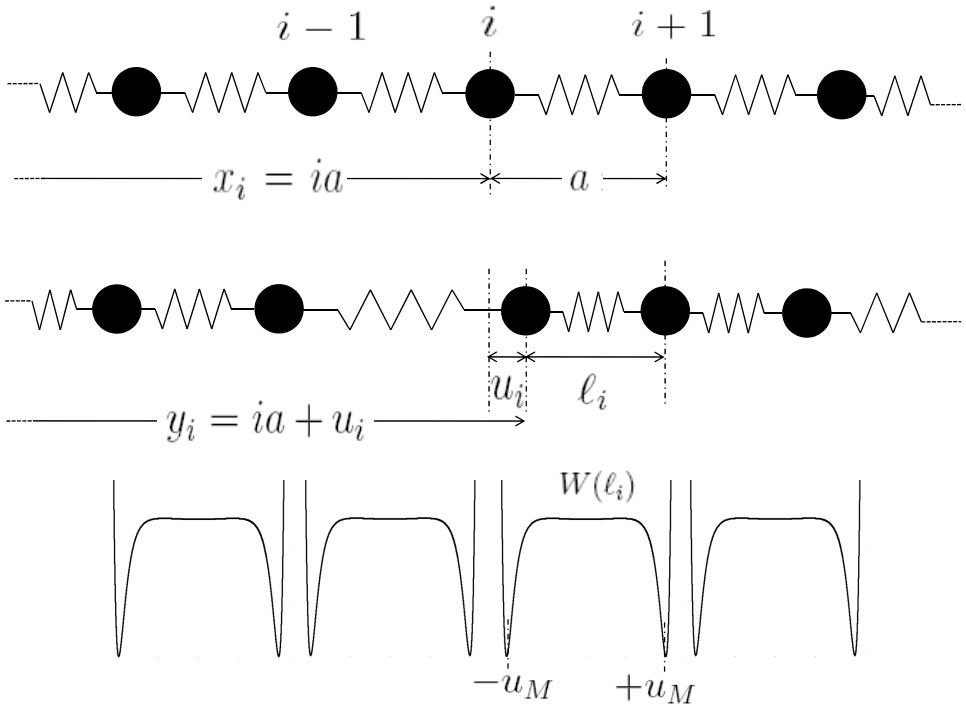

Figure 2.6: Chain of atoms with nearest-neighbor anharmonic interactions, x_i is the reference equilibrium positions of the atoms from a fixed origin, y_i is the current position of the atom from a fixed origin.

energy of martensite wells at $\ell_i = \pm 1$ set to be zero by C. A plot of potential $W(\ell_i)$ is shown in Fig. (2.7).

2.5.2 Interfacial energy

When adjacent unit cells (in our one-dimensional case, the bond lengths) in the material are in different phases or variants, the resulting interface has higher energy than if the cells were in the same phase. The term interfacial energy is used in the context of interaction between adjacent unit cells. When adjacent unit cells are in different variants, this energy provides the interfacial energy. When the adjacent cells are transforming between variants, this provides nearest neighbor (NN) interaction energy. We incorporate this interfacial energy through a simple

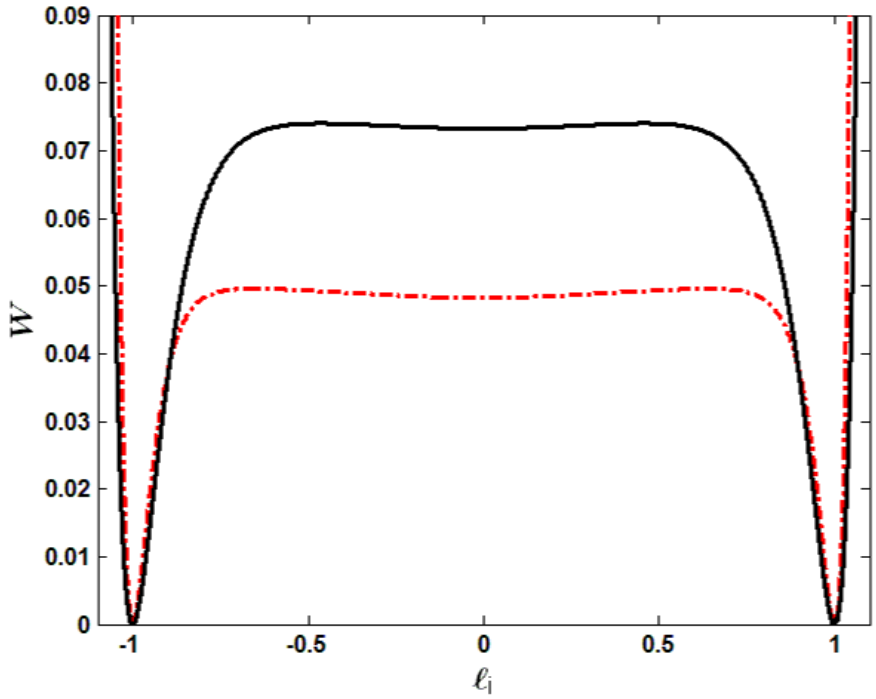

Figure 2.7: A plot of $W(\ell_i)$ for $k_m/k_a = 3, B = 0.15$ (solid line) and $k_m/k_a = 5, B = 0.1$ (dash-dot line). Depth of the austenite well $A = 0.0175$ for both the curves.

gradient energy of the form

$$W_g = \lambda \left(\frac{u_{i+1} - u_i}{2} - \frac{u_i - u_{i-1}}{2} \right)^2, \tag{2.27}$$

where λ is a gradient coefficient. This energy is motivated by harmonic strain-gradient energy terms in augmented continuum theories. The strain- gradient in our case arises from the difference between adjacent bond lengths. In non-dimensional form the gradient energy becomes

$$\bar{W}_g = \frac{\bar{\lambda}}{4} \left(\bar{u}_{i+1} - 2\bar{u}_i + \bar{u}_{i-1} \right)^2 \tag{2.28}$$

where $\bar{W}_g = 3W_g/Au_M^8$ and $\bar{\lambda} = 3\lambda/Au_M^6$.

2.5.3 Equations of motion

Let the masses of the particles in the chain be identical and equal to m. The Langevin equations [68] of motion

$$m\ddot{u}_i = -\frac{\partial W(\ell_i)}{\partial u_i} - \frac{\partial W(\ell_{i-1})}{\partial u_i} - \frac{\partial W_g}{\partial u_i} - \gamma \dot{u}_i + F_i(t), \tag{2.29}$$

Note that $\ell_i = u_{i+1} - u_i$ and $\ell_{i-1} = u_i - u_{i-1}$ are the "strains" of the i and $i-1$ bonds respectively. Letting $\bar{\gamma} = \gamma\sqrt{3m/Au_M^2}$ be a non-dimensionalized counterpart of the friction coefficient γ we obtain the non-dimensional Langevin equations

$$\bar{\ddot{u}}_i = -\frac{\partial \bar{W}(\ell_i)}{\partial \bar{u}_i} - \frac{\partial \bar{W}(\ell_{i-1})}{\partial \bar{u}_i} - \frac{\partial \bar{W}_g}{\partial \bar{u}_i} - \bar{\gamma}\bar{\dot{u}}_i + \bar{F}_i(t), \tag{2.30}$$

where $\bar{F}$ is a non-dimensional distributed Gaussian force whose magnitude is given by the fluctuation-dissipation theorem

$$< F_i(t_1) F_j(t_2) >= 2\gamma k_b(\theta + 1)\delta_{ij}\delta(t_1 - t_2). \tag{2.31}$$

where $k_b = k_B\theta_M\sqrt{Au_M^6 m/3}$ is a non-dimensional Boltzmann's constant.

2.6 Numerical simulations

2.6.1 Thermal cycle

We solve Eqs. (2.30) for a chain of $N = 1000$ atoms using the velocity Verlet algorithm [69] to discretize the equations. A detailed description of the Velocity Verlet algorithm is included in Appendix B. A non-dimensional time step $\Delta t = 10^{-3}$ is used. The non-dimensional friction coefficient is chosen to be $\gamma = 0.002$ based on trial simulations for a series of test systems and observing how well the system maintains the desired temperature. If γ is too high the flow of energy between the physical system and the reservoir is slow. If γ is too low, then the energy oscillates unphysically, causing equilibration problems. The atoms are given small initial random displacements about the equilibrium position and small random velocities. Averages are calculated over a time period of $\tau_{av} = 600$.

We study a thermal cycle of the system by cooling the chain from austenite phase followed by heating. During cooling, the target temperature is divided by a factor $r = 1.2$ and the system is allowed to equilibrate and averages are calculated. Heating is achieved by multiplying the target temperature by the same factor. The atoms at the boundaries are free (they only experience forces from the interior of the domain).

2.6.1.1 Zero interfacial energy

We first study the thermal cycle of the chain of atoms in the absence of interfacial energy by setting $\lambda = 0$. We have chosen a potential well with $k_m/k_a = 5, A = 0.00175, B = 0.1, C = 0.05$ as shown in Fig.2.7.

Figure 2.8(a) shows the bond length between a representative pair of atoms during the cooling and heating cycle. The bond length oscillates around 0 at high-temperature indicating austenite phase. As the temperature is lowered, the bond

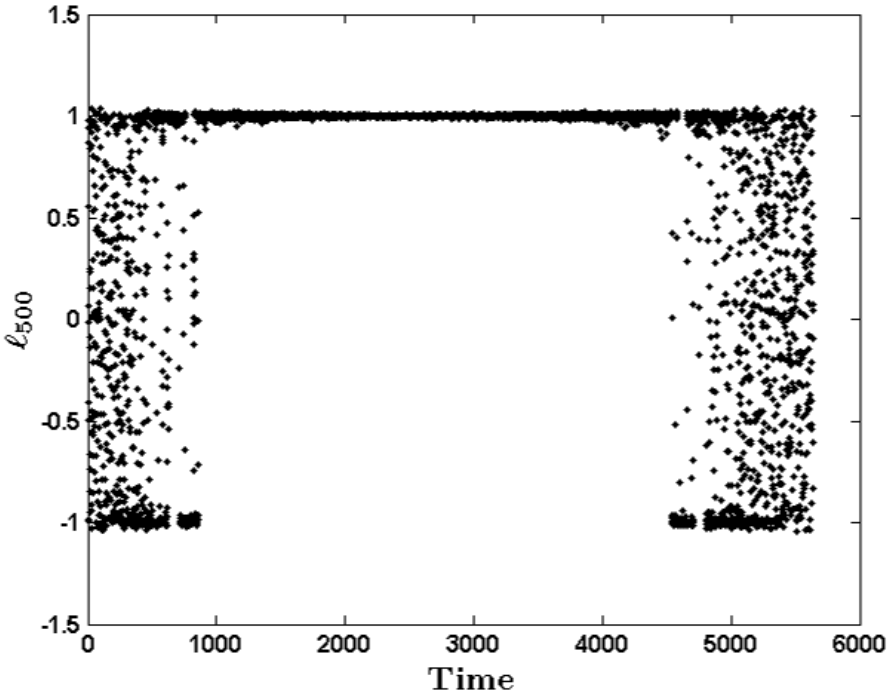

(a)

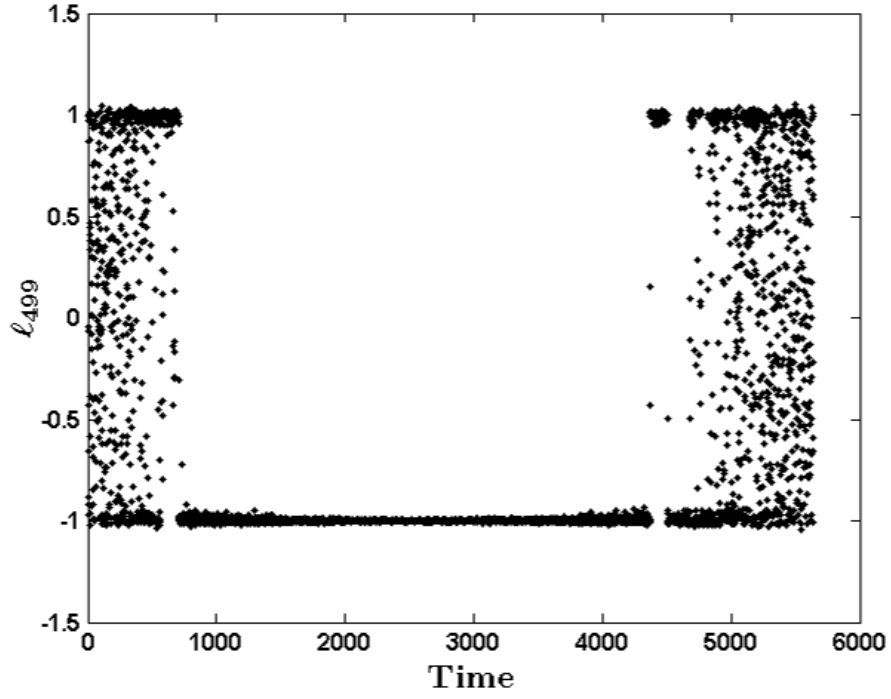

(b)

Figure 2.8: (a) The bond length ℓ_i between representative atoms 500 and 501 in the chain with time. (b) The bond length ℓ_i between atoms 499 and 500 in the chain with time.

length transforms to a value +1 which indicates M^- variant of the martensite phase. The two variants of martensite are energetically equivalent and the atoms can randomly transforms to any one of the variant, see in Figure 2.8(b) the bond length transforms to M^+ variant. At the end of martensite transformation, we plotted the random distribution of twins of M^+ and M^- variants in the middle of the chain from atom number 475 to 525, shown in Fig.2.9(a). The width of the twin is the size of regions of a single variant and the dotted line represent the twin boundaries. In this simulation with 1000 atoms the average twin width is 1.9 unit cells, fine twins formed due to absence of interfacial energy. As the temperature is increased the chain completely transforms to austenite.

The time average of the strain in the bonds in the chain of the atoms during cooling and heating cycle is shown in Fig. 2.9(b). The average positions of the atoms are initially close to 0 indicating the austenite phase. Once cooled, average position of the atoms randomly distributed either to +1 or −1 indicating martensite variants and further heating of the chain transforms all atoms to austenite phase. This is the origin of self-accommodation in these materials.

The transformation temperature of the system depends on the height of the austenite potential energy. The potential energy with the two barrier heights are shown in Fig.2.7. The plot of time averaged total energy $< E >$ with temperature is shown in Fig.2.10(a) for barrier height $B = 0.1$ and $B = 0.15$ by lines with circles and squares respectively, whereas the dashed and solid lines represent the cooling and heating cycle respectively. For a barrier height $B = 0.15$ the curve shifts towards right indicating a higher transformation temperature compared to $B = 0.1$. Due to the absence of the interfacial energy, the internal energy curve of the system during cooling and heating cycles for a certain barrier height does not show hysteresis.

The derivative of the internal energy with respect to temperature is the specific heat of the chain. Figure 2.10(b) shows a plot of the specific heat with temperature. The resulting plot shows the peaks representing the exothermic and endothermic

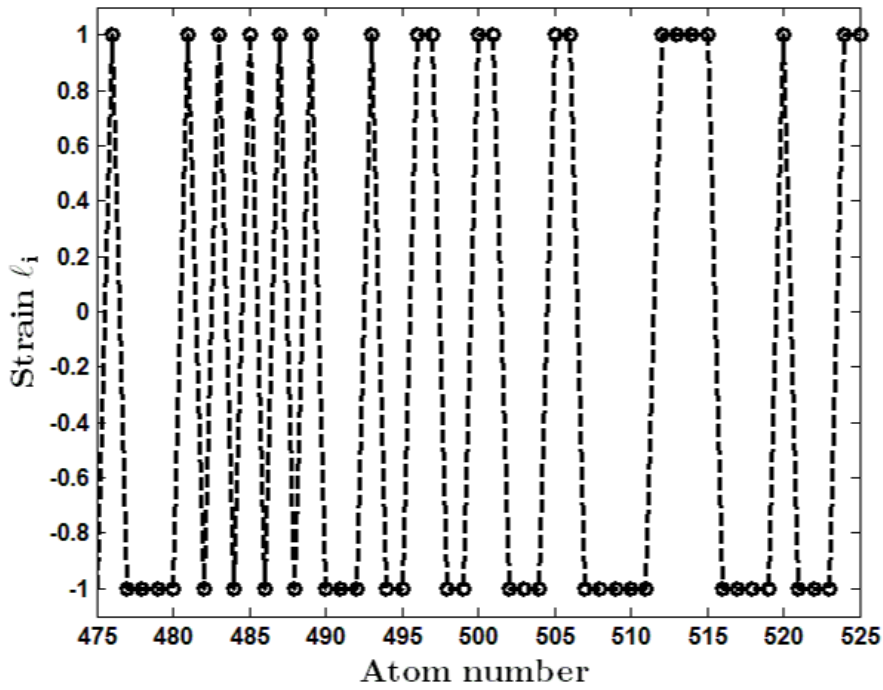

(a)

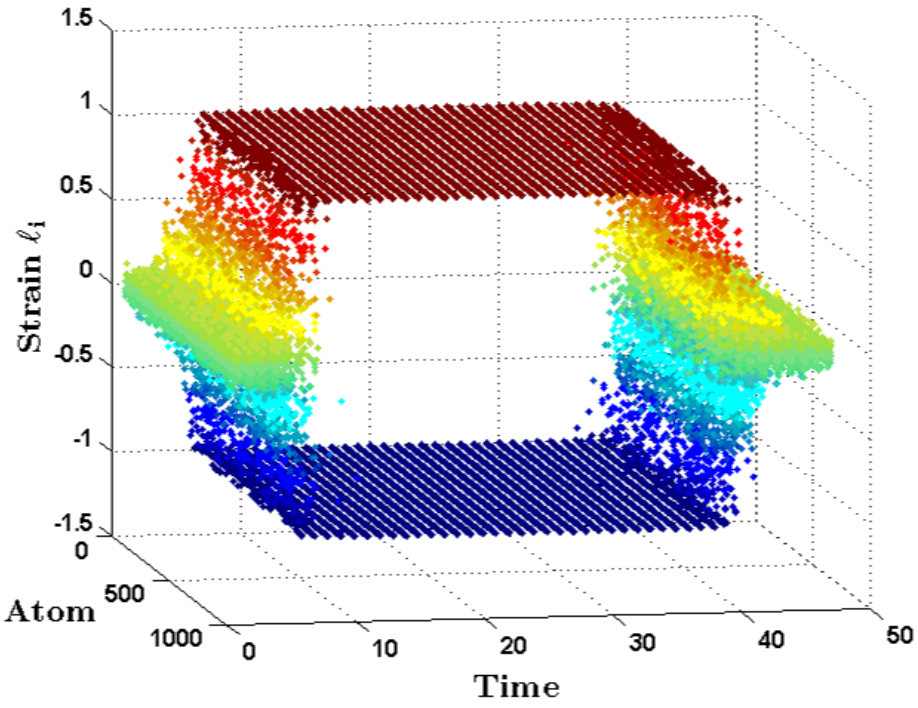

(b)

Figure 2.9: (a) Plot of strain along the middle of the chain at $\tau = 1800$ from atom number 475 to 525. The dotted line represent the twin boundaries. (b) Plot of strain along the chain with time.

processes during the austenite to martensite and martensite to austenite phase transformation respectively. The peaks shift towards right for $B = 0.15$ which represents the higher transformation temperature. This is a realistic representation of the differential scanning calorimetry (DSC) measurements of materials undergoing structural phase transitions, refer Shaw and Kryiakides [70] the experimental DSC thermogram for NiTi alloy.

2.6.1.2 Effect of interfacial energy

We choose a potential with $k_m/k_a = 3$, $A = 0.00175$, $B = 0.1$ and $\lambda = 0.2$ in the following simulations. In Fig. 2.11(a) and Fig. 2.11(b) we plot the average energy per atom with temperature in the absence and presence of interfacial energy, respectively. The presence of a finite interfacial energy increases dispersion of the energy of transformation through lattice vibrations and this contributes to the domain wall entropy, thereby enhancing hysteresis. Note that with zero interfacial energy, the heating and cooling cycles trace the same path.

Another significant feature of the interfacial energy is the formation of wider twins during cooling. In all the simulations, the two variants form in approximately equal amounts resulting in self-accommodation. However, the number of twin decreases with increasing gradient coefficient. In Fig. 2.12, we plot the strain along the middle of chain from atom number 475 to 525. The dotted lines represent the twin boundaries. In Fig. 2.12(a), for $\lambda = 0$ very fine twins are formed, whereas for $\lambda = 0.2$ some wider twins are also formed as shown in Fig. 2.12(b). Generally wider twins are formed near the boundaries of the chain. This is more clearly seen in the plot of the average twin width (Number of atoms/Number of interfaces) as a function of the gradient coefficient λ. In Fig. 2.13 the average twin width in the absence of interfacial energy is about 1.9 unit cells, whereas average twin width for $\lambda = 0.25$ is about 6.3 unit cells.

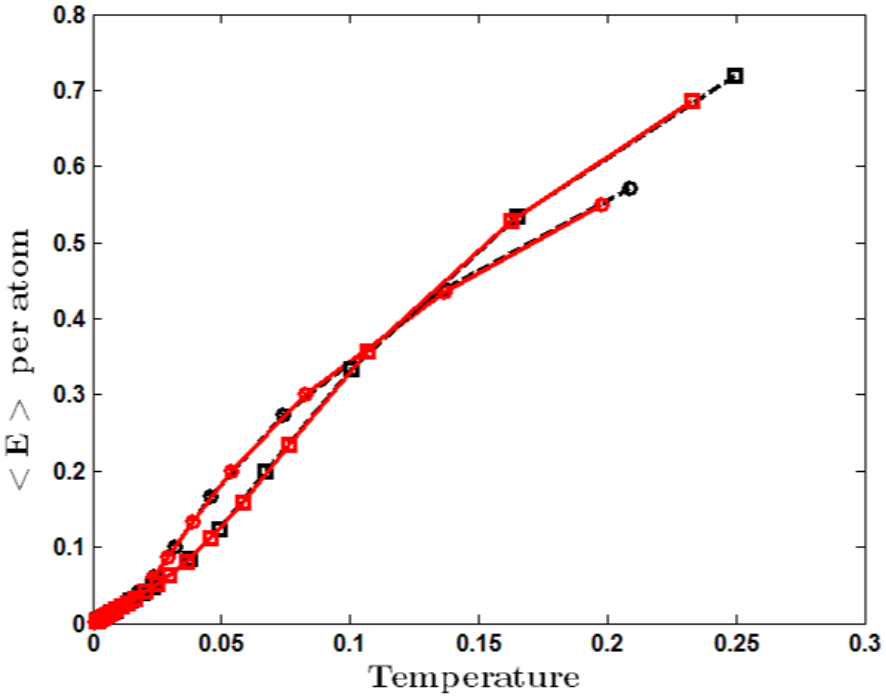

(a) Plot of the average total energy per atom with temperature

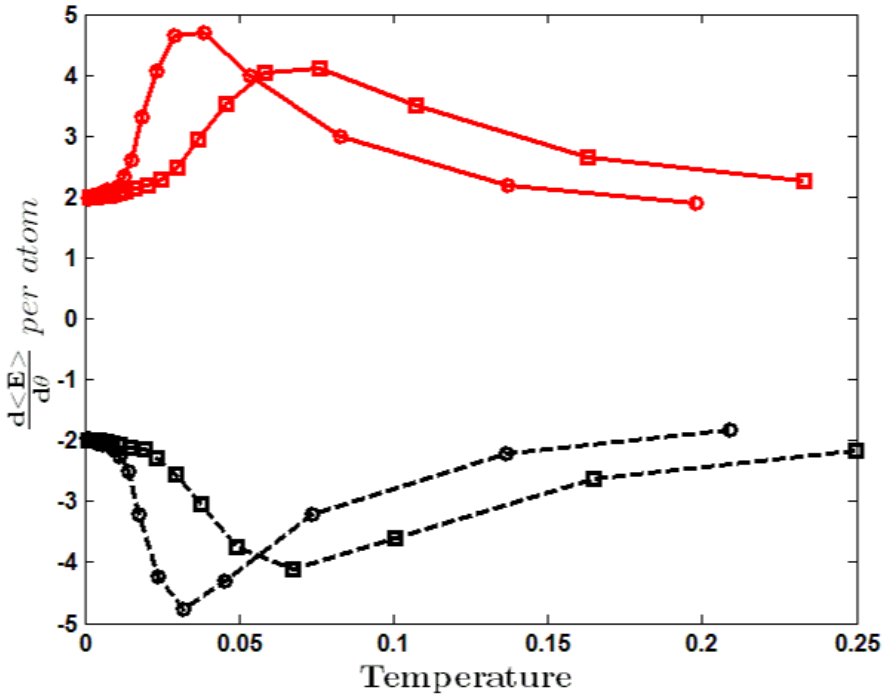

(b) Plot of the specific heat with temperature

Figure 2.10: Lines with circle represents barrier height $B = 0.1$ and lines with squares represents barrier height $B = 0.15$. The heating curve is shown using a solid line and cooling curve is shown using dashed line.

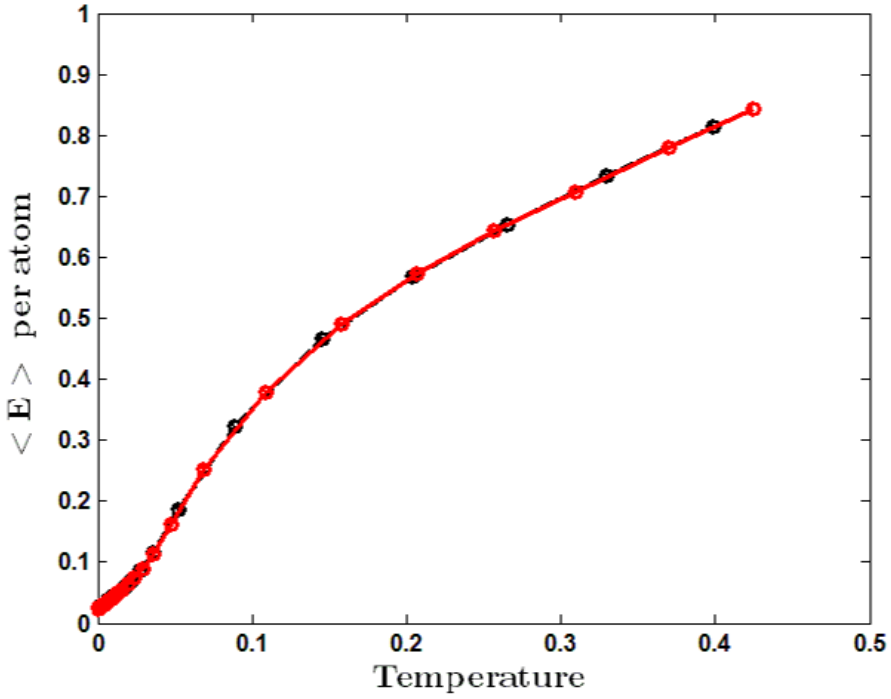

(a) $\lambda = 0$

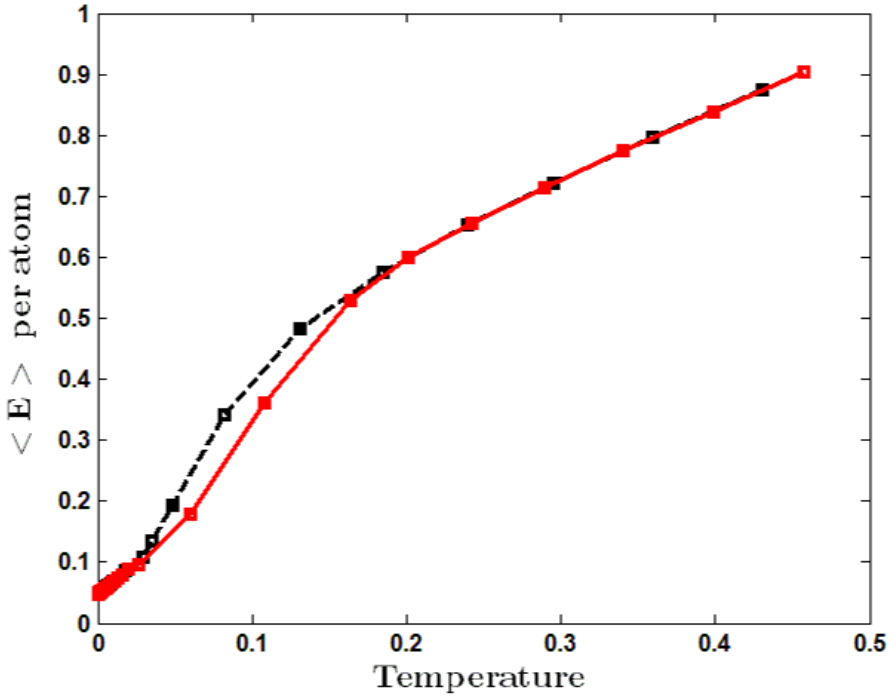

(b) $\lambda = 0.2$

Figure 2.11: Heating path is shown using solid line and the cooling path is shown using dashed line.

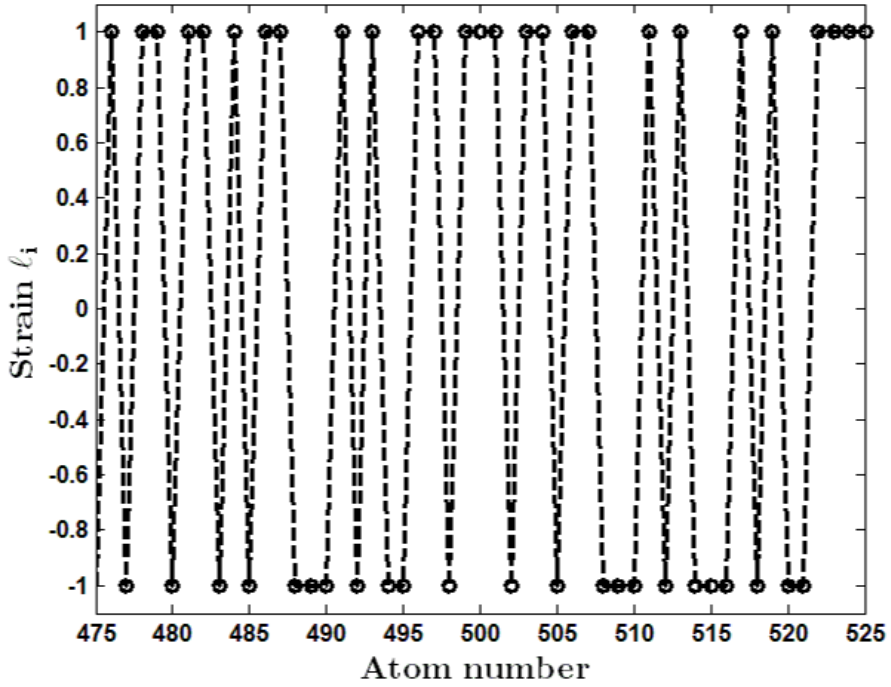

(a) $\lambda = 0$

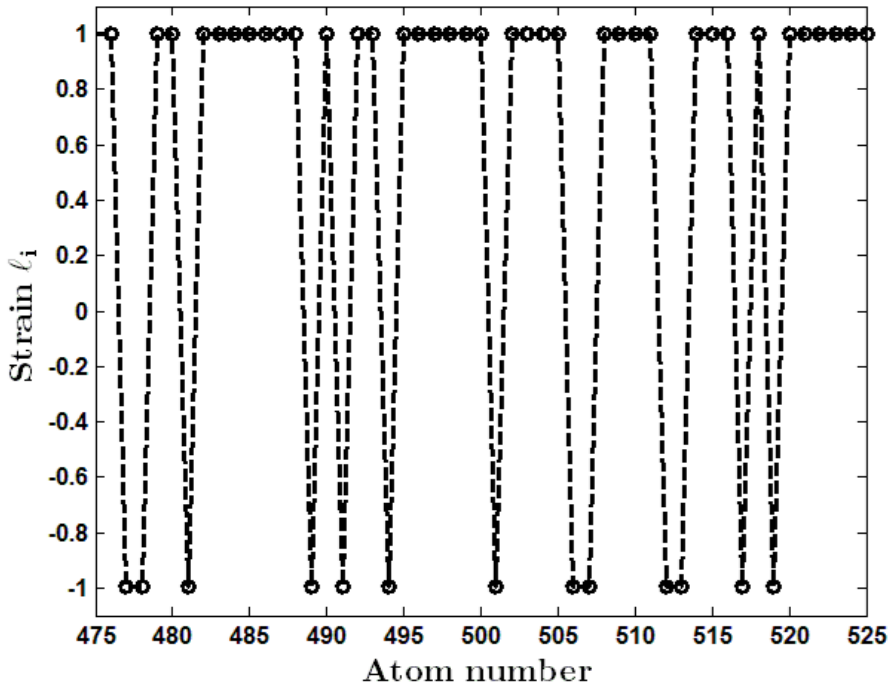

(b) $\lambda = 0.2$

Figure 2.12: Plot of strain along the chain from atom number 475 to 525 (a) in the absence of interfacial energy and (b) for finite interfacial energy. The dotted lines represent the twin boundaries. The width of the twins increases with λ.

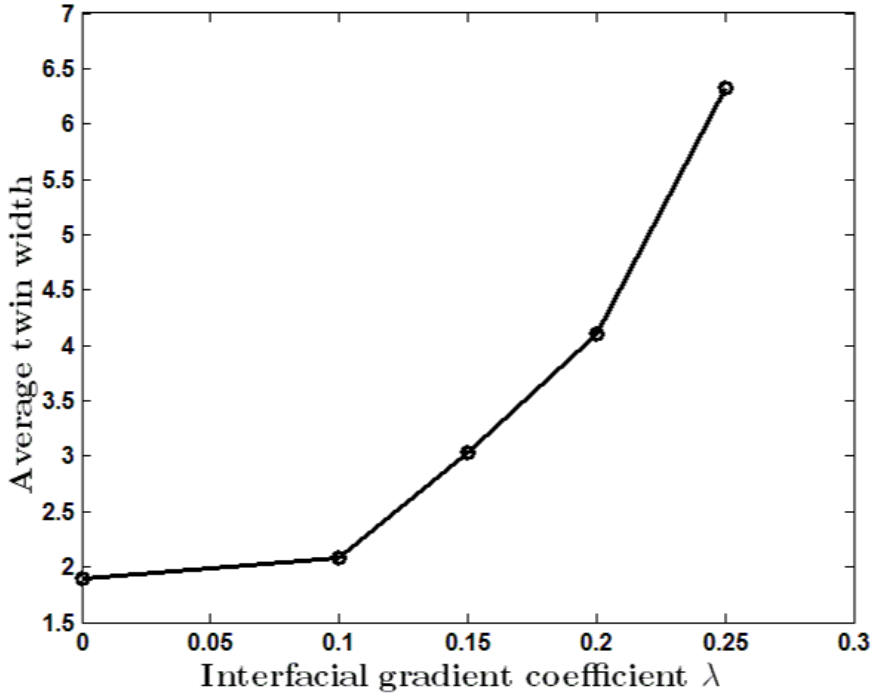

Figure 2.13: A plot of average twin width of the chain of 1000 atoms along with interfacial gradient coefficient λ.

2.6.2 Mechanical cycle

We study pseudoelasticity and the shape memory effect for a chain of $N = 1000$ atoms at a temperature well above and below the transformation temperature respectively. A force is applied to the both ends of the chain as shown in Fig. 2.14 and the system is allowed to equilibrate over a time period of $\tau_{av} = 600$. The cumulative strain of the chain due to the applied force is calculated at each step.

2.6.2.1 Pseudoelasticity

We start the simulation at a high-temperature austenite phase, incremental tensile force applied to the atoms at the either end of the chain. In Fig. 2.15(a) we plot the change in strain ℓ_i of each atom along with the time step. At time $t = 0$ the bond length of atoms oscillates around 0 indicating austenite phase. At each time step a incremental tensile force $f = 0.1$ applied as a result bond length of the atoms gradually moves towards the M^+ variant. At time $t = 20$ the

Figure 2.14: A force applied to the both ends of the chain

bond length of the atoms oscillates around +1 indicating the complete martensite phase transformation. Further loading the chain results in elastic deformation of martensite. Upon unloading the force, bond length of the atoms gradually moves back to austenite phase. At time $t = 68$ the bond length of atoms oscillates around 0 indicating the complete recovery of austenite phase.

In Fig. 2.15(b) we plot the cumulative strain of the chain during loading and unloading cycle. Hysteresis is observed during the pseudoelastic cycle.

2.6.2.2 Shape memory effect

We now study the detwinning and shape memory effect in the chain by loading and unloading at a low-temperature at which martensite is stable. In these simulations we have chosen a potential well with $k_m/k_a = 3$, $A = 0.00175$, $B = 0.15$ and interfacial energy $\lambda = 0.1$. In Fig. 2.16(a) we plot the change in strain ℓ_i of each atom along with the time step. We start the simulation at a high-temperature at which austenite is the stable phase and cool the system to produce twinned martensite, as shown at time $t = 12$ marked **b**. From this point the temperature of the chain is kept constant and a force is applied to the atoms at both ends of the chain. Now the atoms preferentially move in the direction of the applied force and transform to the M^+ variant as shown at the time $t = 20$ marked **d**; this is the detwinning process. Further loading results in the elastic deformation of M^+ variant from time $t = 20$ to $t = 30$ (**d** to **e**). From point **e** the chain is unloaded and all the atoms remain in the M^+ variant (**f**). This results in a residual strain. Upon heating, the chain completely transforms to austenite as shown by point **g**. Residual strain is completely recovered by this heating cycle. Further cooling results in the twinned martensite and this process is the shape memory effect.

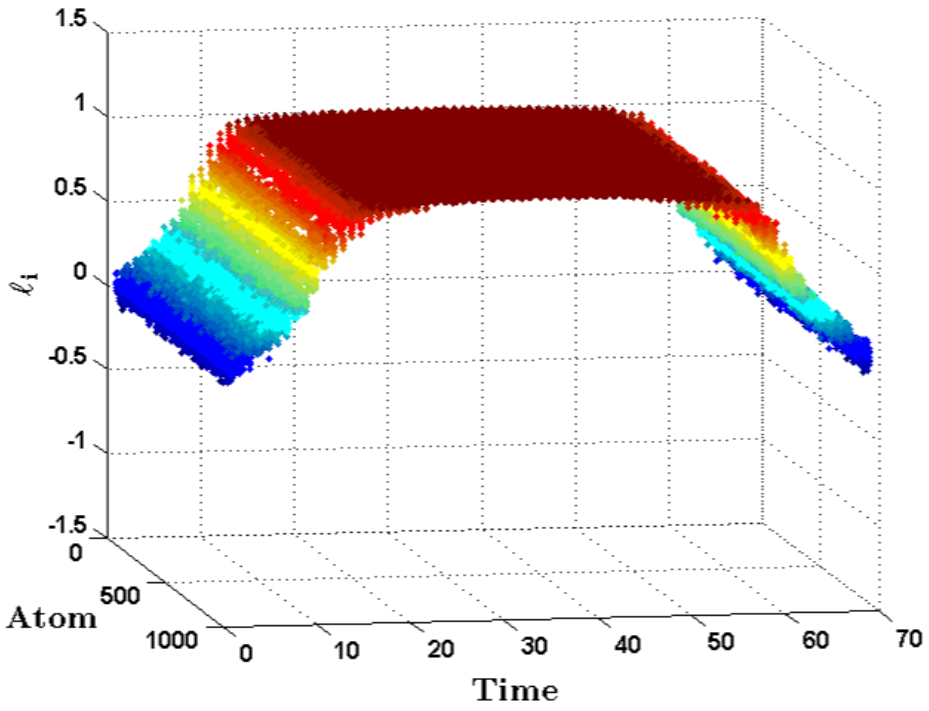

(a)

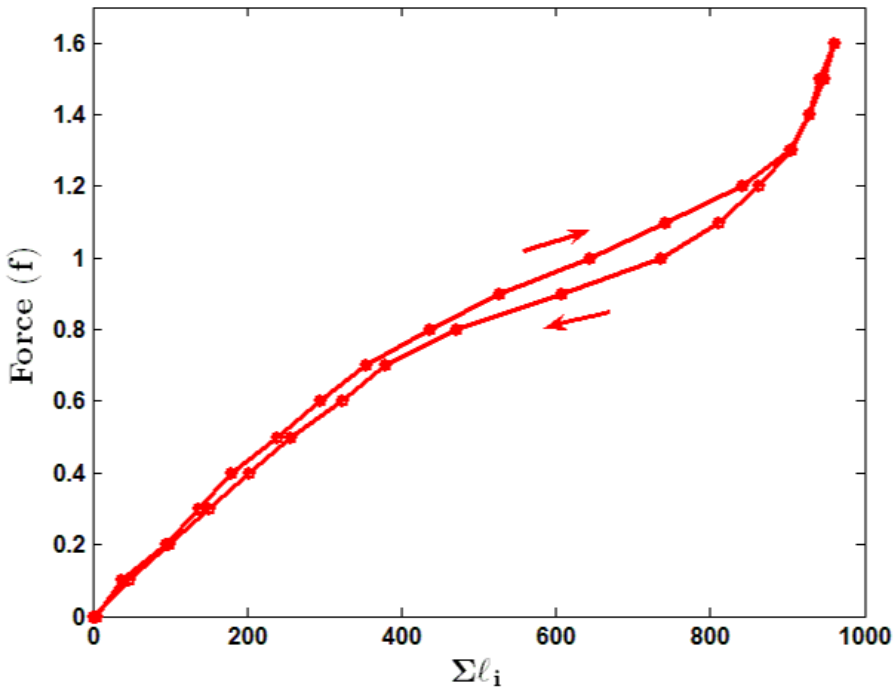

(b)

Figure 2.15: (a) Plot of the strain of each atom in the chain during the simulation cycle. (b) Plot of applied force vs. length of the chain during the simulation cycle.

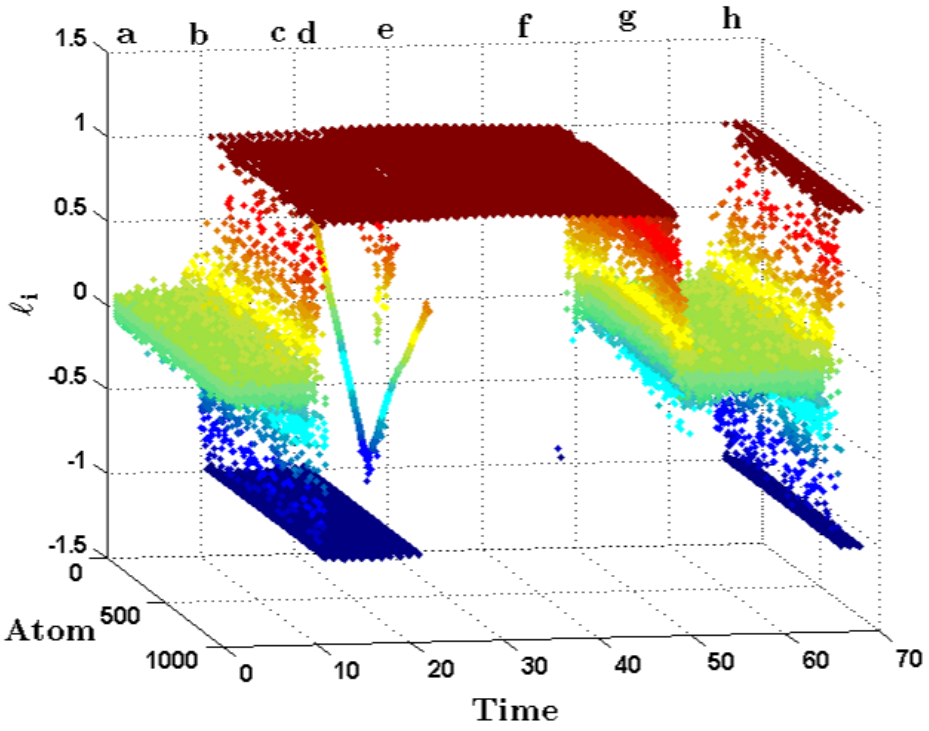

(a)

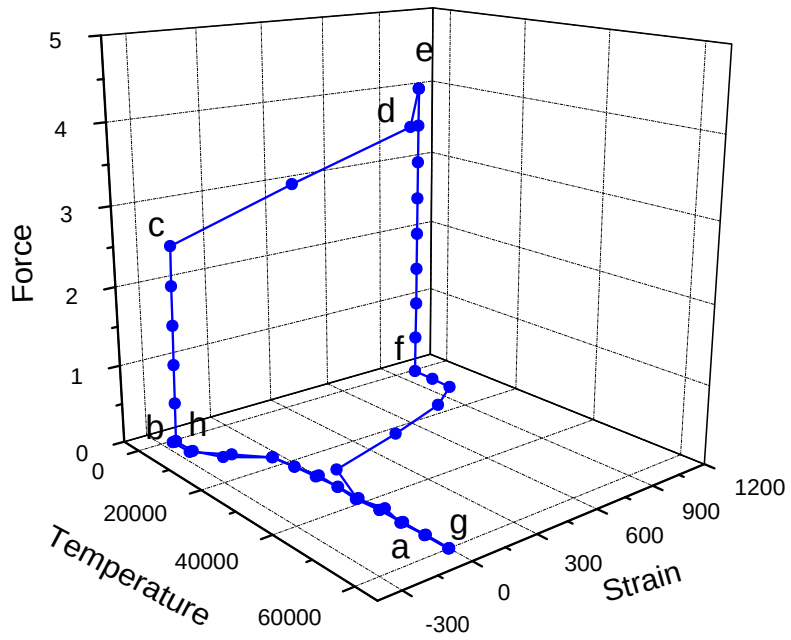

(b)

Figure 2.16: (a) Plot of the strain of each atom in the chain during shape memory effect simulation cycle. (b) Plot of cumulative strain of the chain during shape memory effect simulation cycle.

In Fig. 2.16(b) we plot the respective cumulative strain $\Sigma\ell_i$ of the chain for the shape memory effect simulation cycle. During $\mathbf{a}-\mathbf{b}$, austenite transforms to twinned martensite upon cooling the chain. During $\mathbf{b}-\mathbf{c}-\mathbf{d}$, the applied force at constant temperature causes detwinning. During $\mathbf{d}-\mathbf{e}$, the martensite phase deforms elastically. During $\mathbf{e}-\mathbf{f}$, the unloading cycle resutls in a residual strain (point $\mathbf{f}$). During $\mathbf{f}-\mathbf{g}$, the M^+ variant of martensite transforms to austenite upon heating the chain. Finally, during $\mathbf{g}-\mathbf{h}$, twinned martensite is obtained upon cooling the chain. This is a realistic representation of the shape memory effect, refer [71] the experimental stress-strain-temperature response for NiTi alloy.

2.7 Summary

- Identified physical mechanism for phase transformation in a discrete setting.
- A parameterization of the potential energy indicates the properties required for entropy-driven phase transformation.
- Austenite well need to be softer compared to martensite well.

Chapter 3

Temperature dependent substrate potential

3.1 Introduction

In the previous chapter we proposed a parametrization of the total potential energy of a discrete system to obtain a phase transforming mode and showed that particular properties of the parametrization allow vibrational entropy induced structural phase transitions. This calculation does not directly address the particular form of the individual empirical interatomic potentials to be chosen — only that the parametric slice of the PTM must have certain properties which can be related to the phase transformation. Thus this is only an indirect characterization of the actual interatomic potential.

In this chapter we present a more direct empirical model of the interatomic potential. Our motivation for this model is as follows: consider a single atom in a material capable of undergoing phase transformations. At finite temperature, the atom vibrates with a finite amplitude as do all its surrounding atoms. Calculation of the motion of the atom under consideration is a many-body problem which is extremely difficult to solve. Instead, we take the mean field approach and view the average effect of the surrounding atoms as providing a *substrate potential well* for

the atom[1]. In fact we assume that this substrate potential is harmonic with the minimum about the equilibrium position. When the material undergoes a phase transformation, the atom now vibrates about a new equilibrium position as do its neighbors. Presumably the substrate energy of the atom is now different as is the location of its minimum. We will again assume a harmonic energy with the minimum about the new equilibrium positions in each variant. At high-temperature, the well corresponding to the austenite has lower energy than the wells corresponding to martensite. Conversely, at low-temperatures, the martensite wells have lower energy than the austenite well.

Thus the empirical model that we consider is that of a *temperature dependent* interaction between atoms providing the potential energy for the atoms. In molecular dynamics approaches the interatomic potential is not considered to be dependent on temperature (which is a macroscopic quantity). We view this as a constitutive model for the discrete system for describing temperature dependent phenomena. With this approach, the continuum free energy can be used conveniently to describe the discrete system.

Note that if the interatomic potential is made temperature dependent, the kinetic energy implicitly enters the potential energy calculation and explicitly in the kinetic energy calculation in a MD simulation. Using statistical mechanics calculations, in this chapter we clarify the effect of this possibility for a temperature dependent interatomic potential.

3.2 Single oscillator model

3.2.1 Substrate potential

In the model envisaged here, temperature is manifested in the vibration of a single atom as well as in the potential substrate energy due to the surrounding atoms.

[1]Such an approach is taken in basic statistical mechanics calculations of the high-temperature specific heat of solids. The resulting value of the specific heat with an assumption of a harmonic substrate potential is in very good accord with experimental data of Dulong and Petit [65].

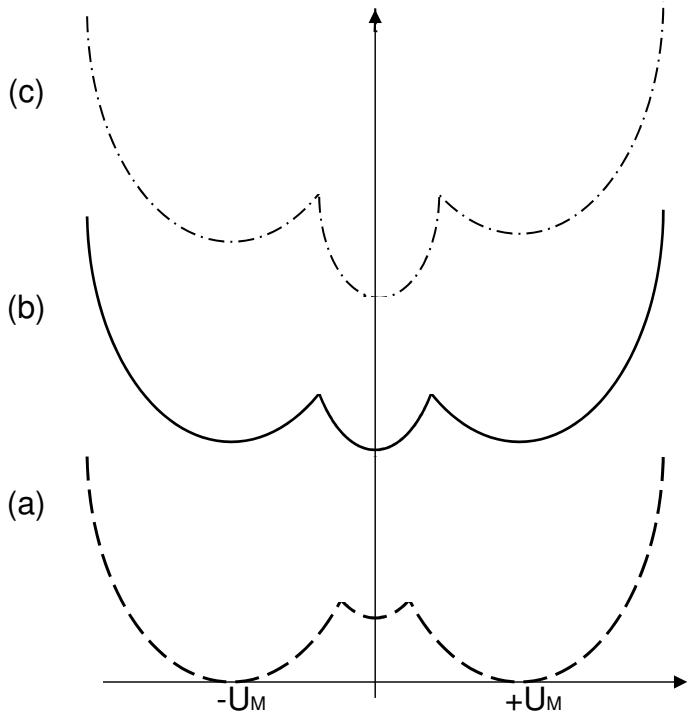

Figure 3.1: Plot of the substrate potential versus atom position for different temperatures: (a) $\Theta < \Theta_t$, (b) $\Theta = \Theta_t$ and (c) $\Theta > \Theta_t$.

This is in contrast to the classical molecular dynamics viewpoint in which the interatomic potentials are independent of temperature.

We begin by considering a single particle of mass M. Let X represent the reference position of the atom and Y, the current position. The displacement is $U = Y - X$. Denoting the absolute temperature by Θ, we assume that the particle experiences a substrate potential (mean effect of all of its neighbors) $W(U, \Theta)$ with the above properties (shown in Fig. 3.1 for three different representative temperatures). The central minimum at $U = 0$ represents austenite and the side wells at $U = \pm U_M$, the two variants of martensite equilibrium positions. As mentioned earlier, the two martensite wells have equal energies at all temperatures since the two variants are symmetry related to each other [72]. We neglect the change in lattice spacing with temperature.

A piecewise harmonic substrate potential energy with the above properties is

given by

$$W(U,\Theta) = \begin{cases} \frac{1}{2}\mu_m(U+U_M)^2 + H_m\Theta, & U \le -U_T, \\ \frac{1}{2}\mu_a U^2 + H_a(\Theta+\Theta_o), & -U_T \le U \le U_T, \\ \frac{1}{2}\mu_m(U-U_M)^2 + H_m\Theta, & U \ge U_T. \end{cases} \tag{3.1}$$

where U_T is the intersection of the austenite and martensite energies, μ_a and μ_m are the elastic moduli of austenite and martensite phase respectively. $H_a\Theta_o$ is the energy of austenite phase at absolute zero temperature. For transition to occur we require that $H_a < H_m$. The transition temperature Θ_t is related to Θ_o through

$$\Theta_t = \frac{H_a\Theta_o}{H_m - H_a}. \tag{3.2}$$

For convenience, we consider the following non-dimensionalization

$$u = \frac{U}{a},\ u_M = \frac{U_M}{a},\ u_T = \frac{U_T}{a},\ w = \frac{W}{\mu_a a^2},\ \theta = \frac{\Theta}{\Theta_t},\ h_m = \frac{H_m\Theta_t}{\mu_a a^2},\ h_a = \frac{H_a\Theta_t}{\mu_a a^2}, \tag{3.3}$$

where a is a lattice constant of the material. Then u is the "strain" and u_M is the "transformation strain". In non-dimensional form, the substrate potential is given by

$$w(u,\theta) = \begin{cases} \frac{1}{2}\mu(u+u_M)^2 + h_m\theta, & u \le -u_T, \\ \frac{1}{2}u^2 + h_a(\theta+\vartheta), & -u_T \le u \le u_T, \\ \frac{1}{2}\mu(u-u_M)^2 + h_m\theta, & u \ge u_T, \end{cases} \tag{3.4}$$

where we have set $\mu = \mu_m/\mu_a$ and $\vartheta = (h_m - h_a)/h_a$ and used Eq. (3.2) to eliminate θ_o. The point of intersection of the austenite and martensite wells u_T is temperature dependent and given by

$$u_T(\theta) = \frac{\sqrt{\mu^2 u_M^2 + (1-\mu)(\mu u_M^2 + 2\vartheta h_a(\theta-1))} - \mu u_M}{1-\mu}, \tag{3.5}$$

where we have chosen the positive root. Note that $0 \leq u_T \leq u_M$.

3.2.2 Motion of an atom in the substrate potential

We now study the motion of an atom under the influence of the above substrate potential. Nondimensionalizing time T using the frequency of oscillations in the austenite well: $t = T\sqrt{\mu_a/M}$, the equation of motion of the atom is

$$\ddot{u} = \begin{cases} -\mu(u + u_M), & u \leq -u_T, \\ -u, & -u_T \leq u \leq u_T, \\ -\mu(u - u_M), & u \geq u_T \end{cases} \tag{3.6}$$

where the superimposed dot represents differentiation with respect to the non-dimensional time t.

Consider the following thought experiment. Let the atom start from a state of rest at the bottom of one of the martensite wells at absolute zero temperature. As the temperature is gradually increased, the average kinetic energy of the atom increases. Solving Eq. (3.6) for an atom in, say, the right martensite well we obtain

$$u(t) = u_M + \frac{v_m}{\sqrt{\mu}} \sin \sqrt{\mu} t, \tag{3.7}$$

where v_m is the maximum speed of the atom (attained at $u = u_M$). The average kinetic energy of the atom is $< K >= \frac{1}{4} v_m^2$. From statistical mechanics we know that the average kinetic energy equals $\frac{1}{2} k_B \Theta$ where k_B is the Boltzmann's constant. Thus the temperature of the system when the atom is localized in the martensite well is given by

$$\theta = \frac{v_m^2}{2k_b} \tag{3.8}$$

where we have set $k_b = k_B\theta_T/(\mu_a a^2)$. Thus we can rewrite Eq. (3.7) as

$$u(t) = u_M + \sqrt{\frac{2k_b\theta}{\mu}}\sin\sqrt{\mu}(t - t_m) \tag{3.9}$$

where t_m is a time at which the atom is at the bottom of the martensite well.

Similarly, after transformation, the atom is localized in the austenite well and its motion can be described by

$$u(t) = \sqrt{2k_b\theta}\sin(t - t_a) \tag{3.10}$$

where t_a is a time at which the atom is at the bottom of the austenite well.

3.2.3 Transformation temperatures and specific heat of pure phases

At very low-temperatures, the austenite well is above the martensite wells and may be considered to be unstable. The temperature at which austenite well begins to become metastable (*austenite start temperature*) can be calculated using the condition $u_T(\theta_{as}) = 0$. The austenite start temperature is thus given by

$$\theta_{as} = 1 - \frac{\mu u_M^2}{2\vartheta h_a}. \tag{3.11}$$

The temperature above which the martensite wells are unstable is given by the condition $u_T(\theta_{af}) = u_M$ which by using Eq. (3.5) gives

$$\theta_{af} = 1 + \frac{u_M^2}{2\vartheta h_a}. \tag{3.12}$$

The calculation of the specific heat in the pure phases is straightforward. Since the average energy at temperature θ in our model is given by $k_b\theta + h_m\theta$ (contributions of $k_b\theta/2$ from the average potential and kinetic energies), the specific heat

of the martensite phase (below the transformation start temperature) is given by

$$c_m = k_b + h_m. \tag{3.13}$$

Similarly the specific heat in the austenite phase (above transformation finish temperature) is given by

$$c_a = k_b + h_a. \tag{3.14}$$

3.3 Statistical mechanics of N uncoupled oscillators

The calculations presented in the last section are for a single oscillator. In reality, there are N atoms moving at different velocities following the Maxwell distribution. In a *canonical NVT ensemble*, the probability distribution of the microscopic quantities is weighted by the factor $\exp(-\beta h)$ where $\beta = 1/k_b\theta$ and h is the Hamiltonian of the system.

In our case, the non-dimensional Hamiltonian is temperature dependent and given by

$$h = w(u, \theta) + \frac{1}{2}\dot{u}^2, \tag{3.15}$$

with w specified by Eq. (3.4).

The one-dimensional single particle partition function $\mathcal{Z}$ is given by

$$\mathcal{Z} = \int_{-\infty}^{\infty}\int_{-\infty}^{\infty} \exp(-\beta h)\mathrm{d}u\,\mathrm{d}\dot{u} \tag{3.16}$$

which can be factored as $\mathcal{Z} = \mathcal{Z}_u\mathcal{Z}_{\dot{u}}$ where $\mathcal{Z}_{\dot{u}}$ is the one-dimensional kinetic energy contribution and can be easily evaluated to be

$$\mathcal{Z}_{\dot{u}} = \int_{-\infty}^{\infty} \exp(-\beta\frac{1}{2}\dot{u}^2)\mathrm{d}\dot{u} = \sqrt{2k_b\pi\theta}. \tag{3.17}$$

The one-dimensional potential energy contribution $\mathcal{Z}_u$ is given by

$$\mathcal{Z}_u = \int_{-\infty}^{\infty} \exp(-w/k_b\theta)\mathrm{d}u. \tag{3.18}$$

Using Eq. (3.4) the potential energy contribution to the partition function is given by

$$\begin{aligned}\mathcal{Z}_u &= \int_{-\infty}^{-u_T} \exp\left(-\frac{(\mu(u+u_M)^2/2 + h_m\theta)}{k_b\theta}\right)\mathrm{d}u \\ &\quad + \int_{-u_T}^{u_T} \exp\left(-\frac{(u^2/2 + h_a(\theta+\vartheta))}{k_b\theta}\right)\mathrm{d}u \\ &\quad + \int_{u_T}^{\infty} \exp\left(-\frac{(\mu(u-u_M)^2/2 + h_m\theta)}{k_b\theta}\right)\mathrm{d}u\end{aligned} \tag{3.19}$$

The integrals can be evaluated in terms of the error function and thus $\mathcal{Z}_u$ can be written explicitly as

$$\begin{aligned}\mathcal{Z}_u &= \sqrt{2k_b\pi\theta}\left\{\exp\left(-\frac{h_a(\theta+\vartheta)}{k_b\theta}\right)\mathrm{erf}\left(\frac{u_T}{\sqrt{2k_b\pi\theta}}\right)\right. \\ &\quad \left. + \frac{1}{\sqrt{\mu}}\exp\left(-\frac{h_m}{k_b}\right)\left[1 + \mathrm{erf}\left(\sqrt{\frac{\mu}{2k_b\pi\theta}}(u_M - u_T)\right)\right]\right\}\end{aligned} \tag{3.20}$$

From the partition function, we can calculate the thermodynamics functions of interest. Specifically, the Helmholtz free energy per atom is given by

$$\begin{aligned}F &= -k_b\theta\ln\mathcal{Z} \\ &= -k_b\theta\ln(2k_b\pi\theta) - k_b\theta\ln\left\{\exp\left(-\frac{h_a(\theta+\vartheta)}{k_b\theta}\right)\mathrm{erf}\left(\frac{u_T}{\sqrt{2k_b\pi\theta}}\right)\right. \\ &\quad \left. + \frac{1}{\sqrt{\mu}}\exp\left(-\frac{h_m}{k_b}\right)\left[1 + \mathrm{erf}\left(\sqrt{\frac{\mu}{2k_b\pi\theta}}(u_M - u_T)\right)\right]\right\}\end{aligned} \tag{3.21}$$

The first term of the right is the standard contribution due to the harmonic potential whereas the second term is the contribution reflecting the exchange of stability of the phases. The Helmholtz free energy is plotted in Fig. 3.2(a) for some representative values of the constants, $\mu = 0.4$, $h_a = 5$, $h_m = 35$, $k_b = 5$ and $u_M = 10$. Notice a sharp change in the slope of the curve around the phase

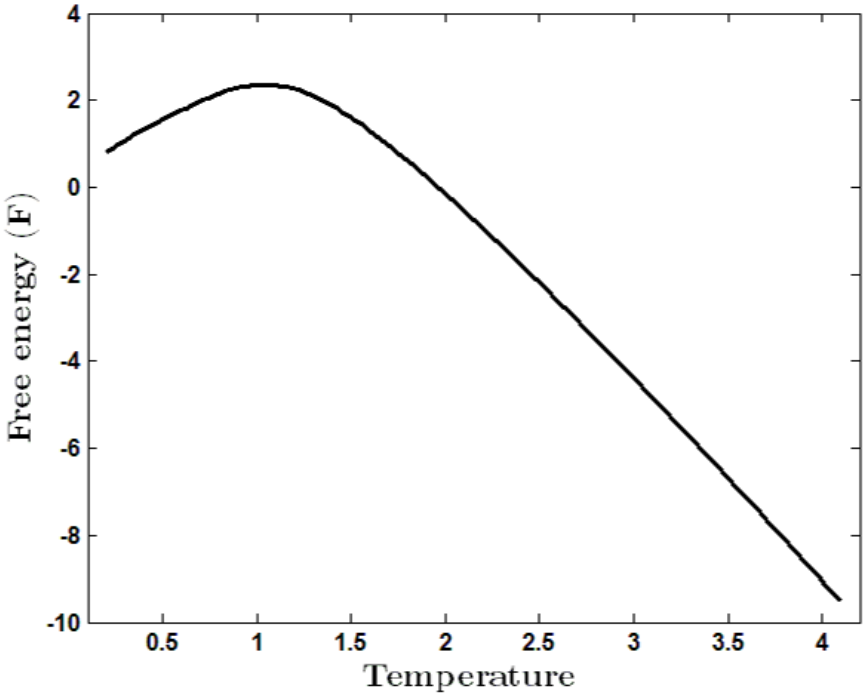

(a)

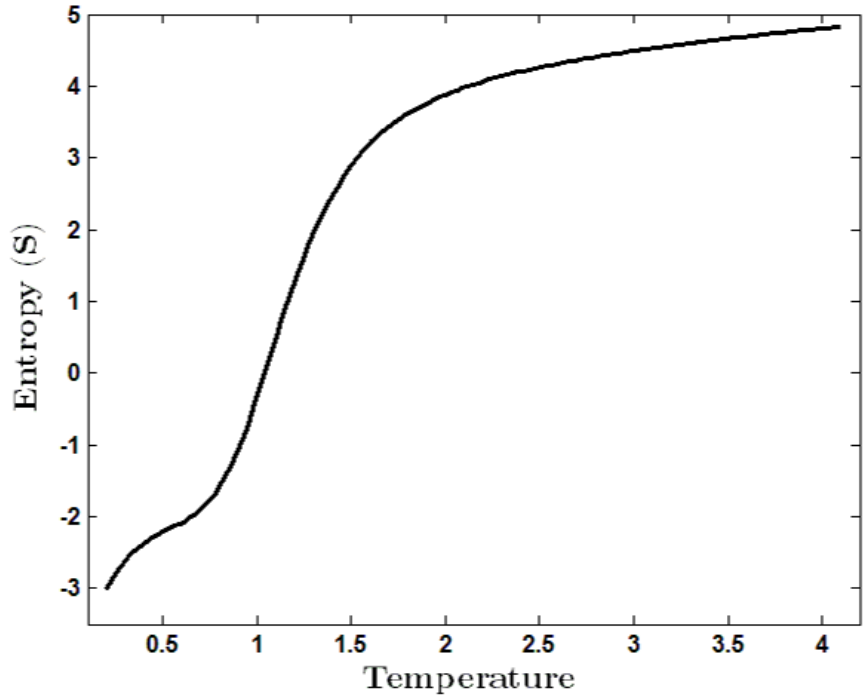

(b)

Figure 3.2: (a) Free energy as a function of temperature. (b) Entropy as a function of temperature.

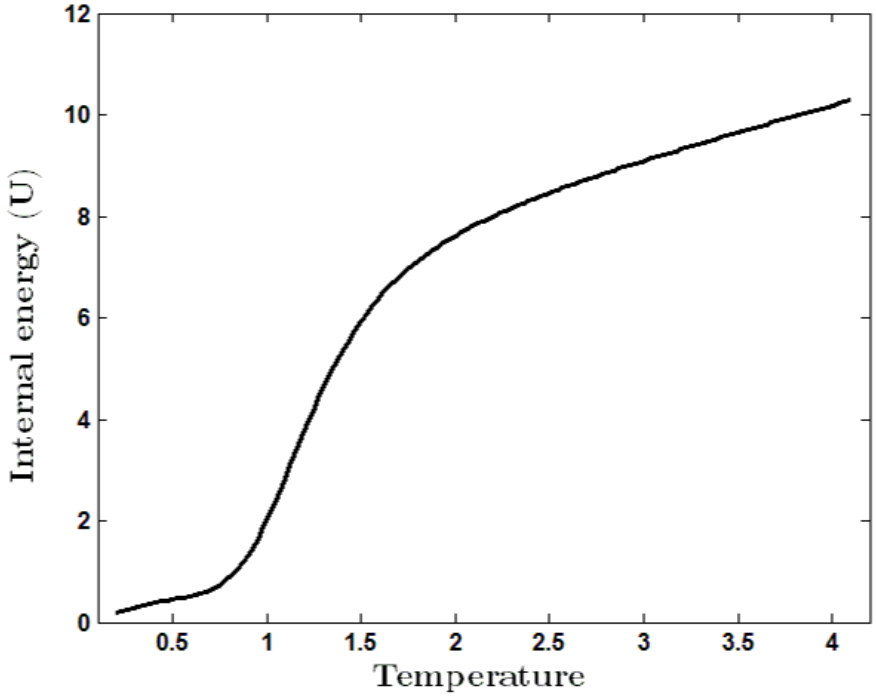

(a)

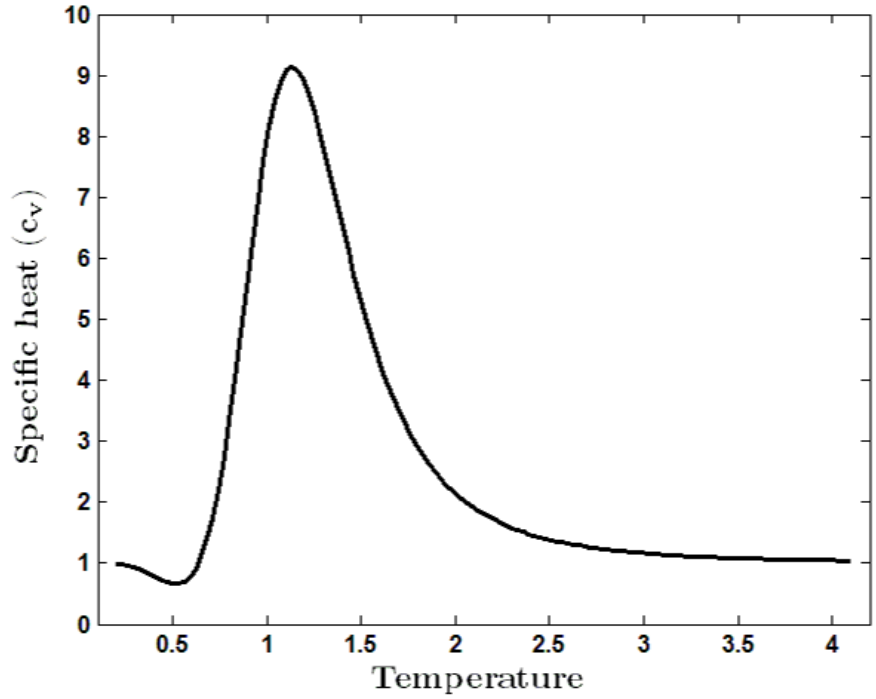

(b)

Figure 3.3: (a) Internal energy as a function of temperature. (b) Specific heat as a function of temperature.

transformation temperature θ_T. The entropy per atom is obtained by

$$S = -\frac{\partial F}{\partial \theta} \tag{3.22}$$

and the internal energy per atom is given by

$$U = F + \theta S. \tag{3.23}$$

The specific heat capacity at constant volume per atom is given by

$$c_V = \frac{\partial U}{\partial \theta}. \tag{3.24}$$

In Fig. 3.2(b) we plot the entropy as a function of temperature. Entropy is constant at low-temperature and at high-temperature, whereas during transformation undergoes a step change indicating the entropy-driven phase transformation.

In Fig. 3.3(a) and Fig. 3.3(b) we plot the internal energy and specific heat respectively. The spike in the specific heat curve indicates the first-order phase transformation and the area under the spike represents the latent heat of the system.

3.4 Summary

The statistical mechanics calculations of the uncoupled oscillators show the role of the temperature dependent parameters in the interatomic potential in the free energy and the specific heats. No contradiction in using temperature dependent potential energy. It is thus possible to interpret the thermodynamic variables in terms of these constitutive parameters.

Chapter 4

Temperature dependent interatomic potential

4.1 Introduction

In the previous chapter we studied the role of a temperature dependent *substrate potential* in a phase transforming material from a statistical mechanical viewpoint. In this chapter we numerically study a chain of coupled oscillators. We do not consider a substrate potential but instead consider temperature dependent nearest-neighbor interactions of the form described in the previous chapter.

In this chapter, we take the latter approach of temperature dependent potentials, but from a different standpoint. Suttan [73] discusses temperature dependent interatomic potentials in detail. The pair potentials in [62, 63] are temperature dependent Lennard-Jones type single well potentials in a multicomponent system. In contrast, we choose a single component system but allow the (nearest-neighbor) interatomic potential to have multiple temperature dependent wells. In a material undergoing a phase transition, the surrounding atoms have different configurations depending on the temperature. Thus an atom under consideration has multiple equilibrium bond lengths relative to its nearest-neighbor atoms corresponding to the lattice constants of the parent and product phases. The configuration of the

surrounding atoms (which depends on temperature) changes the energy of the interaction potential and the location of its minimum. In the previous chapter we studied the effect of an anharmonic temperature dependent *substrate potential* and derive the transformation temperatures and latent heat as a function of the substrate properties. In this paper we use a polynomial Falk-type free energy [74], which is a polynomial expansion of a single strain component, to describe the interaction potential. In the discrete setting here we assume the interaction potential to be a function of the distance between nearest-neighbor pairs of atoms. We restrict our studies in this work to a one-dimensional chain of identical atoms. An additional feature of our model is a gradient energy to penalize the presence of phase boundaries.

In Section 4.2 we describe the features of the interaction potential required to obtain stability of the various phases at different temperatures. We also describe the gradient energy which is a chosen to be a simple quadratic form. The temperature of the system is controlled using a Nosé-Hoover thermostat [75, 76] and the resulting equations of motion are presented. Next, in Section 4.3 we study the model under different loading and unloading conditions and the effect of the interatomic potential on the thermodynamic properties of the material. The model reproduces realistic hysteresis as well as specific heat dependence on temperature. Finally, in Section 4.3.2 we study mechanical loading of the chain and present pseudoelasticity and shape memory effects in this system.

4.2 Model

In this section we describe the interaction potential and gradient energy and obtain the equations of motion of atoms in a one-dimensional chain. Our interatomic potential is motivated by the same considerations as the free energy derived in continuum theories (e.g., [74]).

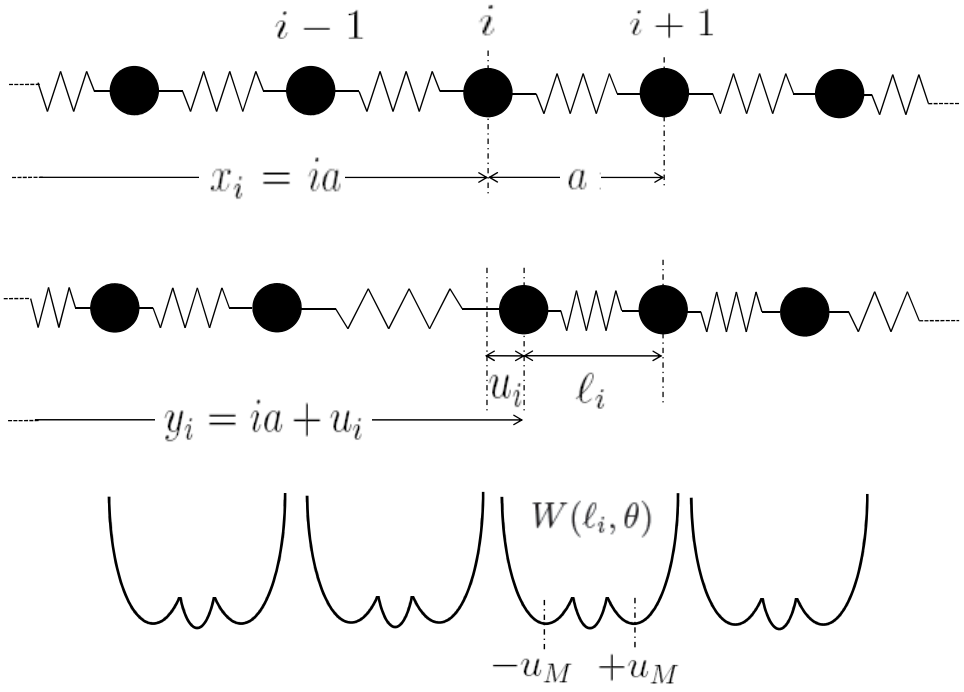

Figure 4.1: Chain of atoms with nearest-neighbor anharmonic interactions.

4.2.1 Energy

4.2.1.1 Interatomic potential

Consider a chain of N equidistant atoms separated by distance a as shown in Figure 4.1. This is the reference configuration and is taken to represent the austenite lattice. Thus a is the lattice constant of the austenite phase. We take the lattice constants of the two variants of martensite ($M^{\pm}$) to be $a \pm u_M$.

Let the reference equilibrium positions of the atoms (in the austenite phase) from a fixed origin be given by x_i; thus $x_i = ia$. Let the current position of the atom i be given by y_i. Then $y_i = ia + u_i$ where u_i is the displacement of the i atom from its reference position. The interatomic potential between adjacent pairs of atoms i and $i+1$ is chosen such that the global minimum of the energy is at $y_{i+1} - y_i = a$ for $\theta > \theta_T$ and at $y_{i+1} - y_i = a \pm u_M$ for $\theta < \theta_T$ in order to reflect the properties of the phase transition described above. In terms of the displacements

the minima occur at $u_{i+1} - u_i = 0$ for the austenite phase and $u_{i+1} - u_i = \pm u_M$ for the two variants of the martensite phase. The energy of the ith bond is chosen as an eighth order polynomial of the bond length $\ell_i = y_{i+1} - y_i$,

$$W(\ell_i, \theta) = A(\ell_i - a)^8 + B(\ell_i - a)^6 + C(\ell_i - a)^4 + D(\ell_i - a)^2 + E. \tag{4.1}$$

Since the two variants of martensite are energetically equal we have retained only the even powers terms in the polynomial expansion. We choose A, B to be temperature independent and $E = 0$. We allow the coefficient of the harmonic term to be temperature dependent; when the harmonic coefficient $D(\theta) < 0$, austenite is unstable whereas when $D(\theta) > 0$ austenite is metastable. The temperature at which the coefficient D becomes negative is the *martensite finish* temperature θ_M. Next we take the martensite lattice parameter to be independent of temperature and accordingly obtain $C = -D/2$. Finally, setting the martensite wells to be at $\ell_i = a \pm u_M$ we obtain $A/B = -3/4$. The fitting of the coefficients to the properties of the free energy are described in more detail in Falk [74]. The main difference between our potential and the Falk free energy is that we require our martensite bond length to be independent of temperature and hence we choose an eighth order polynomial in contrast to the Falk-type sixth order polynomial.

For convenience we operate in a non-dimensional setting in which our energy is written as

$$\bar{W}(\bar{\ell}_i, \bar{\theta}) = 3\bar{\ell}_i^8 - 4\bar{\ell}_i^6 - 2\bar{\theta}\bar{\ell}_i^4 + 4\bar{\theta}\bar{\ell}_i^2, \tag{4.2}$$

where $\bar{\ell}_i = (\ell_i - a)/u_M$, $\bar{W} = 3W/Au_M^8$ and $\bar{\theta} = (\theta - \theta_M)/\theta_M$. We note that $\bar{\ell}_i = \bar{u}_{i+1} - \bar{u}_i$ where $\bar{u}_i = u_i/u_M$ is the non-dimensional displacement. Thus $\bar{\ell}_i$ is proportional to the "strain" in bond i. We will drop the bars for convenience henceforth.

The features of the interatomic energy for the ratios of the coefficients given by Eq. (4.2) are:

1. Austenite becomes unstable at $\theta = 0$ and martensite becomes unstable

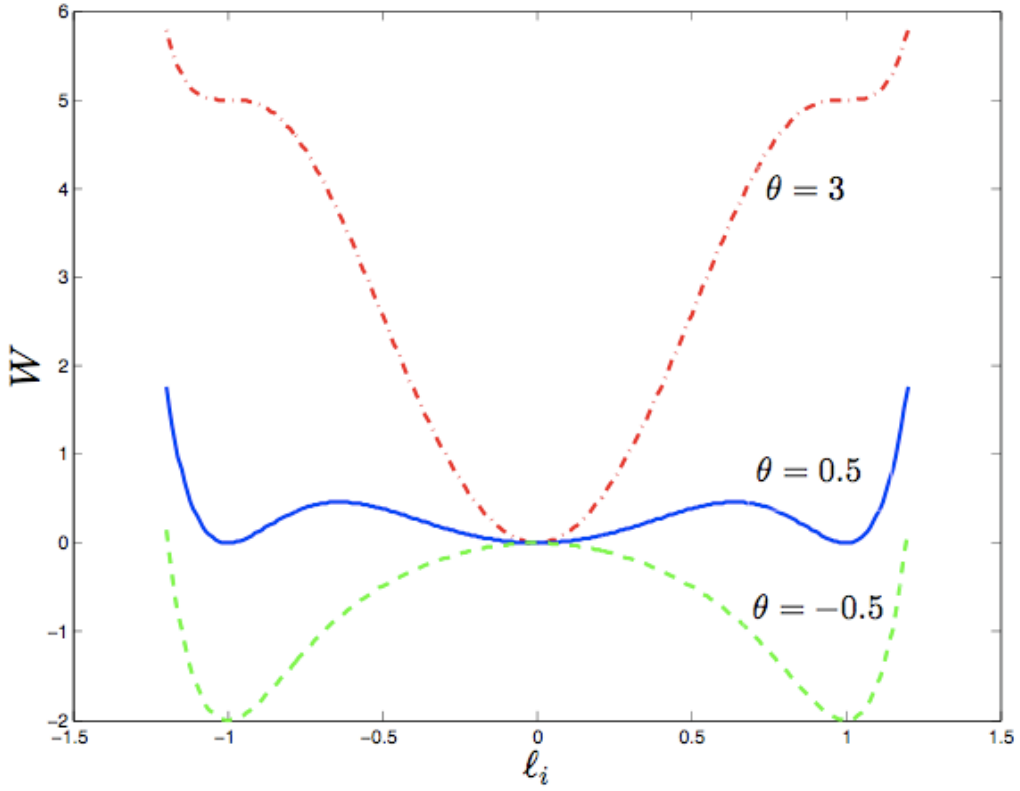

Figure 4.2: A plot of $W(\ell_i, \theta)$ for three different θ. For $\theta > 3$ the martensite phase is unstable whereas for $\theta < 0$ austenite is unstable. At $\theta = 0.5$ both phases have equal energy.

(austenite finish temperature) at $\theta = 3$. The transformation temperature at which both phases have equal energy is given by $\theta_T = 0.5$.

2. The martensite wells are at $\ell_i = \pm 1$ for $\theta < 3$.

3. The austenite elastic modulus is given by $\mu_a(\theta) = 8\theta$ and the martensite modulus is given by $\mu_m(\theta) = 48 - 16\theta$.

A plot of the potential $W(\ell_i, \theta)$ is shown in Fig. (4.2) for $\theta = -0.5$ (dashed line), $\theta = 0.5$ (solid line) and $\theta = 3$ (dash-dot line).

4.2.1.2 Interfacial energy

When adjacent unit cells (in our one-dimensional case, the bond lengths) in the material are in different phases or variants, the resulting interface has higher energy than if the cells were in the same phase. When the adjacent cells are transforming

between variants, this provides nearest neighbor (NN) interaction energy. We incorporate this interfacial energy through a simple gradient energy of the form

$$W_g = \lambda \left(\frac{u_{i+1} - u_i}{2} - \frac{u_i - u_{i-1}}{2} \right)^2, \tag{4.3}$$

where λ is a gradient coefficient. This energy is motivated by harmonic strain-gradient energy terms in augmented continuum theories. The strain-gradient in our case arises from the difference between adjacent bond lengths. In non-dimensional form the gradient energy becomes

$$\bar{W}_g = \frac{\bar{\lambda}}{4} \left(\bar{u}_{i+1} - 2\bar{u}_i + \bar{u}_{i-1} \right)^2 \tag{4.4}$$

where $\bar{W}_g = 3W_g/Au_M^8$ and $\bar{\lambda} = 3\lambda/Au_M^6$.

4.2.2 Equations of motion

Let the masses of the particles in the chain be identical and equal to m. Setting the non-dimensional time $\bar{t} = t\sqrt{Au_M^6/3m}$, we obtain the non-dimensional equations of motion

$$\ddot{u}_i = -\frac{\partial W(\ell_i, \theta)}{\partial u_i} - \frac{\partial W(\ell_{i-1}, \theta)}{\partial u_i} - \frac{\partial W_g}{\partial u_i}, \tag{4.5}$$

where we have, once again, dropped the bars for convenience. Note that $\ell_i = u_{i+1} - u_i$ and $\ell_{i-1} = u_i - u_{i-1}$ are the "strains" of the i and $i-1$ bonds respectively.

In order to mimic the presence of a heat bath at temperature θ in contact with the system we use the Nosé-Hoover thermostat [75, 76]. The Nosé-Hoover thermostat introduces an additional degree of freedom which evolves according to the difference between the temperature of the system and the reservoir (target)

temperature. With the Nosé-Hoover thermostat, the equations of motion are

$$\begin{aligned} \ddot{u}_i &= 8\ell_i(3\ell_i^4 - \theta)(\ell_i^2 - 1) - 8\ell_{i-1}(3\ell_{i-1}^4 - \theta)(\ell_{i-1}^2 - 1) + \lambda(u_{i+1} - 2u_i + u_{i-1}) - \gamma\dot{u}, \\ \dot{\gamma} &= \frac{1}{Q}\left(\sum_{i=1}^{N} \frac{1}{2N}\dot{u}_i^2 - k_b(\theta + 1)\right), \end{aligned} \tag{4.6}$$

where $k_b = k_B\theta_M/Au_M^8$ is a non-dimensional Boltzmann's constant.

4.3 Numerical simulation

4.3.1 Thermal cycle

We solve Eqs. (4.6) for a chain of $N = 1000$ atoms using the velocity Verlet algorithm to discretize the equations. A non-dimensional time step $\Delta t = 10^{-4}$ is used. The thermal inertia parameter is chosen to be $Q = 0.002$. The atoms are given small initial random displacements about the equilibrium position and small random velocities. Averages are calculated over a time period of $\tau_{av} = 100$.

We study a thermal cycle of the system by cooling the chain from austenite phase followed by heating. During cooling, the target temperature is divided by a factor $r = 1.1$ and the system is allowed to equilibrate and averages are calculated. Heating is achieved by multiplying the target temperature by the same factor. The atoms at the boundaries are free (they only experience forces from the interior of the domain).

4.3.1.1 Zero interfacial energy

We first study the thermal cycle of the chain of atoms in the absence of interfacial energy by setting $\lambda = 0$.

Figure 4.3(a) shows the bond length between a representative pair of atoms during the cooling and heating cycle for $k_b = 0.1$. The bond length oscillates around 0 at high-temperatures indicating the austenite phase. As the temperature is lowered, the bond length transforms to a value -1 which indicates M^- variant of

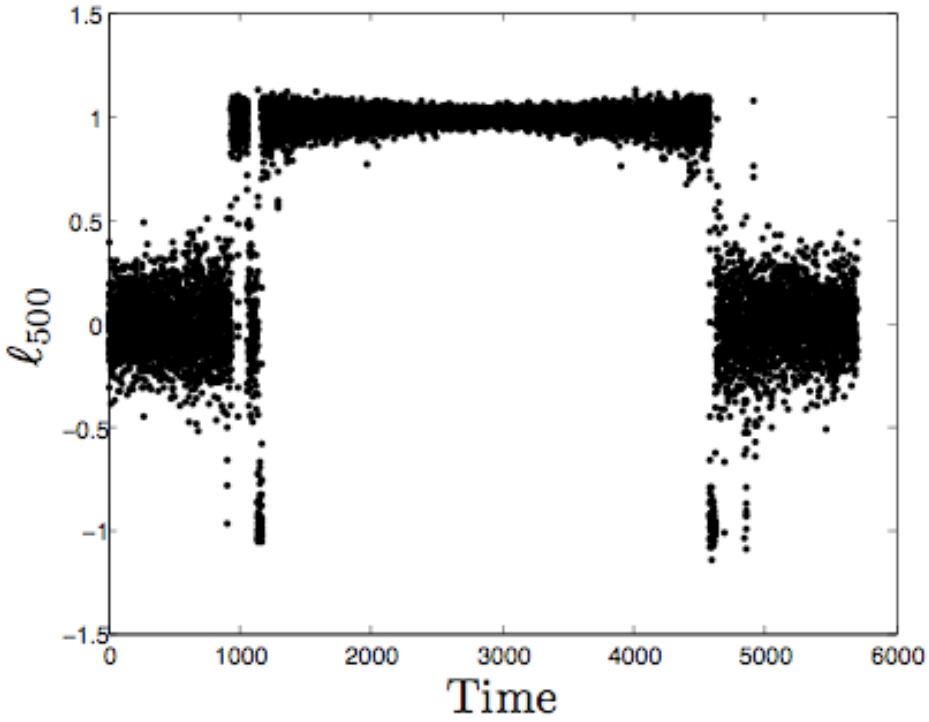

(a) $k_b = 0.1$

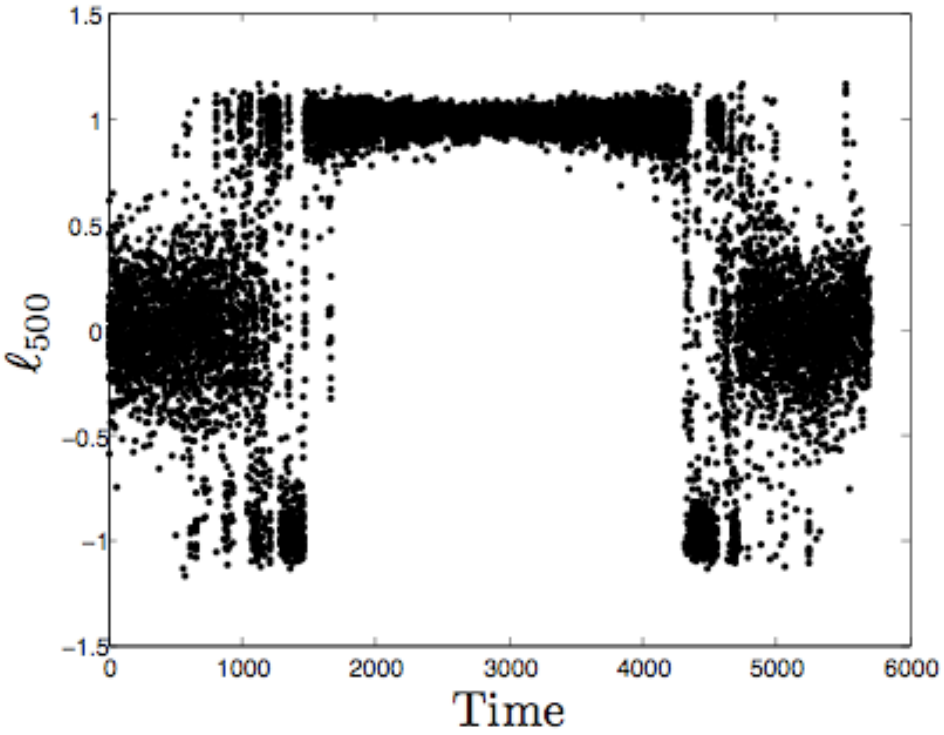

(b) $k_b = 0.2$

Figure 4.3: The bond length ℓ_{500} between atoms 500 and 501 in the chain with time. The chain is initially at high-temperature $\theta = 3$ and is cooled to $\theta = -0.7$ after which it is reheated to $\theta = 3$.

the martensite phase. At $\tau \approx 3000$ the chain is heated and transforms to austenite. It may be noted that the amplitude of oscillations decrease with temperature (more clearly seen away from the transformation) as is to be expected. The non-dimensional Boltzmann's constant k_b relates the interatomic potential energy to the amplitude of the thermal oscillations. This can be seen by the amplitude of oscillation of the representative atom for two values of k_b. In Fig. 4.3(a), $k_b = 0.1$ and the amplitude of oscillation is higher than in Fig. 4.3(b) in which $k_b = 0.2$.

We next plot the instantaneous energy per atom in Fig. 4.4. The instantaneous potential energy of the chain is calculated using

$$V = \sum_{i=1}^{N-1} \left(3\ell_i^8 - 4\ell_i^6 - 2\theta\ell_i^4 + 4\theta\ell_i^2 + 2\phi_i\theta\right) + \sum_{i=2}^{N-1} \frac{\lambda}{4} \left(u_{i+1} - 2u_i + u_{i-1}\right)^2, \quad (4.7)$$

where $\phi_i = 1$ if the bond is in the martensite phase and $\phi_i = 0$ otherwise. The lowest curve in Fig. 4.4 is the instantaneous kinetic energy of the chain per atom. Note that the instantaneous kinetic energy per atom is equal to the Boltzmann constant times the absolute temperature. The middle curve is the potential energy. The phase transition can be observed from the sharp changes in the potential energy during the heating and cooling cycles.

The plot of time averaged total energy $< E >$ (internal energy of the chain) with temperature is shown in Fig. 4.5(a) for $k_b = 0.1$ and Fig. 4.5(b) for $k_b = 0.2$. It is seen that the hysteresis is larger for smaller k_b. As the amplitude of oscillations becomes close to zero, the width of the hysteresis tends towards the difference between the temperatures at which the austenite wells and martensite wells become unstable, which for this potential is $\Delta\theta = 3$. For finite amplitude oscillations, the nucleation of the austenite (resp. martensite) occurs at lower (resp. higher) temperatures and the width of the hysteresis loops is smaller. Henceforth we use $k_b = 0.2$ in the rest of our simulations.

The derivative of the internal energy with temperature is the specific heat of the chain. Figure 4.6 shows a plot of the specific heat with temperature. The

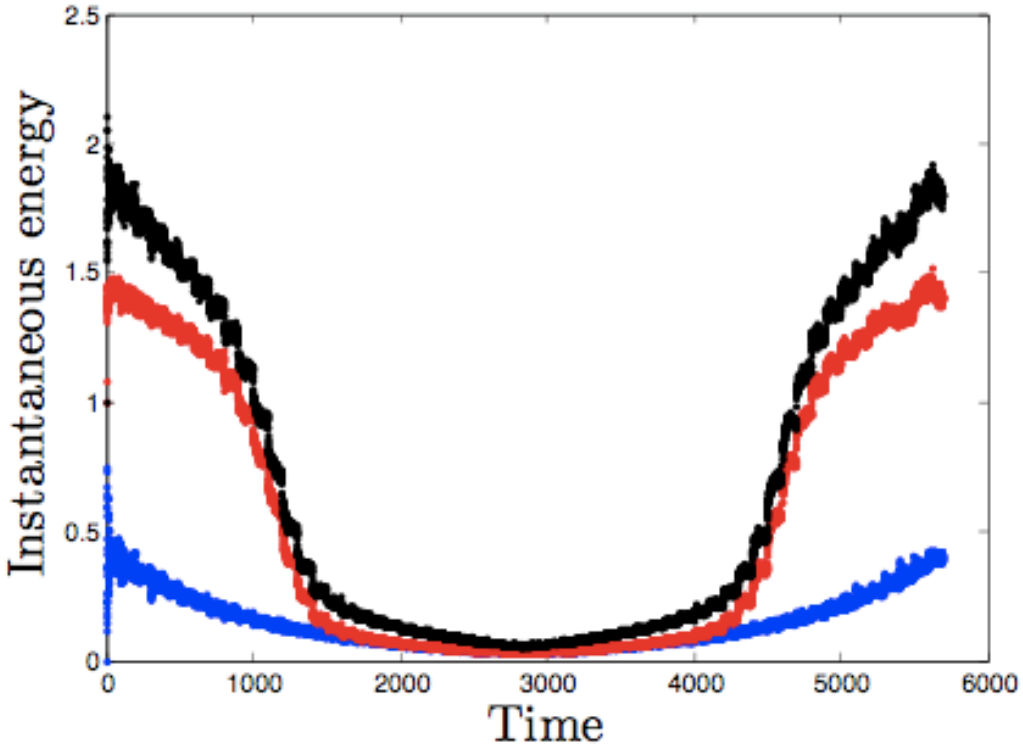

Figure 4.4: Plot of the instantaneous energy as a function of time. The lowest curve is the instantaneous kinetic energy per atom ($= \frac{1}{2}k_b(\theta + 1)$), the middle curve is the instantaneous potential energy per atom and the upper curve is the instantaneous total energy per atom.

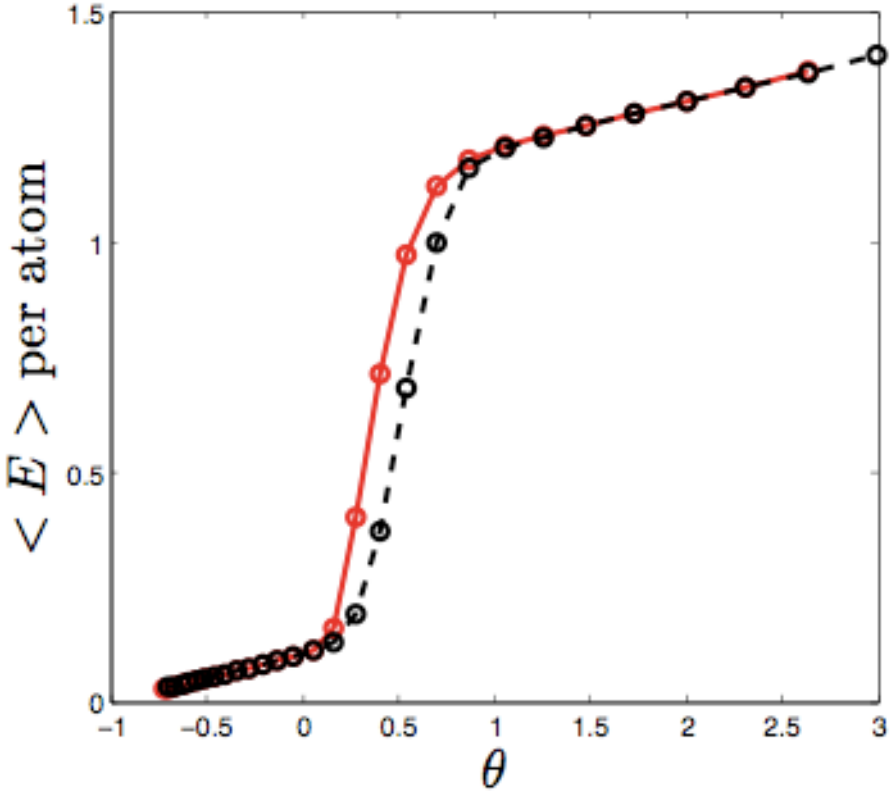

(a) $k_b = 0.1$

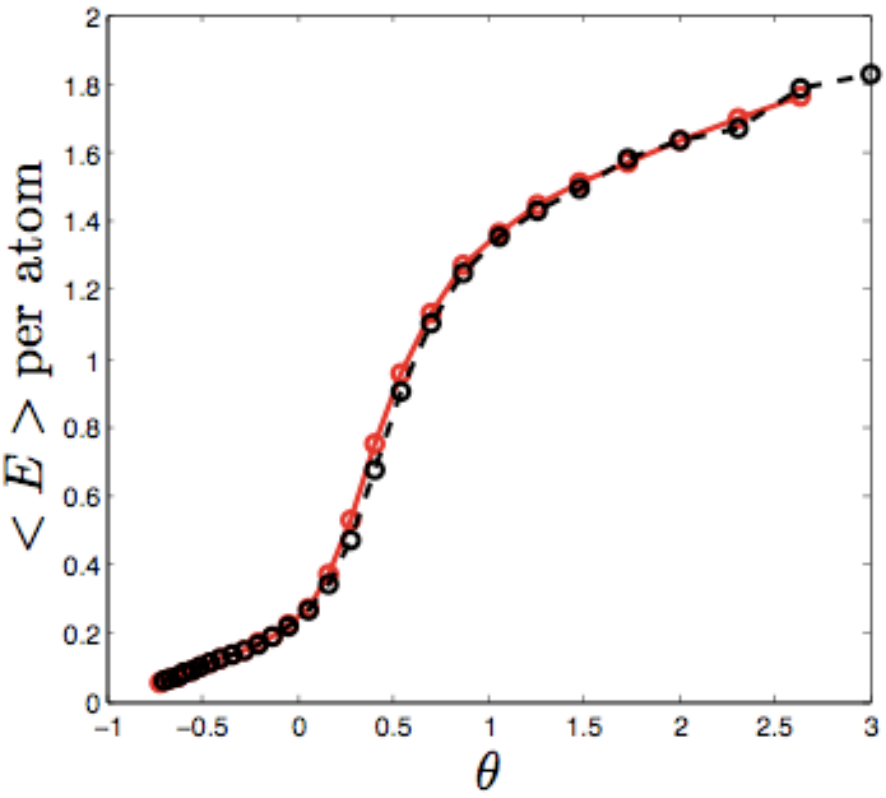

(b) $k_b = 0.2$

Figure 4.5: Plot of the average total energy per atom with temperature.

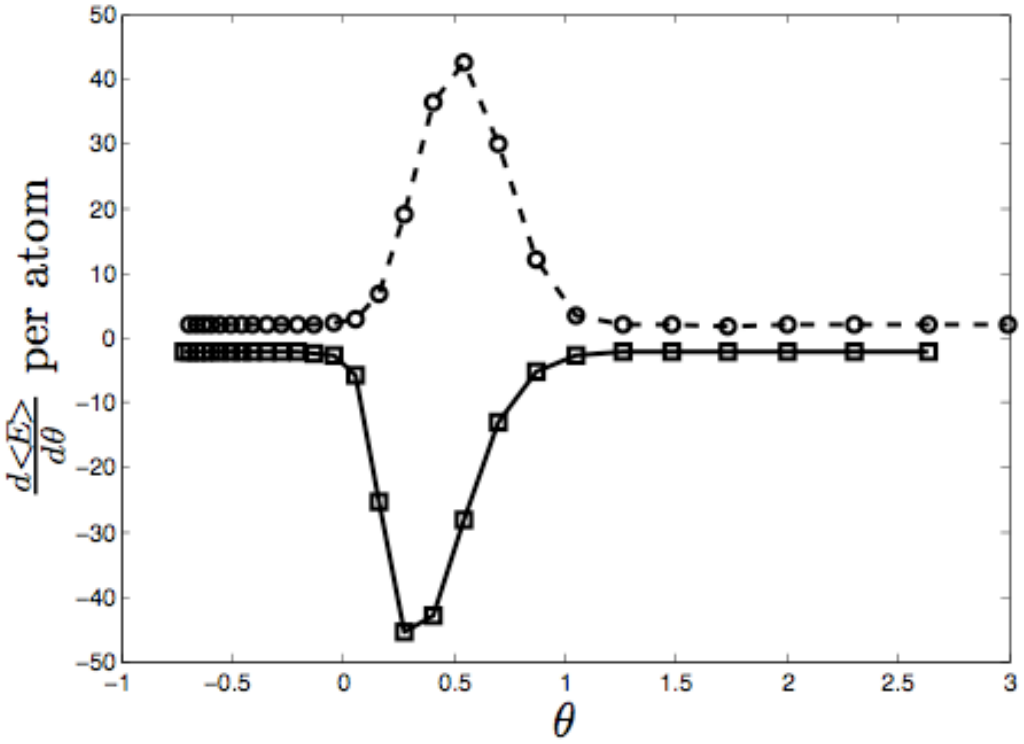

Figure 4.6: Plot of the specific heat with temperature. The heating curve is shown using dashed line whereas the cooling curve is shown using a solid line.

resulting plot shows constant specific heat in each of the pure phases and peaks representing the exothermic and endothermic processes during the austenite to martensite and martensite to austenite phase transformations respectively. This is a realistic representation of differential scanning calorimetry (DSC) measurements of structural phase transitions, refer Shaw and Kryiakides [70] the experimental DSC thermogram for NiTi alloy.

Figure 4.7(a) shows the time averaged strain in the bonds along the chain of the atoms during the cooling and heating cycle. The solid curve shows the cooling curve and the dashed curve shows the heating curve. The average positions of the atoms are initially close to 0 indicating the austenite phase. As the temperature is lowered, martensite phase is formed with an approximately equal distribution of the two variants. At time $\tau \approx 3000$, the chain is heated and the austenite phase is recovered. In the martensite phase, the two variants are formed with a random distribution of *twins* of M^+ and M^- variants. The width of a twin is the size of

regions of a single variant. In Fig. 4.7(b) we show a close up of a region in the middle of the chain from atom number 475 to atom number 525. It can be seen that several fine twins of just unit cell width are formed. This is possible since there is no energy penalty associated with twin boundaries in these simulations.

4.3.1.2 Effect of interfacial energy

In the absence of interfacial energy, very fine twins are formed. In the simulation shown in Fig. 4.7(a), there are 493 interfaces which implies that the average width of the twin is 1.97 unit cells. In the presence of a finite interfacial energy, obtained by setting the gradient coefficient $\lambda = 0.5$, wider twins are formed especially near the boundaries. The average twin width in the presence of interfacial energy is about 2.3 unit cells.

In Fig. 4.8 we plot of the average energy per atom with temperature to study the effect of the interfacial energy. The energy of the martensite phase in the presence of the interfacial energy at a given temperature. Another significant feature is the presence of higher hysteresis in the case with interfacial energy. The presence of interfacial energy increases dispersion of energy of transformation of a bond through the chain and this contribution to the domain wall entropy enhances the hysteresis in the process.

4.3.2 Mechanical cycle

We study the pseudoelasticity and shape memory effect for a chain of $N = 200$ atoms. Thermal inertial parameter is chosen to be $Q = 0.002$ and a non-dimensional time step $\Delta t = 10^{-4}$. The non-dimensional Boltzmann's constant $k_b = 0.1$, and the temperature of the system is kept constant by Nosé-Hoover thermostat. A force is applied to the both ends of the chain as shown in Fig. 4.9 and the system is allowed to equilibrate over a time period of $\tau_{av} = 700$.

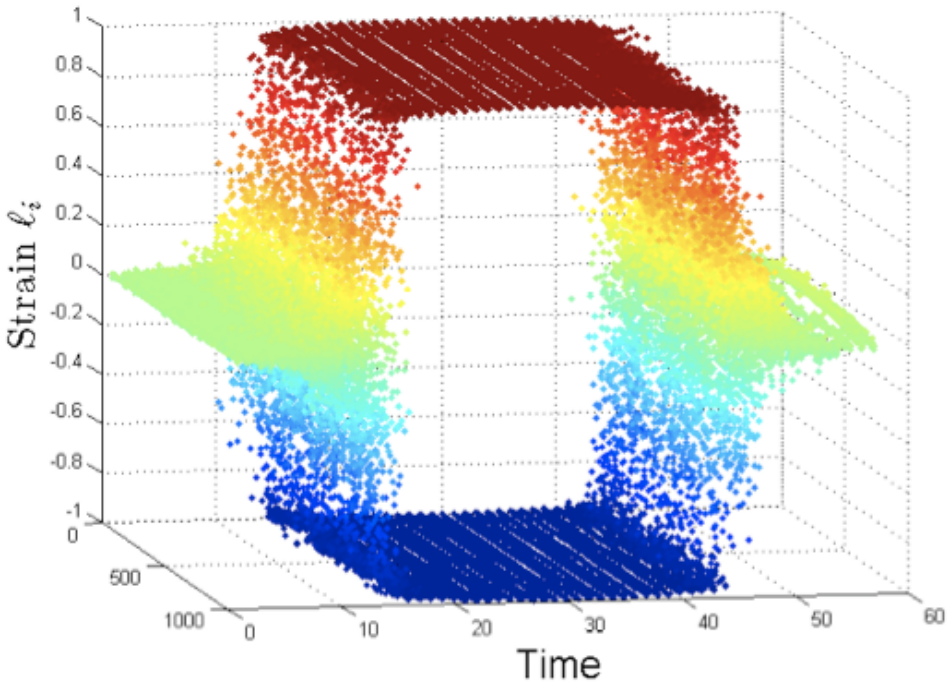

(a)

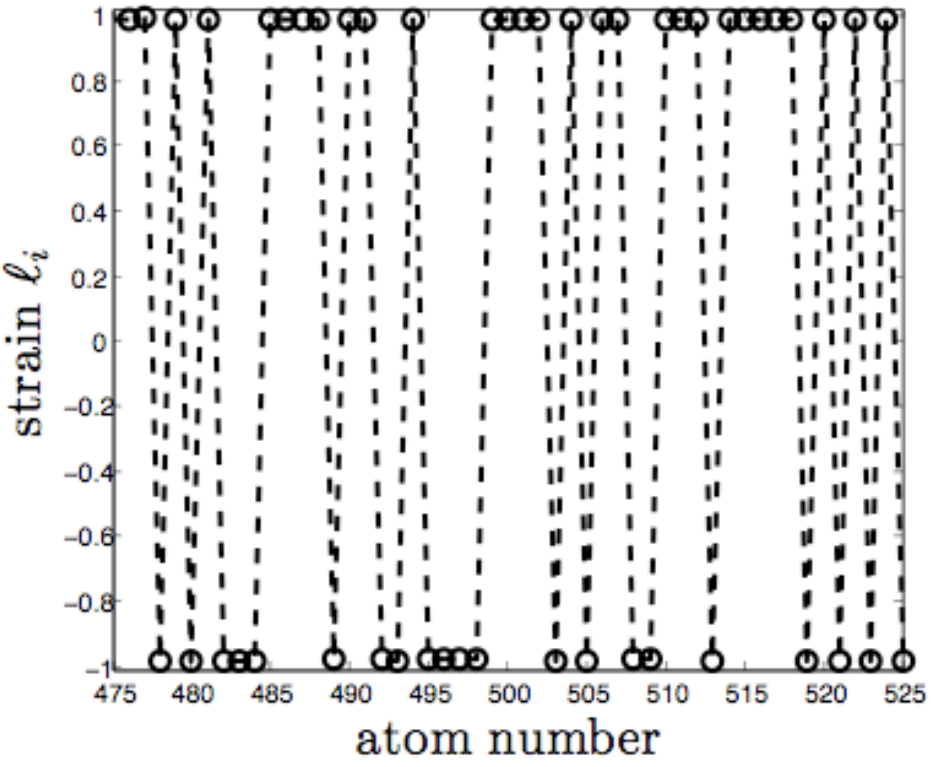

(b)

Figure 4.7: (a) Plot of strain along the chain with time. (b) Plot of strain along the middle of the chain at $\tau = 3000$ from atom number 475 to 525. The dotted lines represent the twin boundaries.

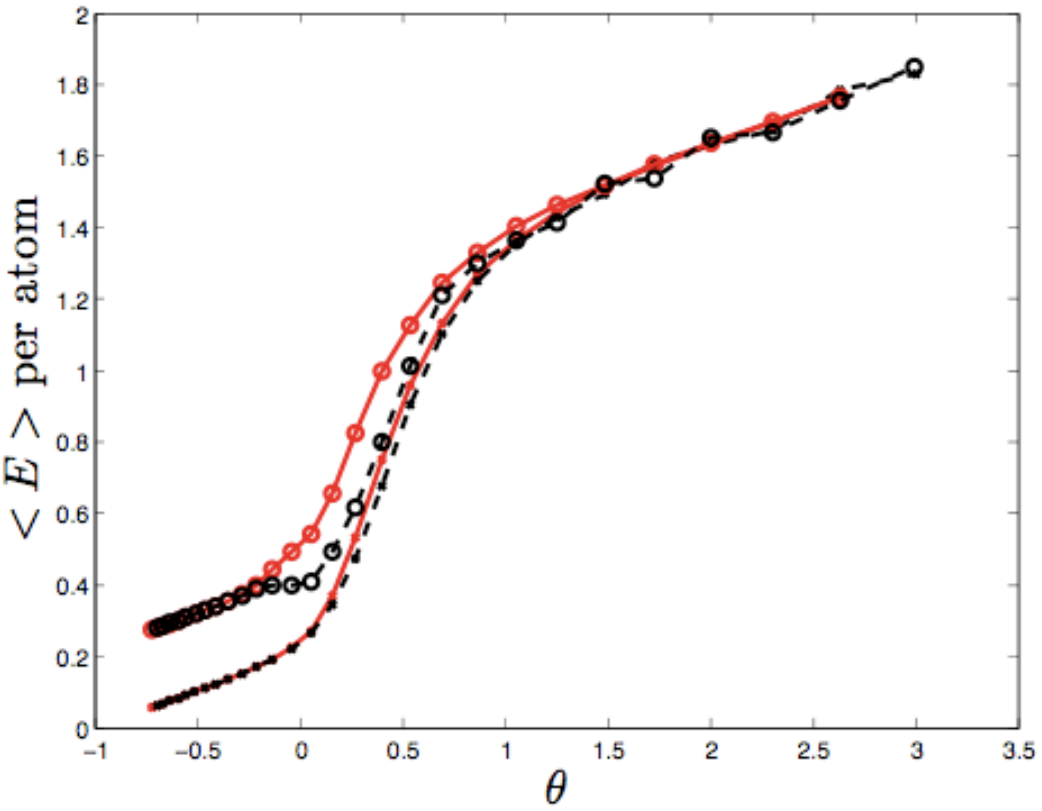

Figure 4.8: Plot of the average energy with temperature. The lines without circles show the case of $\lambda = 0$ whereas the lines with circles represent the case with $\lambda = 0.5$. In both cases, the solid lines represent the cooling curve and the dashed lines represent the heating curve.

Figure 4.9: A force applied to the both ends of the chain

4.3.2.1 Pseudoelasticity

The atoms are set in the austenite equilibrium positions and small initial random velocities are given. The system temperature is kept at $\theta = 2.5$ at which the austenite is stable. The interfacial energy of the chain is chosen to be $\lambda = 35$. Once the system reaches the austenite stable phase, a incremental tensile force $f = 0.25$ is applied to first and last atom in the chain and averages of the martensite volume fraction and cumulative strain of the chain are calculated. Fig. 4.10(a) shows a plot of the force-% of martensite volume fraction of the chain. The chain is initially in the austenite phase, applied force at the end of chain causes only elastic deformation of the austenite phase. At some critical force (point **a** in Fig. 4.10(a)) austenite becomes unstable and martensite starts to form. With further applied force, martensite spreads in the chain with very less incremental applied force and at point **b** in Fig. 4.10(a) the chain is completely transformed to martensite phase. Further loading results in the elastic deformation of martensite (as shown in path $\mathbf{b} - \mathbf{c}$). Unloading the force at this point results in the complete recovery of the deformation of the chain, at point **d** martensite is unstable and austenite starts to spread in the chain. At point **e** the chain is completely recovered to austenite phase. Fig. 4.10(b) shows the strain of the each atom in the chain during loading and unloading cycle. At time $t = 0$ the strain of the individual atom in the chain is close to 0, representing the austenite phase and at time $t = 50$ the strain is close to 1.1 representing elastically strained martensite. Upon unloading at this stage the complete recovery to austenite is achieved and the strain is 0 at time step 100. This is a realistic representation of the pseudoelasticity in shape memory alloys, refer [71] the experimental stress-strain response for NiTi alloy.

Next we study the pseudoelastic behavior of the chain at different system temperatures. In Fig. 4.11(a) we plot the cumulative strain of the chain with the applied force at temperatures $\theta = 3.5, 2.5$ and 1.5. Strain in the chain is completely recovered. Hysteresis is due to the energy dispersion in the chain due to interfacial energy. In Fig. 4.11(b) we plot the required transformation

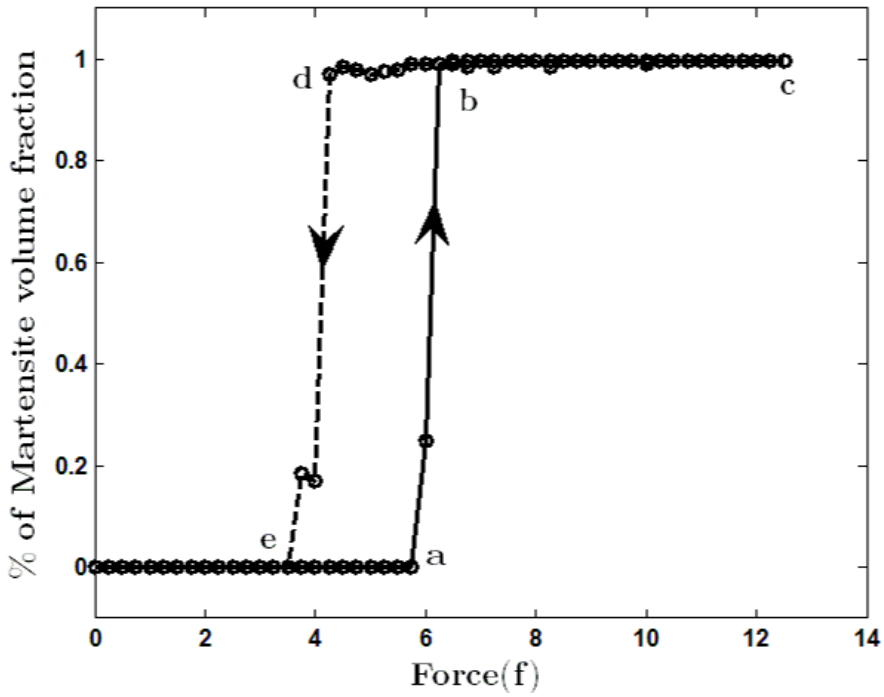

(a)

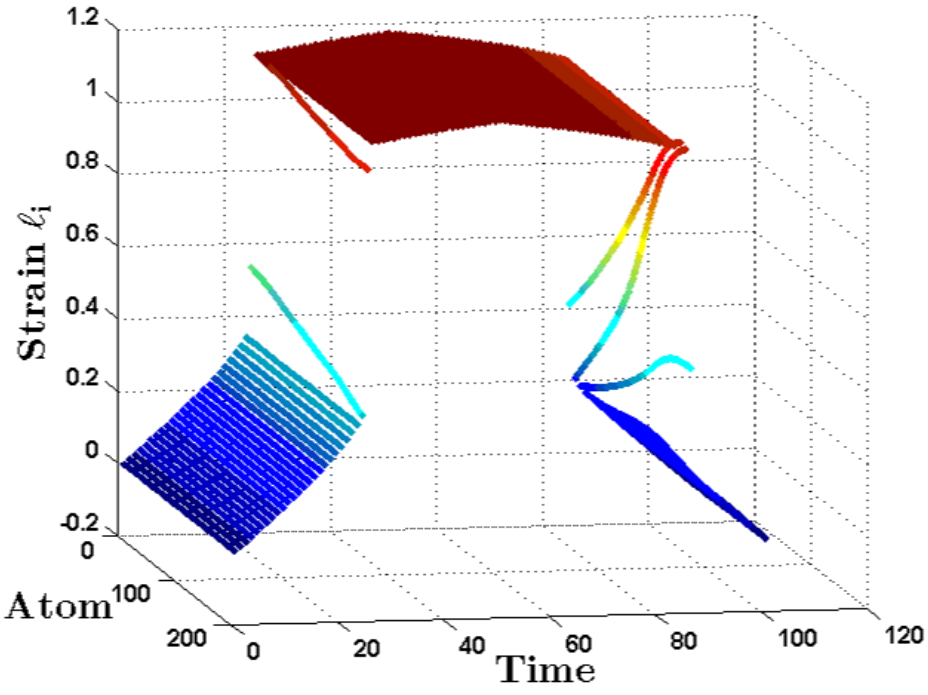

(b)

Figure 4.10: (a) Plot of the change in the martensite volume fraction with applied force. Loading path is shown in solid line and unloading path is shown in dashed line. (b) Plot of the strain in each atom with time

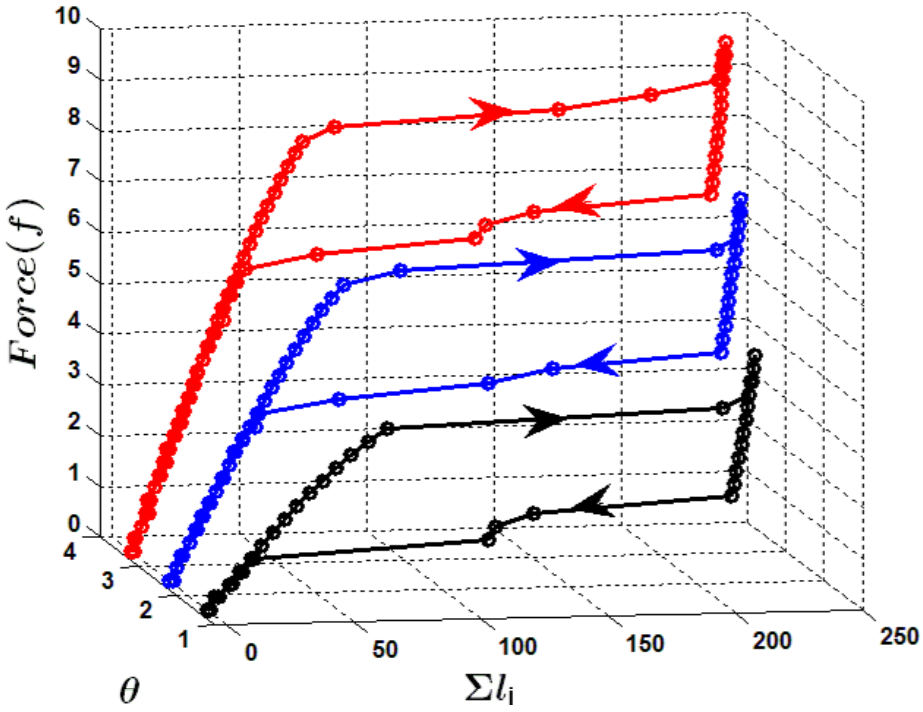

(a)

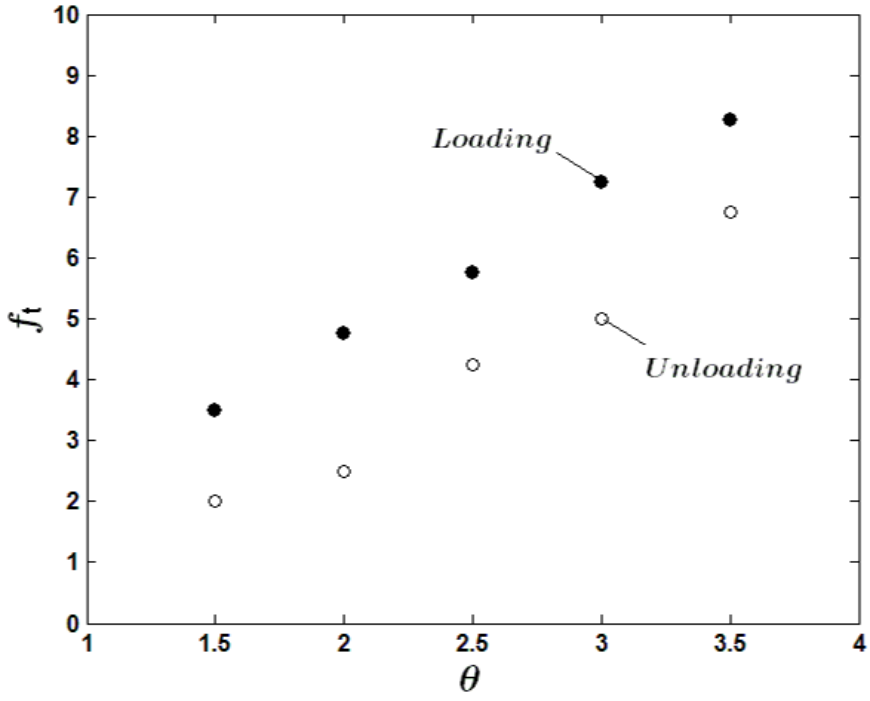

(b)

Figure 4.11: (a) Plot of pseudoelasticity in the chain at temperatures $\theta = 3.5, 2.5$ and 1.5. (b) Plot of the transformation force as function of temperature.

force f_t during loading and unloading at different temperatures, force required for forward and reverse transformation increases with increase in temperature. Shaw and Kyriakides [70] report experimental observations of increasing transformation stress with temperature but report a growth in the width of hysteresis loops with increasing temperature.

4.3.2.2 Shape memory effect

We now study detwinning and the shape memory effect in the chain by loading and unloading at a low-temperature $\theta = -0.5$, at which martensite is stable. For this study we choose the interfacial energy $\lambda = 0.1$. In Fig. 4.12(a) we plot the change in strain ℓ_i of each bond with time. We start the simulation at a high-temperature austenite stable phase and cool the system to produce twinned martensite, as shown at time $t = 14$ marked as point **b**. From this point the temperature of the chain is kept constant and force is applied to the atoms at the either end of chain. Now the atoms preferentially move towards the direction of applied force. All the atoms are moved to M^+ variant as shown at the time $t = 36$ marked **d**, this process is detwinning. Further loading results in the elastic deformation of M^+ variant, time $t = 37$ to $t = 53$ (**d** to **e**). From the point **e** the chain is unloaded and all the atoms are still at M^+ variant (**f**), this results in a residual strain. Upon heating, the chain completely transforms to austenite as shown by point **g**. The residual strain is completely recovered by this heating cycle. Further cooling results in the twinned martensite and this process is shape memory effect.

In Fig. 4.12(b) we plot the respective cumulative strain $\Sigma\ell_i$ of the chain for the shape memory effect simulation cycle. Path $\mathbf{a} - \mathbf{b}$, austenite to twinned martensite by cooling the chain. Path $\mathbf{b} - \mathbf{c} - \mathbf{d}$, detwinning by the applied force at constant temperature. Path $\mathbf{d} - \mathbf{e}$, elastic deformation of the martensite phase. Path $\mathbf{e} - \mathbf{f}$, unloading cycle ends up with a residual strain (point **f**). Path $\mathbf{f} - \mathbf{g}$, martensite to austenite by heating the chain. Path $\mathbf{g} - \mathbf{h}$, back to twinned martensite by cooling the chain. This is a realistic representation of the shape memory effect, refer [71]

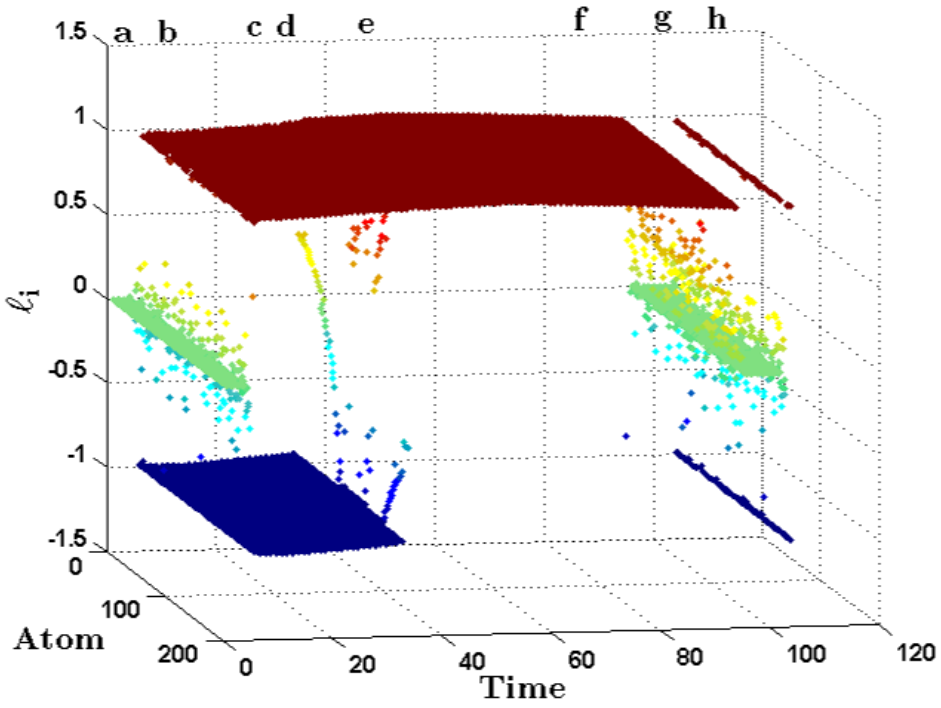

(a)

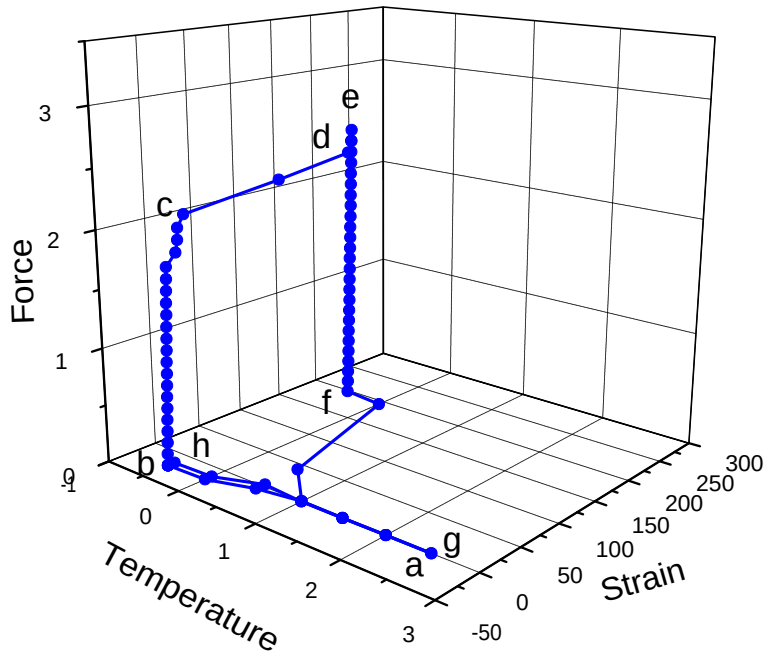

(b)

Figure 4.12: (a) Plot of the strain of each atom in the chain with time. (b) Plot of shape memory effect in the chain.

the experimental stress-strain-temperature response for NiTi alloy.

4.4 Summary

- The model shows that it is possible to use a form of the continuum free energy for the interatomic potential energy and the dispersion of energy by the strain gradient term causes hysteresis.
- We studied the numerical simulation of this model for temperature-induced phase transition, pseudoelasticity and shape memory effect.

Chapter 5

Conclusions and Future Work

5.1 Conclusions and discussion

In this thesis we examined discrete models for materials undergoing structural phase transitions. Our focus was on the properties of interatomic potentials which allow phase transitions. We first showed that the properties of the phase transforming mode are critical in allowing a material to undergo phase transitions. In particular the potential energy slice in the phase transforming mode must have energy wells corresponding to the low-temperature phase as well as a relatively flat region corresponding to the high-temperature phase. This allows the vibrational entropy to dominate at high-temperatures allowing the free energy of the high-temperature phase to become smaller than the low-temperature phase and thus an exchange of phase stability.

In Chapter 2 we presented a one-dimensional discrete model, in which the interatomic potential energy of the discrete masses is assumed to be independent of the system temperature. We assumed a potential well with two minima for two martensite variants and a flat region for austenite phase. Such discrete models allow the atoms to oscillate between the three wells in the potential well with the mean position of the oscillating atoms determining the phase of the atom. At high-temperature the atoms spend most of the time in the flat region and

their mean position is that of the austenite phase and at low-temperature the atoms spend most of the time in one of the martensite wells. Interfacial energy between different phases or variants is incorporated as a gradient energy term. The vibrational entropy controls the structural phase transition. We studied the temperature-induced phase transition for a one-dimensional chain of atoms by numerical simulation. The results represent a realistic temperature-induced phase transition by exothermic and endothermic dissipation of energy during forward and reverse transformation respectively. Hysteresis arises due to energy dissipation and the width of the twins increases with the interfacial energy. The transformation temperature of the chain of atoms increases with increase in barrier height of the potential well. Pseudoelastic simulations are done by applying a force to the atoms at the either end of the chain, and the temperature of the atoms is maintained above the transformation temperature. The cumulative strain in the chain along with the force applied represents a transformation to martensite variants and a complete recovery to austenite phase. The shape memory effect simulations show a realistic recovery of twinned martensite.

In continuum theories, free energy of system incorporates temperature dependent parameters. Motivated by these theories we developed a discrete model, in which the interatomic potential changes with the temperature. In Chapter 3, we presented a discrete phenomenological model in which a temperature dependent substrate potential provides a mean field effect of the surrounding atoms. The possibility of double counting the effect of the kinetic energy in the potential and that of the atoms is examined. The phenomenological parameters are adjusted to avoid this possibility.

In Chapter 4 we assume an atom under consideration has multiple equilibrium bond lengths relative to its nearest-neighbor atoms corresponding to the lattice constants of the parent and product phases. The configuration of the surrounding atoms (which depends on temperature) changes the energy of the interaction potential and the location of its minimum. We use a polynomial Falk-type free en-

ergy, which is a polynomial expansion of a single strain component, to describe the interaction potential. At high-temperatures the potential well has one minimum, representing the austenite phase. At low-temperatures the potential well has two minima, representing the martensite phase with two variants and at transformation temperature all the three wells exist. We studied the numerical simulation of this model for temperature-induced phase transition, pseudoelasticity and shape memory effect.

5.2 Future work

In this thesis our main focus was to develop discrete models to study the temperature dependent phase transition, pseudoelasticity and shape memory effect in SMA. We simplified the problem by assuming model to be one-dimensional chain of discrete masses with two energetically equivalent martensite variants. The three models we developed are capable of qualitatively depicting the phenomena of SMA. However complex nucleation phenomena, twin formation and phase boundary motion with temperature and stress cannot be studied with a one-dimensional model. Two- and three-dimensional models will be useful in studying the kinetic relation of moving boundaries and also their dependency on temperature.

The potentials to be used in higher dimensional models are a simple generalization of the one-dimensional model. We outline the basic framework to extend the interatomic potential energy of the type discussed in Chapter 4 to a two-dimensional lattice shown in Figure 5.1.

Each discrete mass is assumed to be interacting with four nearest-neighbours.The nearest-neighbours form the four quadrants surrounding each lattice. Based on the atomic positions of the nearest-neighbour atoms, we calculate the deformation gradient $\mathbf{F}_I(u_{i,j}, u_{i+1,j}, u_{i,j+1})$, $\mathbf{F}_{II}(u_{i,j}, u_{i-1,j}, u_{i,j+1})$, $\mathbf{F}_{III}(u_{i,j}, u_{i-1,j}, u_{i,j-1})$, $\mathbf{F}_{IV}(u_{i,j}, u_{i+1,j}, u_{i,j-1})$ of each quadrant. The potential energy of a lattice point (ϕ) is a function of energy of four quadrants ($\phi_I(\mathbf{F}_I), \phi_{II}(\mathbf{F}_{II}), \phi_{III}(\mathbf{F}_{III}), \phi_{IV}(\mathbf{F}_{IV})$).

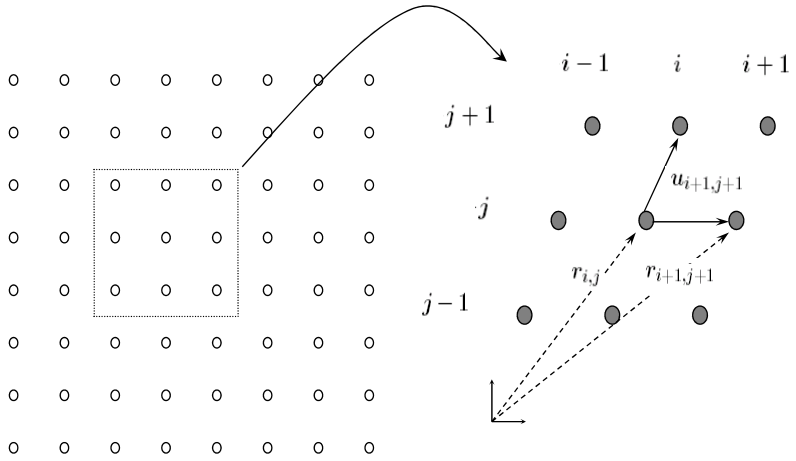

Figure 5.1: Two-dimensional discrete model.

Thus the total potential energy of the atom under consideration is given by

$$\phi = f(\phi_I, \phi_{II}, \phi_{III}, \phi_{IV}). \tag{5.1}$$

The interatomic potential energy of each quadrant can be a function of temperature as in Chapter 4 (and a particular choice of the potential energy can be the continuum free energy).

The molecular dynamics of the atoms can be performed by solving the Newton's equations

$$\ddot{u}_{i,j} = -\frac{\partial \phi}{\partial u_{i,j}}. \tag{5.2}$$

Similar to quasi-continuum models, two dimensional discrete models can be coupled with the finite element nodes to study the temperature dependent structural property of SMA.

Bibliography

[1] G.B. Olson and W.S. Owen (Eds), *Martensite*, ASM International, Metals Park, OH, USA, 1992.

[2] E.K.H. Salje, *Phase transitions in ferroelastic and co-elastic crystals*, Cambridge Univ. Press, Cambridge, U.K., 1993.

[3] K. Otsuka and C.M. Wayman, *Shape memory materials*, Cambridge Univ. Press, Cambridge, U.K., 1999.

[4] J.A. Gonzalo and B. Jimenéz, *Ferroelectricity*, Wiley, New York, 2005.

[5] K. Bhattacharya, S. Conti, G. Zanzotto, and J. Zimmer, "Crystal symmetry and the reversibility of martensitic transformations", *Nature*, vol. 428, pp. 55–59, 2004.

[6] R. Abeyaratne and S. Vedantam, "A lattice-based model of the kinetics of twin boundary motion", *Journal of the Mechanics and Physics of Solids*, vol. 51, pp. 1675–1700, 2003.

[7] Ph. Boullay, D. Schryvers, and J.M. Ball, "Nano-structures at martensite macrotwin interfaces in Ni65Al35", *Acta Materialia*, vol. 51, pp. 1421–1436, 2003.

[8] C. Chu, *Hysteresis and microstructures: a study of biaxial loading on compound twins of copper-aluminium-nickel single crystals*, Ph.D. dissertation, University of Minnesota, Minneapolis, MN, USA, 1993.

[9] R. Abeyaratne, C. Chu, and R.D. James, "Kinetics of materials with wiggly energies: Theory and application to the evolution of twinning microstructures in a CuAlNi shape memory alloy", *Philosophical Magazine A*, vol. 73, pp. 457–497, 1996.

[10] G.Lu, N. Kioussis, V. Bulatov, and E. Kaxiras, "Generalized-stacking-fault energy surface and dislocation properties of aluminum", *Physical Review B*, vol. 62, pp. 3099–3108, 2000.

[11] L.Q. Chen and Y.Z. Wang, "The continuum field approach to modeling microstructural evolution", *Journal of the Minerals Metals and Materials Society*, vol. 48, pp. 13–18, 1996.

[12] C. Ratsch, M.F. Gyure, R.E. Caflisch, M. Petersen, M. Kang, J. Garcia, and D.D. Vvedensky, "Level-set method for island dynamics in epitaxial growth", *Physical Review B*, vol. 65, pp. 195403–195415, 2002.

[13] F.F. Abraham, J. Broughton, N. Bernstein, and E. Kaxiras, "Spanning the length scales in dynamic simulation", *Computers in Physics*, vol. 12, pp. 538, 1998.

[14] J. Broughton, F. Abraham, N. Bernstein, and E. Kaxiras, "Concurrent coupling of length scales: Methodology and application", *Physical Review B*, vol. 60, pp. 2391–2403, 1999.

[15] K. Ohsawa and E. Kuramoto, "Flexible boundary condition for a moving dislocation", *Journal of Applied Physics*, vol. 86, pp. 179–185, 1999.

[16] F.F. Abraham and H. Gao, "How fast can cracks propagate", *Physical Review Letters*, vol. 84, pp. 3113–3116, 2000.

[17] S.J. Zhou, P.S. Lomdahl nad R. Thomson, and B.L. Holian, "Dynamic crack processes via molecular dynamics", *Physical Review Letters*, vol. 76, pp. 2318–2321, 1996.

[18] S.J. Carroll, P.D. Nellist, R.E. Palmer, S. Hobday, and R.Smith, "Shallow implantation of size-selected ag clusters into graphite", *Physical Review Letters*, vol. 84, pp. 2654–2657, 2000.

[19] M. Moseler, J. Nordiek, and H. Haberland, "Reduction of the reflected pressure wave in the molecular-dynamics simulation of energetic particle-solid collisions", *Physical Review B*, vol. 56, pp. 15439–15445, 1997.

[20] E.B. Tadmor, M. Ortiz, and R. Phillips, "Quasicontinuum analysis of defects in solids", *Philosophical Magazine A*, vol. 73, pp. 1529–1563, 1996.

[21] E.B. Tadmor, R. Phillips, and M. Ortiz, "Mixed atomistic and continuum models of deformation in solids", *Langmuir*, vol. 12, pp. 4529–4534, 1996.

[22] V.B. Shenoy, R. Miller, E.B. Tadmor, R. Phillips, and M. Ortiz, "Quasicontinuum models of interfacial structure and deformation", *Physical Review Letters*, vol. 80, pp. 742–745, 1998.

[23] J.M. Ball and R.D. James, "Fine phase mixtures as minimizers of energy", *Archive for Rational Mechanics and Analysis*, vol. 100, pp. 13–52, 1987.

[24] M.S. Wechsler, D.S. Lieberman, and T.A. Read, ", *Trans. AIME J. Met.*, vol. 197, pp. 1503–1515, 1953.

[25] K. Bhattacharya, "Wedge-like microstructure in martensites", *Acta Metallurgica et Materialia*, vol. 39, pp. 2431–2444, 1991.

[26] J.M. Ball, P.J. Holmes, R.D. James, R.L. Pegp, and P.J. Swart, "On the dynamics of fine structure", *Journal of Nonlinear Science*, vol. 1, pp. 17–70, 1991.

[27] G. Friesecke and J.B. McLeod, "Dynamics as a mechanism preventing the formation of finer and finer microstructure", *Archive for Rational Mechanics and Analysis*, vol. 133, pp. 199–247, 1996.

[28] P. Leo, T. Shield, and O. Bruno, "Transient heat transfer effects on the pseudoelastic behavior of shape-memory wires", *Acta Metallurgica et Materialia*, vol. 41(8), pp. 2477–2485, 1993.

[29] N. Bubner, "Landau-ginzburg model for a deformation-driven experiment on shape memory alloys", *Continuum Mechanics and Thermodynamics*, vol. 8, pp. 283–308, 1996.

[30] S. Turteltaub, "Viscosity and strain gradient effects on the kinetics of propagating phase boundaries in solids", *Journal of Elasticity*, vol. 46(1), pp. 53–90, 1997.

[31] S. C. Ngan and L. Truskinovsky, "Thermal trapping and kinetics of martensitic phase boundaries", *Journal of the Mechanics and Physics of Solids*, vol. 47, pp. 141–172, 1999.

[32] J. Shaw, "Simulations of localized thermo-mechanical behavior in a niti shape memory alloy", *International Journal of Plasticity*, vol. 16, pp. 541–562, 2000.

[33] A. Vainchtein, "Dynamics of non-isothermal martensitic phase transitions and hysteresis", *International Journal of Solids and Structures*, vol. 39, pp. 3387–3408, 2002.

[34] C. Faciu and M. Mihailescu-Suliciu, "On modeling phase propagation in smas by a maxwellian thermo-viscoelastic approach", *International Journal of Solids and Structures*, vol. 39, pp. 3811–3830, 2002.

[35] A. Vainchtein, "Non-isothermal kinetics of a moving phase boundary", *Continuum Mechanics and Thermodynamics*, vol. 15, pp. 1–19, 2003.

[36] L. Truskinovsky, "Dynamics of nonequilibrium phase boundaries in a heat conducting elastic medium", *Journal of Applied Mathematics Mechanics*, vol. 51, pp. 777–384, 1987.

[37] R. Abeyaratne and J.K. Knowles, "Kinetic relations and the propagation of phase boundaries in solids", *Archive for Rational Mechanics and Analysis*, vol. 114, pp. 119–154, 1991.

[38] G. Caginalp, "An analysis of a phase field model of a free boundary.", *Archive for Rational Mechanics and Analysis*, vol. 92(3), pp. 205–245, 1986.

[39] A. A. Wheeler, W. J. Boettinger, and G. B. McFadden, "Phase field models for isothermal phase transitions in binary alloys", *Physical Review A*, vol. 45, pp. 7424–7439, 1992.

[40] E. Fried and M. E. Gurtin, "Continuum theory of thermally induced phase transitions based on an order parameter", *Physica D*, vol. 68, pp. 326–343, 1993.

[41] Y. M. Jin A. Artemev and A.G. Khachaturyan, "Three-dimensional phase field model and simulation of cubic to tetragonal martensitic transformation in polycrystals", *Philosophical Magazine A*, vol. 82, pp. 1249–1270, 2002.

[42] S. Vedantam, "Constitutive equations for rate-dependent pseudoelastic behaviour of shape memory alloys", *Smart Materials and Structures*, vol. 15, pp. 1172, 2006.

[43] E. C. Aifantis, "On the microstructural origin of certain inelastic models", *Journal of Engineering Materials and Technology*, vol. 106, pp. 326–330, 1984.

[44] N. Triantafyllidis and E. C. Aifantis, "A gradient approach to localization of deformation. I - Hyperelastic materials", *Journal of Elasticity*, vol. 16, pp. 225–237, 1986.

[45] N. Triantafyllidis and S. Bardenhagen, "On higher order gradient continuum theories in 1-d nonlinear elasticity. derivation from and comparison to the corresponding discrete models", *Journal of Elasticity*, vol. 33(3), pp. 259–293, 1993.

[46] N. Triantafyllidis and S. Bardenhagen, "The influence of scale size on the stability of periodic solids and the role of associated higher order gradient continuum models", *Journal of the Mechanics and Physics of Solids*, vol. 44, pp. 1891–1928, 1996.

[47] A. Vainchtein, "Stick-slip motion of interfaces as a singular limit of the viscosity capillarity model", *Mathematics and Mechanics of Solids*, vol. 6(3), pp. 323–341, 2001.

[48] M.E. Gurtin and L. Anand, "A theory of strain-gradient plasticity for isotropic, plastically irrotational materials. part I: Small deformations", *Journal of the Mechanics and Physics of Solids*, vol. 53, pp. 1624–1649, 2005.

[49] L. Truskinovsky and A. Vainchtein, "The origin of nucleation peak in transformational plasticity", *Journal of the Mechanics and Physics of Solids*, vol. 52, pp. 1421–1446, 2004.

[50] L. Truskinovsky and A. Vainchtein, "Dynamics of martensitic phase boundaries: discreteness, dissipation and inertia", *Continuum Mechanics and Thermodynamics*, vol. 20(2), pp. 97–122, 2008.

[51] N.M. Ghoniem, E.P. Busso, N. Kioussis, and H Huang, "Multiscale modeling of nano and micro-mechanics: an overview", *Philosophical Magazine*, vol. 83, pp. 3475, 2003.

[52] L. Truskinovsky and A. Vainchtein, "Kinetics of martensitic phase transitions: Lattice model", *SIAM Journal on Applied Mathematics*, vol. 66, pp. 533–553, 2005.

[53] J. Frenkel and T. Kontorova, ", *Phys Z. Sowjet Union*, vol. 13, pp. 1, 1938.

[54] W. Atkinson and N. Cabrera, "Motion of a frenkel-kontorova dislocation in a one-dimensional crystal", *Physical Review A*, vol. 138(3), pp. 763–766, 1965.

[55] Y. Zhen and A. Vainchtein, "Dynamics of steps along a martensitic phase boundary I: Semi-analytical solution", *Journal of the Mechanics and Physics of Solids*, vol. 56, pp. 496–520, 2008.

[56] Y. Zhen and A. Vainchtein, "Dynamics of steps along a martensitic phase boundary II: Numerical simulations", *Journal of the Mechanics and Physics of Solids*, vol. 56, pp. 521–541, 2008.

[57] K. Tounak, F. Carrion, and S. Yip, "Molecular dynamics study of structural instability of two-dimensional lattices", *Journal of Applied Physics*, vol. 56, pp. 1455–1461, 1983.

[58] O. Kastner, "Molecular-dynamics of a 2D model of the shape memory effect", *Continuum Mechanics and Thermodynamics*, vol. 18, pp. 63–82, 2006.

[59] S. Ozgen and O. Adiguzel, "Investigation of the thermoelastic phase transformation in a NiAl alloy by molecular dynamics simulation", *Journal of Physics and Chemistry of Solids*, vol. 65, pp. 861–865, 2004.

[60] F. E. Hildebrand and R. Abeyaratne, "An atomistic investigation of the kinetics of detwinning", *Journal of the Mechanics and Physics of Solids*, vol. 56, pp. 1296–1319, 2008.

[61] M. Rao and S. Sengupta, "Nucleation of solids in solids: Ferrites and martensites", *Physical Review Letters*, vol. 91, pp. 045502, 2003.

[62] R.S. Elliott, J.A. Shaw, and N. Triantafyllidis, "Stability of thermally-induced martensitic transformations in bi-atomic crystals", *Journal of the Mechanics and Physics of Solids*, vol. 50, pp. 2463–2493, 2002.

[63] R.S. Elliott, J.A. Shaw, and N. Triantafyllidis, "Stability of pressure-dependent, thermally-induced displacive transformations in bi-atomic crystals", *International Journal of Solids and Structures*, vol. 39, pp. 3845–3856, 2002.

[64] J.R. Morris and R.J. Gooding, "Vibrational entropy effects at a diffusionless first-order solid-to-solid transition", *Physical Review B*, vol. 43, pp. 6057–6067, 1991.

[65] C. Kittel, *Introduction to solid state physics*, Wiley, New York, USA, 8th edition.

[66] R.P. Feymann, "Atomic theory of the two-fluid model of liquid helium", *Physical Review*, vol. 94, pp. 262–277, 1954.

[67] A. Einstein, B. Podolsky, and N. Rosen, "Can quantum-mechanical description of physical reality be considered complete", *Physical Review*, vol. 47, pp. 777–780, 1935.

[68] F. Reif, *Fundamentals of Statistical and Thermal Physics. See section 15.5 Langevin Equation*, McGraw Hill, New York, 1965.

[69] L. Verlet, "Computer experiments on classical fluids", *Physical Review*, vol. 159, pp. 98–103, 1967.

[70] John A. Shaw and Stelios Kyriakides, "Thermomechanical aspects of NiTi", *Journal of the Mechanics and Physics of Solids*, vol. 43, pp. 1243–1281, 1995.

[71] P. Thamburaja, H. Pan, and F. Chau, "Martensitic reorientation and shape-memory effect in initially textured polycrystalline Ti-Ni sheet", *Acta Materialia*, vol. 53, pp. 3821–3831, 2005.

[72] S. Vedantam and R. Abeyaratne, "A helmholtz free-energy function for a CuAlNi shape memory alloy", *International Journal of Non-Linear Mechanics*, vol. 40, pp. 177–193, 2005.

[73] A. P. Sutton, "Temperature-dependent interatomic forces", *Philosophical Magazine A*, vol. 60, pp. 147–159, 1989.

[74] F. Falk, "Model free energy, mechanics, and thermodynamics of shape memory alloys", *Acta Metallurgica*, vol. 28, pp. 1773–1780, 1980.

[75] S. Nosé, "A unified formulation of the constant temperature molecular dynamics methods", *Journal of Chemical Physics*, vol. 81, pp. 511–519, 1984.

[76] W.G. Hoover, "Canonical dynamics: Equilibrium phase-space distributions", *Physical Review A*, vol. 31, pp. 1695–1697, 1985.

[77] J. W. Gibbs, *Elementary principles in statistical mechanics*, Longmans Greens, New York, 1972, v.2, pt.1 of the collected works of J.Willard Gibbs, Chap.4.

Appendix A

Review of statistical mechanics

Consider a system of interest, whose *microstate* refers to a specific detailed microscopic configuration and macrostate refers to its macroscopic properties such as temperature and pressure. In statistical mechanics, the macrostate is characterized by a probability distribution on a certain set of microstates, and this provides a framework for relating microscopic properties of individual atoms and molecules to the macroscopic properties of materials. Gibbs [77] first introduced the concept of an ensemble of systems. An ensemble is a collection of a very large number of systems. Macroscopic environmental constraints lead to different types of ensembles such as, for example, a thermally isolated system which is referred as microcanonical ensemble with volume V, number of particles N and energy E fixed. A canonical ensemble is one in which N, V and temperature θ are fixed. An ensemble of this system can exchange its energy with a heat reservoir. A grand canonical ensemble exchanges particles along with energy with the reservoir. Our focus here is on a canonical ensemble to study the macroscopic properties of coupled oscillators. In this section we will review the thermodynamic variables obtained using canonical ensemble.

A.1 Canonical ensemble

In a canonical or NVT ensemble, the probability distribution P_i is given by Boltzmann distribution.

$$P_i = \frac{e^{-\beta E_i}}{\mathcal{Z}}. \tag{A.1}$$

where $\beta = 1/k_B\theta$ and k_B is Boltzmann's constant. E_i is the energy of the ith microstate of the system. The probabilities of the various microstates must add to one $\Sigma P_i = 1$, and the normalization factor in the denominator, $\mathcal{Z}$, is the canonical partition function.

A.2 Partition function

Physically, the partition function encodes the underlying physical structure of the system. The partition function is given by $\mathcal{Z} = \mathcal{Z}_p\mathcal{Z}_q$ where

$$\mathcal{Z}_q = \int_{-\infty}^{+\infty} \exp\left(-\frac{\bar{V}(q)}{k_B\theta}\right) dq, \tag{A.2}$$

and

$$\mathcal{Z}_p = \int_{-\infty}^{+\infty} \exp\left(-\frac{\bar{K}(p)}{k_B\theta}\right) dp, \tag{A.3}$$

where $\mathcal{Z}_p$ and $\mathcal{Z}_q$ are the partition functions associated with the momentum and position respectively. The potential energy is $V(q)$ and the kinetic energy is $K(p)$ and thus the total Hamiltonian is

$$H = V + K. \tag{A.4}$$

A.3 Thermodynamic functions

The thermodynamic variables of the system, such as the average energy $< E >$, entropy S and free energy F can be expressed in terms of the partition function

or its derivatives. Total energy of the system is the sum of the microstate energies weighted by their respective probabilities

$$< E >= \Sigma_i E_i P_i = \frac{1}{\mathcal{Z}} \Sigma_i E_i e^{-\beta E_i} = -\frac{1}{\mathcal{Z}} \frac{d\mathcal{Z}}{d\beta}. \tag{A.5}$$

Internal energy U can be interpreted as average total energy

$$< E >= U = -\frac{d \log \mathcal{Z}}{d\beta}, \tag{A.6}$$

and entropy can be calculated by logarithm of the number of microscopic configurations

$$S = -k_B \Sigma_i P_i \log P_i = \log \mathcal{Z} + \beta U. \tag{A.7}$$

Finally, the Helmholtz free energy of a system F is given by

$$F = U - \theta S = -\frac{\log \mathcal{Z}}{\beta} = -k_B \theta \log \mathcal{Z}. \tag{A.8}$$

Thus with knowledge of the Hamiltonian, the macroscopic thermodynamic variables can be obtained.

Appendix B

Velocity Verlet algorithm

Verlet algorithm [69] is a numerical method used to integrate Newton's equations of motion. It is frequently used to calculate trajectories of particles in molecular dynamics simulations. The basic form of the Verlet algorithm is derived by adding Taylor expansions for the positions of the particles at a forward-time and backward-time as given in Eq. (B.1) and E. (B.2) respectively

$$r(t+\Delta t) = r(t) + v(t)\Delta t + \frac{1}{2}a(t)\Delta t^2 + \frac{1}{6}b(t)\Delta t^3 + O(\Delta t^4) \tag{B.1}$$

$$r(t-\Delta t) = r(t) - v(t)\Delta t + \frac{1}{2}a(t)\Delta t^2 - \frac{1}{6}b(t)\Delta t^3 + O(\Delta t^4) \tag{B.2}$$

Where $r(t)$ is the position of the particle at time t and Δt is the incremental time step. $v(t)$ is the velocity and $a(t)$ is the acceleration.

By adding Eq. (B.1) and E. (B.2),

$$r(t+\Delta t) = 2r(t) - r(t-\Delta t) + a(t)\Delta t^2 + O(\Delta t^4) \tag{B.3}$$

From Newton's equations, $a(t)$ is the force divided by mass as given in Eq. (B.4). The force in molecular simulation is a function of the positions.

$$a(t) = -\frac{1}{m}\nabla V(r(t)) \tag{B.4}$$

The truncation error of the algorithm when evolving the system by Δt is of the order of Δt^4. This algorithm is simple to implement. A problem with this version of the Verlet algorithm is that the velocities are not directly generated. Velocity is important to evaluate the kinetic energy of the system and verify the conservation of the total energy. Velocities can be computed indirectly from the positions by using Eq. (B.5)

$$v(t) = \frac{r(t + \Delta t) - r(t - \Delta t)}{2\Delta t} \tag{B.5}$$

The error associated is of the order of Δt^2 rather than Δt^4. Velocity Verlet scheme overcome this difficulty by calculating the positions, velocities and accelerations at time $t + \Delta t$ from the same quantities at time t in the following way

$$r(t + \Delta t) = r(t) + v(t)\Delta(t) + \frac{1}{2}a(t)\Delta t^2 \tag{B.6}$$

$$v(t + \frac{\Delta t}{2}) = v(t) + \frac{1}{2}a(t)\Delta t \tag{B.7}$$

$$a(t + \Delta t) = -(\frac{1}{m})\nabla V(r(t + \Delta t)) \tag{B.8}$$

$$v(t + \Delta t) = v(t + \frac{\Delta t}{2})) + \frac{1}{2}a(t + \Delta t)\Delta t \tag{B.9}$$